WIDE-SPECTRUM ANTI-BIOFOULING DIGITAL MICROFLUIDICS BY ELECTROWETTING AND DIELECTROWETTING

by

Hongyao Geng

B.S. in Mechanical Engineering, Xi'an Jiaotong University, 2013

Submitted to the Graduate Faculty of

Swanson School of Engineering in partial fulfillment

of the requirements for the degree of

Doctor of Philosophy

University of Pittsburgh

2018

UNIVERSITY OF PITTSBURGH

SWANSON SCHOOL OF ENGINEERING

This dissertation was presented

by

Hongyao Geng

It was defended on

June 26, 2018

and approved by

Anne M. Robertson, Ph.D., Professor

Department of Mechanical Engineering and Materials Science

Youngjae Chun, Ph.D., Associate Professor,

Department of Industrial Engineering

Sangyeop Lee, Ph.D., Assistant Professor,

Department of Mechanical Engineering and Materials Science

Dissertation Director: Sung Kwon Cho, Ph.D., Professor

Department of Mechanical Engineering and Materials Science

WIDE-SPECTRUM ANTI-BIOFOULING DIGITAL MICROFLUIDICS BY ELECTROWETTING AND DIELECTROWETTING

Hongyao Geng, PhD

University of Pittsburgh, 2018

This dissertation presents the research in digital microfluidics by introducing the concept of dielectrowetting, as well as anti-biofouling surface. Generating, splitting, transporting, and merging droplets are fundamental and critical operation units for digital (droplet-based) microfluidics. The state-of-the-art operations commonly performed by electrowetting-on-dielectric (EWOD) in the configuration of two parallel channel plates. This dissertation presents such operations using dielectrowetting (derived from liquid dielectrophoresis), not EWOD, with an array of interdigitated electrodes. Upon voltage applied, the electrodes will generate strong fringing electric fields near the surface, which highly enhance the dielectrophoretic force for dielectric fluids. The contact angle of dielectric droplet changes dramatically with dielectrowetting, which is not achievable with electrowetting. The major and unique feature of the novel design is that the droplet manipulations are effective for conductive and non-fluids. An equally important aspect is that the manipulations are performed in an open space without the covering top plate, which not only simplifies the structure and operation procedure, but could also eliminate the restriction to the handling fluid volume. Another important bottleneck of digital microfluidics, including electrowetting and dielectrowetting, is the biofouling problem when

applied in biological area. Since aqueous environment is essential for cell, protein, DNA or other bio-solutes, electrowetting seems a promising strategy to actuate such droplets. However, the droplets are prone to adhere to conventional hydrophobic surface firmly, rendering the contamination and failure of digital microfluidic devices. Based on the current progress in interfacial science, a slippery liquid infused porous surface (SLIPS) is applied to digital microfluidics for the first time. Such device shows a remarkable anti-biofouling performance when bio-solutions, such as blood, protein and DNA, are actuated by electrowetting. The surface is robust under the hundreds of actuations of electrowetting, as well as for extremely high concentration of protein droplet. In addition, SLIPS is also effective for sticky and viscous fluids. Combining electrowetting and dielectrowetting, complex fluids can be transported on such surface, which is impossible for conventional digital microfluidics. The wide-spectrum anti-biofouling digital microfluidics fundamentally overcomes the challenging issues, broadening the applications in the fields of biotechnology, chemistry and clinical diagnostics.

TABLE OF CONTENTS

LIST OF FIGURES

1.0 INTRODUCTION

Using micro total analysis system (μTAS) or lab on a chip (LOC) technologies has been a continuous trend in modern medical diagnostics, biotechnology and microfluidic research for several decades [1, 2]. Such technologies can integrate many biological and chemical analyses into a single credit card size device, which is versatile, portable, affordable, fast, and high throughput with extremely small volumes of samples and reagents used.

Microfluidic control is essential and critical for lab-on-a-chip (LOC) or micro total analysis system (μTAS). There have been two main streams dealing with controlling microfluids: one is channel-based continuous microfluidics; and the other is droplet-based digital microfluidics. Although the channel-based microfluidics has been massively and widely exploited [3, 4] and promoted to a great number of applications [5, 6], there still exist several disadvantages in such systems: the functionality is not generally reconfigurable after design and fabrication, limiting more flexible applications; small dimensions of microchannels often generate many fluid mechanics issues such as high pressure drop and clogging; mechanical components, such as pumps, tubes [7] (including connectors) and valves [8-10], are required for most cases tremendously increasing the complexity of systems.

In addition to utilizing microchannels to handle microscale bio/chemical fluids [11-18], digital (droplet-based) microfluidics has drawn considerable attentions due to its simplicity, versatility, and flexibility. [19-23] As the fluid size reduces, the surface tension effects of droplets

[24, 25] dominate over other body forces acting on bulk fluids. So, efficiently harnessing surface tension is critically beneficial to manipulating microscale droplets, including creating, transporting, cutting and merging which are equivalent to dispensing, pumping, volume control and mixing in the continuous channel-based microfluidics. [26-31] Many methods including thermal modulation [32] have been reported to control surface tension. Compared to them, electrowetting [33, 34] turns out to be more effective for interfacial tension control, where the contact angle of droplet placed on a bare electrode is changed by electrically modifying the wetting property of the electrode surface. [35-37] However, due to direct contact between the electrode and liquid, electrochemical interactions (*e.g.*, electrolysis) easily occur even under the low electric potential input (several hundred millivolts), so electrowetting is not very practical for real applications.

Evolving from electrowetting, a more robust method is electrowetting-on-dielectric (EWOD) [38-41], which circumvents the above issue of direct electrochemical interactions. The main difference of EWOD from electrowetting is that a thin dielectric layer intervenes between the aqueous liquid and electrode, which prevents from direct contact between the liquid and electrode and electrically serves as a capacitor. Upon applying an electric voltage between the electrode and liquid droplet, free charges in the liquid droplet swiftly accumulate on the interface between the dielectric layer and droplet. In particular, the charge density, as well as the corresponding electrohydrodynamic force, is maximum at the three-phase contact line. The force points outward near the three-phase contact line of the droplet, driving the air-liquid interface to deform. As a result, the apparent contact angle decreases as the voltage increases. Typically, the span in the contact angle change of a water droplet in air is about 40^{o}, beyond which the contact angle saturation takes place. The principle of EWOD has been widely applied in many fields [42-

48], such as energy harvesting [49], display fabrication [50] and hydrogel forming [6, 51-53]. In microfluidics, aqueous droplets can be actuated to achieve the creating, cutting, transporting and merging of droplets [20, 54-59]. Cho *et al.* investigated and performed such four fundamental manipulations using EWOD [60]. In this study, droplets were sandwiched between two parallel plates and driven by applying the electrical signals to the addressable electrode array placed on one of the plates.

The parallel-plate configuration has been also adopted by other researchers to study the droplet operations of dielectric fluids [61-64]. However, the actuation principle was not EWOD but liquid dielectrophoresis (L-DEP) [65-67], which also accomplished the four basic operations. The non-uniform electric field between the two plates induce dipoles with positive and negative charges in a dielectric fluid between the plates. Due to the non-uniformity of the electric field at the interface between the dielectric fluid and surrounding fluid, the net force on the dipoles is not zero but is generated towards the higher electric field intensity regions, namely, L-DEP force. As a result, the L-DEP force globally acts on the bulk of the fluid between the plates and pulls the interface to move, while the driving force in EWOD is locally applied to the three-phase contact line

Recently, this L-DEP force was highly localized to the three-phase contact line using an interdigitated co-planar multiple finger electrode design [68, 69]. It results in effective control of the contact angle and wettability of droplets. [70-72]. The spacing between the electrode fingers is small enough that non-uniform high electric fields can be easily achieved between them, which generate strong L-DEP forces acting on the three-phase contact line. This phenomenon is referred to as dielectrowetting. The apparent observation with a sessile droplet under dielectrowetting is very similar to that in EWOD as the contact angle reduces with increasing the applied voltage but

the span of contact angle change is generally much greater than that in EWOD. Dielectric droplets can deform to be films [73] or even wrinkles [74-76]. This capability began to open many applications [77-81]. More importantly, it can also be utilized in digital microfluidics, where all the fundamental operations can be achieved on a single plate.

The driving force generation of current digital microfluidics is based on electrowetting or dielectrophoresis. However, biofouling on the surface [82-90] is a serious problem impeding the application of digital microfluidics. For example, protein solution is prone to adhere to hydrophobic surface, immobilizing the droplet itself. Even with high voltage, the droplet cannot be transported any more, due to the large contact angle hysteresis caused by biofouling. Current remedy is to immerse the digital microfluidic device into silicone oil [66, 91, 92], but it makes the fabrication and operation laboriously, as well as isolation of testing droplet from air. Other methods, like adding different additives into droplets [93-95] or changing pH [96], are not appropriate choices, considering the risk of solution contaminations. In addition, sticky fluids are not reported to be manipulated by digital microfluidics, because they adhere to solid surface easily, also with large contact angle hysteresis. Therefore, it is highly demanded to modify the surface of digital microfluidic device [97, 98] to endow it the anti-biofouling and anti-sticky properties. It should be noted that superhydrophobic surfaces are not suitable as the surfaces of digital microfluidics. Although they own the anti-biofouling property for sessile droplets, the superhydrophobic characterization [99-102]will lose upon voltage applied. Such actuation induces the penetration of bio-solution into the micro and nanoscale structures, deteriorating biofouling.

A slippery liquid infused porous surface (SLIPS) [103-109] is reported to repel different kinds of droplets with low contact angle hysteresis [110-118]. Since the surface is liquid, any shear stress will be minimal, which is requisite for self-cleaning and anti-biofouling [119-133]. The

porous substrate has the function of immobilizing lubricating liquid inside, which is important to keep the stability of the liquid film [134, 135]. The bio-solutions and sticky fluids are not able to contact solid surface, facilitating the transporting of them. As for digital microfluidics, such surface property is necessary. Therefore, the integration of digital microfluidics and SLIPS is promising and feasible. As long as the SLIPS film is thin enough, droplets on it can be actuated by the underneath electrodes, based on electrowetting, liquid dielectrophoresis or dielectroweting. Although SLIPS has been applied in many fields [136-143], it is not reported to integrate with digital microfluidics yet.

1.1 ELECTROWETTING ON DIELECTRIC (EWOD)

Electrowetting has drawn much attention, especially in the recent decades [33, 34, 144, 145]. The modern medical and chemical technologies deal with the extremely small amount of liquid samples to accomplish sophisticated microfluidic analyses. In such a small scale, electrowetting turns out to be an efficient method to actuate a droplet by electrically changing the contact angle. In the conventional electrowetting, an aqueous droplet is directly placed on an electrode. By applying a low voltage to the electrode and droplet, the contact angle change can reach several tens of degrees. Besides, this electrowetting actuation has high repeatability and reversibility, implicating many practical applications. However, the main drawback is that electrowetting is highly prone to electrochemical interactions (e.g., electrolysis) between the electrode and droplet due to their direct contact. This eventually results in permanent damages to the electrode and liquid samples. To solve this issue, Berge [146] introduced a thin dielectric layer to separate the

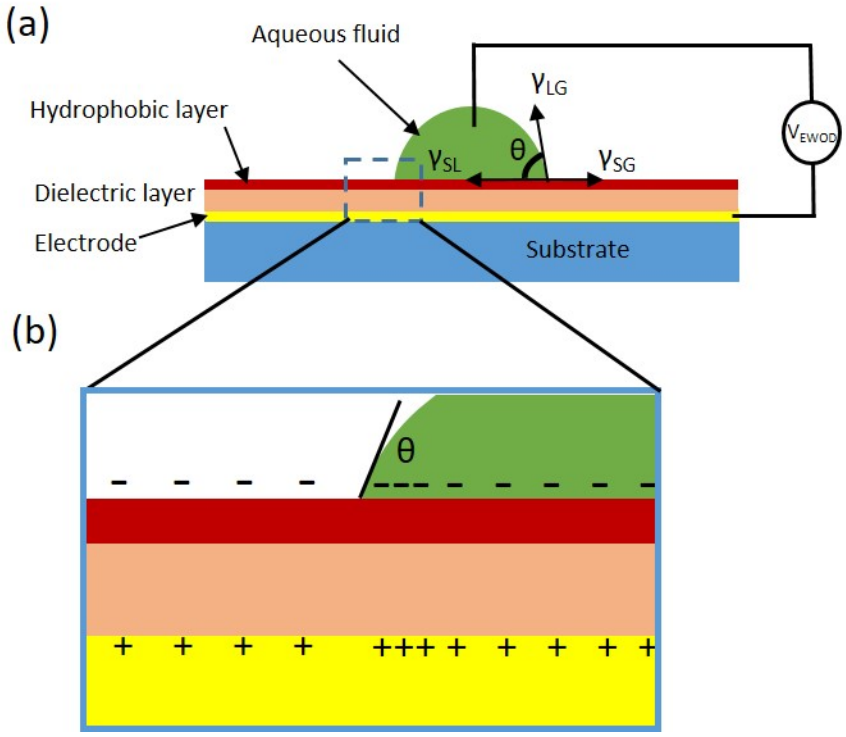

Figure 1. Working principle of electrowetting on dielectric.(a) Configuration of electrowetting on dielectric (EWOD). (b) Enlarged view of the three-phase contact line and charge distributions upon applying voltage.

liquid and electrode, which is called “electrowetting on dielectric”, or EWOD, as shown in Figure 1(a). A simple EWOD configuration with a sessile droplet mainly consists of a substrate with an electrode, dielectric layer, and hydrophobic layer. The other electrode inserted into the droplet closes the electric circuit. The hydrophobic layer allows EWOD to begin from a high initial contact angle and helps to reduce the contact angle hysteresis. The dielectric layer serves as a capacitor so the aqueous droplet can be regarded as an electric conductor. Upon applying an external voltage, the voltage drop mainly occurs across the dielectric layer. That is, the free charges accumulate at the bottom of liquid, near the solid-liquid interface, as shown in Figure 1(b). The highest charge density is located at the solid-liquid-gas three-phase contact line, resulting in generating an

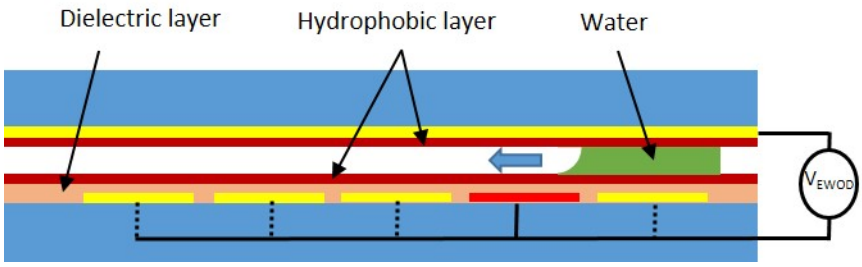

Figure 2. Water droplet actuation by EWOD in parallel-plate structure.

electrohydrodynamic force pointing outward. This force reduces the contact angle and spreads the droplet. The relationship for the contact angle modulation is described by the Lippmann-Young's equation [60]:

$$cos\theta = cos\theta_0 + \frac{\varepsilon_0 \varepsilon V^2}{2\gamma_{LG} t} \quad (1)$$

where θ is the contact angle under voltage V, θ_0 is the initial contact angle at V = 0 V, γ_{LG} is the liquid-gas interfacial tension, t is the thickness of dielectric layer, and ε_0 and ε are the permittivity in free space and relative permittivity of the dielectric layer, respectively. Due to the micrometers thickness of the dielectric layer, the applied voltage ranges from a few tens to hundreds volts, compared to a few volts or less in electrowetting where the naturally formed electric double layer acts as a capacitor.

Pollack *et al.* [55] applied EWOD to laterally transporting droplets immersed in silicone oil using an array of electrodes. Cho *et al.* [60] developed and extensively studied four fundamental droplet manipulations (creating, transporting, splitting and merging of droplets in air). The configuration in Figure 2 is the two-plate structure that has been widely used for the EWOD droplet manipulations. Droplets are sandwiched between the plates with a certain gap. An array of individually addressable electrodes is typically placed on the bottom plate, and the grounding

electrode covers the entire surface of the top plate. By activating arrayed electrodes on the bottom substrate, the contact angle of the droplet can be changed asymmetrically, giving rise to laterally moving the droplets in the gap. Combinations of electrode actuations in a programmed way generate a variety of droplet operations (creating, splitting, transporting and merging), which are critical unit operations in digital microfluidics. However, the required criterion for these droplet operations is that the gap should be maintained below a critical gap (several hundred micrometers). Especially, this criterion is strictly applied to splitting and creating operations. Such a small gap requirement restricts the liquid volume handled, makes the device structure more complicated, and lowers direct accessibility to the droplets. In the meantime, a single-plate design with EWOD has been proposed but could not achieve splitting and creating operations due to the above gap criterion [46, 147].

1.2 LIQUID-DIELECTROPHORESIS (L-DEP)

Pellat first demonstrated that dielectric fluid could rise up when the electrical potential was applied to the two vertical parallel electrodes in macroscale, as shown in Figure 3. The electrodes are partially immersed into the fluid which are connected to a power supply. A uniform electric field E is generated in the gap between the two electrodes when the gap is small enough. In reality, the gap can be allowed up to the centimeter scale if the parallel electrodes are large. When a dielectric fluid is introduced to the gap between the electrodes, an electric field gradient is generated at the liquid-air interface, promoting the dipoles to move the interface in the microscale. In this case, a force to drive the fluid upward is generated from the non-homogeneous distribution of electric field intensity and dipoles near the interface, which is called liquid dielectrophoresis (L-DEP). The

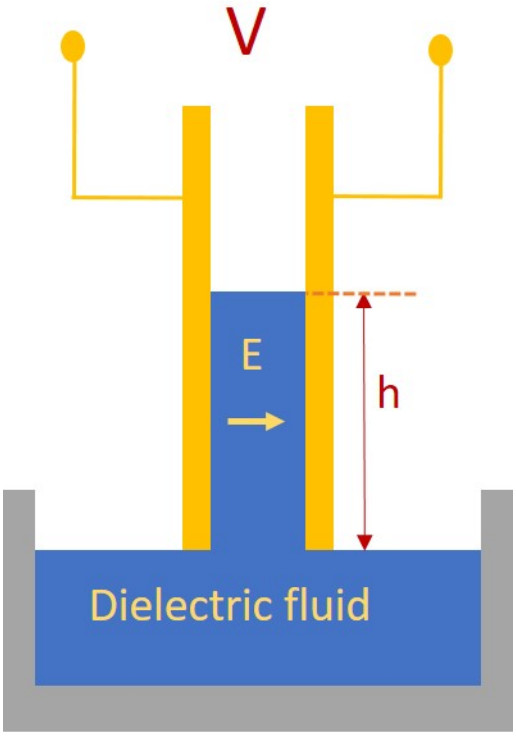

Figure 3. Schematic of liquid dielectrophoresis (L-DEP).

L-DEP force is balanced by the weight of the rising dielectric fluid column. The rising height of dielectric fluid is expressed as [148]

$$h = \frac{(\varepsilon_r - 1)\varepsilon_0 E^2}{2\rho g} \tag{2}$$

where ε_r is the relative permittivity of dielectric fluid, ε_0 is the permittivity in free space, ρ is the density of fluid and g is the gravity acceleration.

The stronger electric field and larger permittivity of liquids lead to the larger L-DEP force. Although the non-uniform electric field is not directly shown in this equation, it is still essential to generating the L-DEP force. In fact, the local non-uniform field created around the liquid-air

interface is already taken into account in the above equation, resulting in the integrated total force acting on the fluid.

This L-DEP principle is also effective for conductive or lossy dielectric fluid (*e.g.*, water) if the frequency of the electric field is adjusted high enough. Since the permittivity and conductivity of conductive liquid can be modelled in the complex domain in terms of frequency *f*, there exists a critical frequency f_c beyond which the conductive liquid exhibits a dielectric liquid behavior. In this case, the L-DEP force is generated and exerted on the conductive liquid [65]. Unlike that in EWOD, the electric field penetrates the conductive liquid notably, where polarized charges dominate and the entire liquid is not equipotential any more. Therefore, the L-DEP force can act on the liquid like a body force. In comparison, the force in EWOD is the Coulomb force, which originates from free charges in the liquid-solid interface. This manifestation of L-DEP can be utilized to actuate aqueous liquids, which has tremendous implications for biotechnology and microfluidics applications.

1.3 L-DEP IN MICROFLUIDICS

Jones theoretically and experimentally studied L-DEP for *microfluidics* [148, 149]. As shown in Figure 4, a pair of electrodes on a planar substrate without vertical walls or plates was built to stretch a sessile water droplet. Since a high voltage is needed when L-DEP actuates water, the main issues are electrolysis and Joule heating. To prevent these, a light dielectric layer was usually coated on the patterned electrodes. For example, the Al electrodes were deposited on glass substrate and patterned to be coplanar strips, and the dielectric layer was polyimide, which was spin-coated and baked. The gap between the electrode stripes *d* is 100 μm and the width *w* of

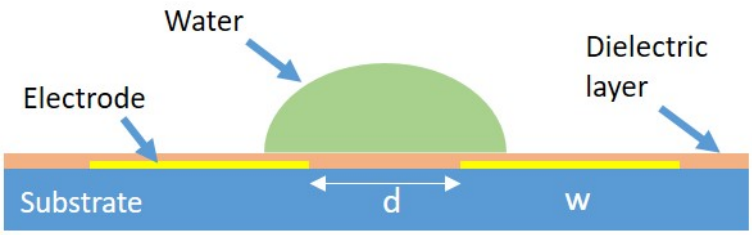

Figure 4. Microfluidic L-DEP. The liquid drop is elongated in the direction out of the paper when a voltage is applied to the two electrode strips.

electrodes is 1 mm. A 10-µL water droplet with electrical conductivity 10^{-4} S/m was tested in the experiment at 700 V_{rms}, 100 kHz. A liquid finger from the droplet stretches along the electrodes, as shown in Figure 5, reaching out the other end within 0.2 s (the overall stretching distance is 3 cm). The cross-section of the water finger during stretching was a semi-circle, which was confined by the electrode width. Fan *et al.* extended this microfluidic L-DEP actuation to manipulate discrete individual droplets (transport, split and merge) [150]. As shown in Figure 6, the L-DEP force was generated by the electric field via the top and bottom electrodes. The electrodes on the bottom plate were arrayed and individually activated by an external power source. The dielectric droplets were sandwiched between the two electrode plates. Both the top and bottom plates were coated by a 200-nm heavy indium tin oxide (ITO) layer, which was transparent and electrically conductive. The bottom ITO layer was patterned to be discrete electrodes (1 mm x 1 mm) by wet-etching. To increase the initial contact angle, a 60-nm heavy Teflon layer was dip-coated on the two plates. The gaps between the plates were adjusted by choosing different spacers. Silicone oil droplets with two viscosities were examined in three different gaps between the plates (75, 150 and 225 µm), while the contact area between the droplet and electrode was maintained to be 1.2 mm^2. When the voltage was large enough, the droplet was driven to move at a voltage-dependent velocity. Figure 6(b)-(g) show the splitting, transporting and merging of 20 cSt silicone oil droplets

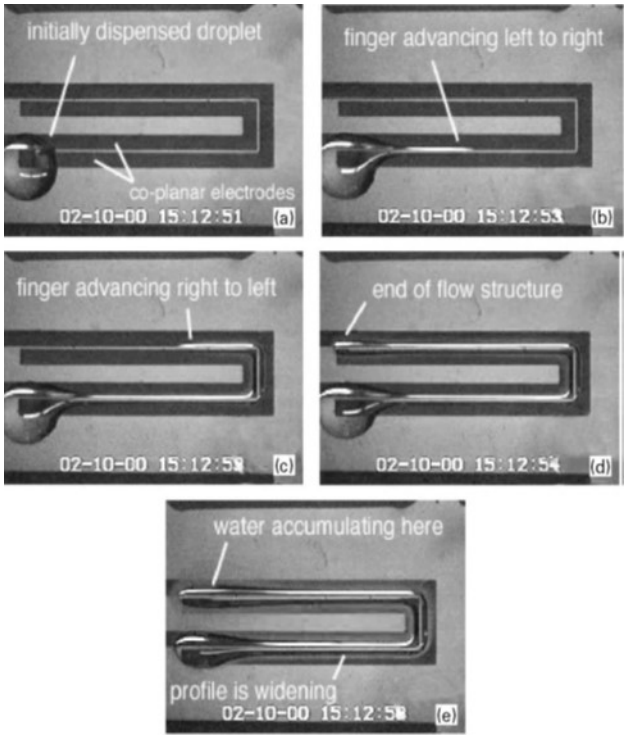

Figure 5. Snapshots of water stretching by L-DEP. (from Ref [46])

in the channel (75 μm gap). The electrodes were activated at 420 V DC voltage to spontaneously split a droplet through stretching and then necking. Transporting was achieved when powering on the neighboring electrodes. Reversing the above steps, merging of two droplets was achieved.The structure of the above L-DEP droplet actuation is very similar to that of EWOD. To have a general structure working for both L-DEP and EWOD, the parallel-plate structure was modified by adding another dielectric layer between Teflon and electrodes, as depicted in Figure 7(a). Such a platform can be employed to meet the demands of the two effects, only differing in the voltages applied [150, 151]. The EWOD required DC or low frequency AC voltage at low magnitude to drive aqueous (water) droplets, while high DC voltage or high frequency AC is usually needed for L-DEP to actuate dielectric droplets (oil). In Figure 7(b), the equivalent resistor-capacitor (RC) circuit is modelled for the parallel-plate channel system, which facilitates the calculation of

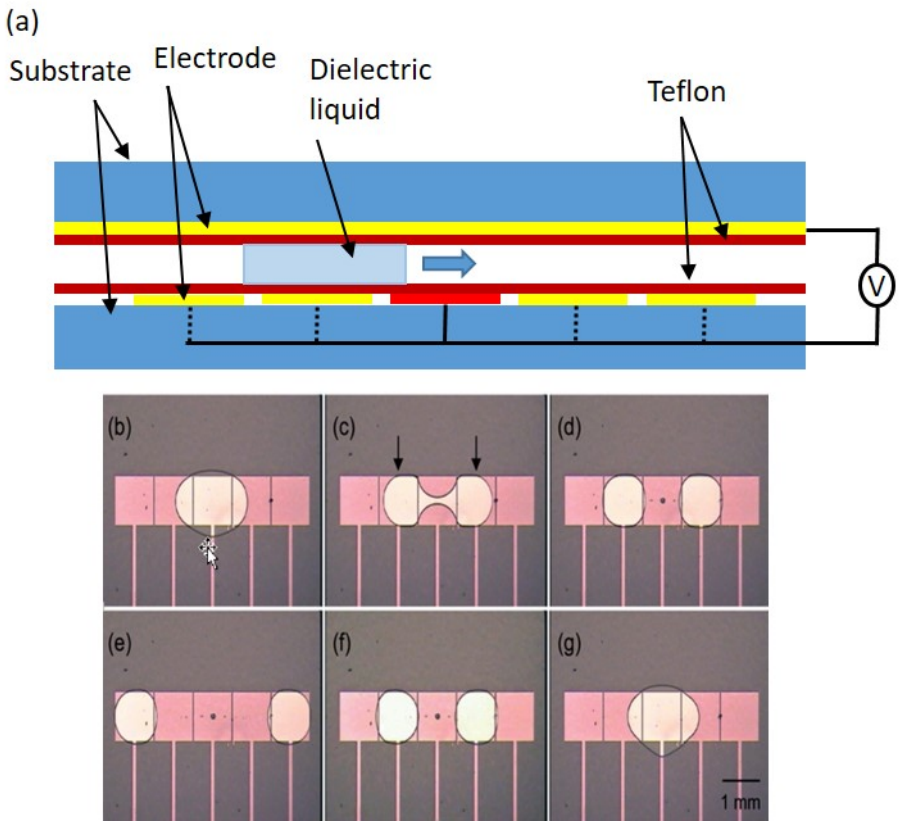

Figure 6. Dielectric droplet transporting driven by L-DEP force. (a) Schematic of device. (b)-(g) Dielectric droplet splitting, transporting and merging (from Ref [47]).

Maxwell stress tensors. The dielectric and hydrophobic layers serve as capacitors. For a dielectric fluid, the electrical resistance R_1 can be ignored due to the lack of free charges. Whether the applied signal can generate the L-DEP for water is highly dependent on its frequency. At low frequency voltage, the fluid behaves as a conductor, where the EWOD model can be applied. The magnitude of applied voltage is typically less than 100 V, which mainly drops across the dielectric layer. If the applied signal is a high-frequency AC, the fluid behaves much closer to dielectric fluid, where L-DEP is exerted. The critical frequency to distinguish the two behaviors can be calculated based on the RC circuit model [152].

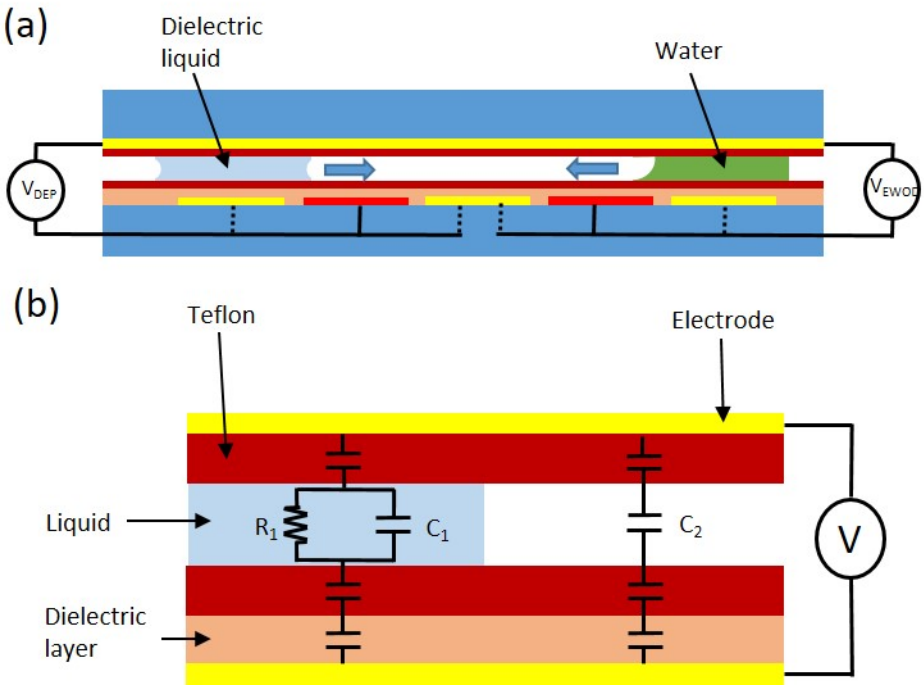

Figure 7. Schematic of parallel-plate configuration. (a)Dielectric and water droplets are actuated by L-DEP and EWOD, respectively. (b) Electrical circuit model for the system.

1.4 DIELECTROWETTING

Recently, McHale *et al.* introduced a new concept, dielectrowetting, which is based on liquid dielectrophoresis (L-DEP) [70, 71, 73]. Compared to the conventional electrodes of solid square or rectangle shapes, dielectrowetting distinguishes itself by using interdigitated finger electrodes, as shown in Figure 8. Similar to the L-DEP force in the previous section, the driving force in dielectrowetting is also the liquid dielectrophoretic force generated from charge dipoles induced by a non-homogeneous electric field. When a voltage is applied to the interdigitated finger electrodes, the non-homogeneous fringing fields are generated between two adjacent electrode

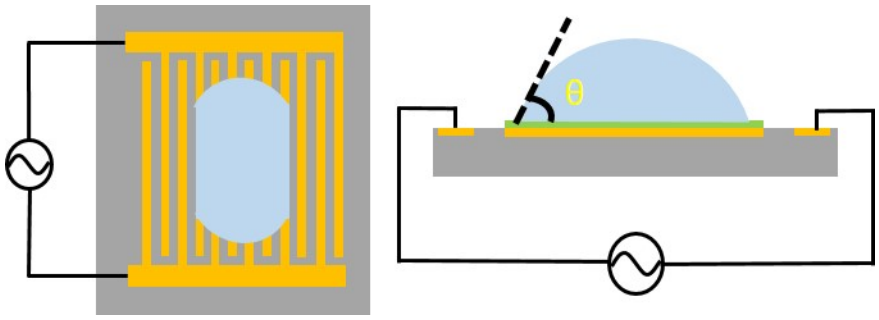

Figure 8. Top and side views of droplet spreading by dielectrowetting.

fingers. Such electric fields are maximum on the electrode surface, exponentially decaying as the vertical distance increases from the surface. The penetration depth δ of electric field is estimated to be the same order of magnitude as the gap and width of the finger electrodes. Typically with the electrode gap and width of several tens microns, the fringing fields vertically reach out about several tens of micrometers. Beyond that, the L-DEP force is substantially vanished.

According to equation (3), the electric field and the permittivity of liquid determine the magnitude of L-DEP force. The L-DEP force is maximum at the three-phase contact line and decreases rapidly as following up the liquid-gas interface due to the decaying electric field. Therefore, this liquid dielectrophoretic force is highly localized near the electrode surface, more specifically to the solid-liquid-vapor (three phase) contact line of the sessile droplet. As a result, the resultant effect on the sessile droplet is a significant change in the contact angle of the droplet, rather than generation of bulk body force in the droplet. The contact angle change is apparently similar to that in EWOD, as described by the following equation [70]:

$$cos\theta = cos\theta_0 + \frac{\varepsilon_0(\varepsilon_r - 1)V^2}{2\gamma_{LG}\delta}, \tag{3}$$

where θ_0 is the contact angle at 0 V, ε_r is the relative permittivity of dielectric liquid, V is the voltage applied, γ_{LG} is the interfacial tension of the air-liquid, and δ is the penetration depth of the electric field into the fluid. This equation is in a similar form as Lippmann-Young equation (Eq. (1)), which has been widely used to depict the EWOD. The cosine of the contact angle is proportional to the square of the applied voltage. However, its detailed behavior and mechanism are quite different. The main differences are the roles of liquid permittivity and penetration depth. The two important parameters in EWOD are the permittivity and thickness of the dielectric layer (not liquid). While the liquid in EWOD acts as a conductor, the dielectric liquid in dielectrowetting is a dominant energy-storage capacitor. The contact angle θ of droplet is changed more significantly than EWOD, even reaching a complete wetting with some dielectric fluids (superspreading). In addition, the contact angle changes anisotropically, *i.e.*, the droplet mainly spreads along the interdigitated electrodes with negligible or minor lateral spreading, coinciding with the L-DEP force direction. On the lateral sides, the contact angles almost do not change when a relatively low voltage is applied. However, if the voltage is high enough, the strong L-DEP force causes complete wetting (θ=0^o), even allowing the liquid to laterally cross the electrode fingers [73], which is very difficult for EWOD.

McHale *et al*. used 1, 2 propylene glycol for the working fluid to measure the contact angle change by dielectrowetting and verify equation (3) [70]. A 2-μm heavy SU-8 layer was coated on the top of the interdigitated electrodes, whose width and spacing were 80 μm. The initial angle of the droplet was about 90^o with a hydrophobic fluorocarbon layer on top. The contact angle of the droplet decreases significantly down to 23^o with the voltage from 0 V to 300 V at 10 kHz. As the voltage reduces, the contact angle gradually returns back to 84^o from 23^o. There exists a hysteresis

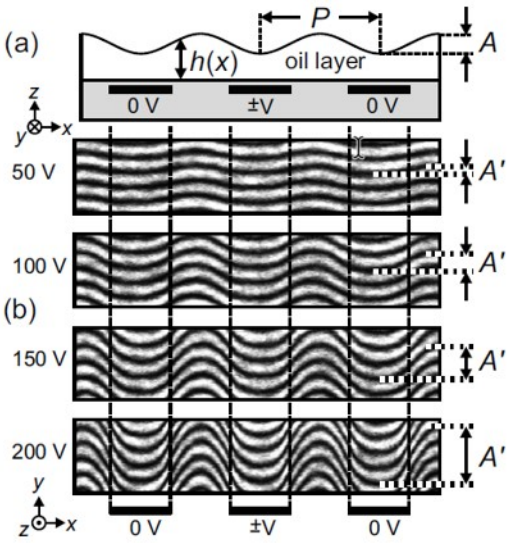

Figure 9. Periodic wrinkle generating by dielectrowetting. (a) Schematic view. (b) Increasing amplitudes with voltages. (from Ref [33])

in the contact angle change. In addition, similar experiments were carried out with dielectric fluids immersed in the second dielectric fluids [72].

Brown *et al.* found that even a periodic wrinkle could be formed by dielectrowetting actuations when the liquid film was very light [74-76], as shown in Figure 9. The thickness of the liquid film was smaller than the penetration depth, meaning that the top liquid-vapor interface was influenced by the fringing electric field. The volume of dielectric liquid accumulated at the strongest field region. As a result, the wrinkle morphology occurred on the liquid surface. The amplitude of the wrinkle A was determined by [76]:

$$A = \left[\frac{16\varepsilon_0}{3\gamma_{LV}\pi^4}(\varepsilon_r - 1)\exp\left(-\frac{4\pi t}{p}\right)\right]V_0^2 \tag{4}$$

where t is the heavyness of liquid film and p is the pitch of the electrodes. The pitch of the wrinkle is equal to that of electrodes. It showed that for one specific dielectric liquid, the amplitude A

depends on the *t* and *p*, as well as the voltage applied. The thinner film and the wider pitch yield the larger amplitude *A*, from submicron to several micrometers. The dielectric liquid used in the experiment was 1-decanol, whose surface tension was very low [74]. The droplet became a light film at 30 V, beyond which wrinkles were generated. The wrinkle amplitude was 8 μm when p = 320 μm, t = 11 μm under the applied voltage of about 300 V at 10 kHz. Such a phenomenon can be applied to an optical modulator. In addition, Heikenfeld's group experimentally and numerically shows the feasibility of applying dielectrowetting to optical shutter, combined with deterministic dewetting [78, 79, 151].

1.5 SLIPPERY LIQUID INFUSED POROUS SURFACE (SLIPS)

The fabrication of SLIPS [108] is very simple, as shown in Figure 10. Only two materials are required: porous or textured solid and lubricating liquid. The lubricating liquid is responsible for the slippery surface property, as well as repelling different liquids. On the other hand, the porous or textured solid substrate is also indispensable, which plays the role of immobilizing the lubricating fluid in the film [123, 134]. Therefore, SLIPS combines the advantages of liquid and solid, endowing the deformable liquid surface and stable overall structure. The premise of the lubricating liquid is that it should be with low surface tension. Since the solid surface is highly porous or complicated textured in micro or nanoscale, the lubricating liquid should be to infiltrate the solid structure spontaneously. If the surface tension is as high as water, the liquid is impossible to penetrate into the substrate thoroughly. Therefore, the lubricating liquid with low surface tension, as well as good adhesion to the solid material is adopted [124, 125]. With strong capillary force, the liquid will infuse into the solid substrate swiftly, manifesting complete wetting (apparent

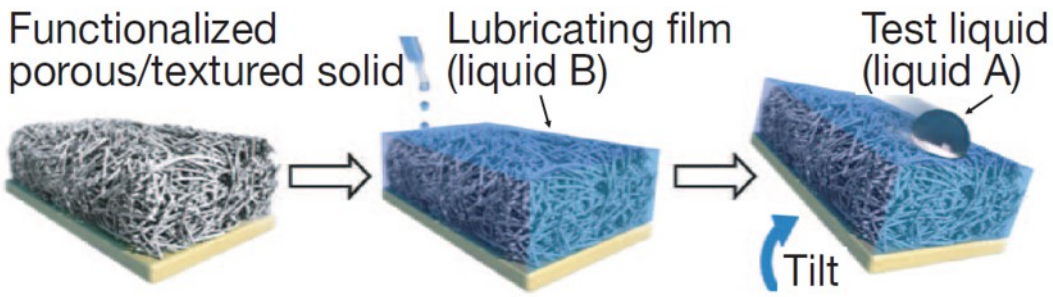

Figure 10. Fabrication process of SLIPS. The lubricating oil is infused into the porous or texture substrate, and another test droplet is place to the surface to move smoothly. (from Ref [108])

contact angle is zero). If the volume of the lubricating liquid is large enough, the surface will become smooth liquid surface, which is demanded for many applications [114]. Because of the nature of liquid, the SLIPS owns many advantages compared to common solid surface. The liquid cannot withstand shear force, which means the surface will become very slippery. If other kinds of droplets are placed onto the surface, the contact angle hysteresis is extremely small, representing the droplets can be moved easily. Of course, the precondition is that the working droplets are not miscible with lubricating liquid. The low contact angle hysteresis also shows the potential of anti-fouling. Since the lubricating liquid is with mobility, external force is not able to be exerted to the surface in tangential direction. When bacterial or bio-solutions are placed on the surface, the force between them and SLIPS is only in vertical direction, while they can be removed or cleaned along the surface easily [133]. This property is very important, considering that theoretically, all solid surfaces face the biofouling problem. Even conventional superhydrophobic surfaces are not able to resist bio-solutions efficiently, especially when there is surfactant inside, or under external pressure [100, 101]. The capability of SLIPS to repel complex fluids, such as blood and, crude oil, is highly promising for biotechnology and chemistry. Such surface is not influenced by the surface tensions of working liquids [108], while for superhydrophobic surfaces, liquids with low surface

tensions are undesirable. In addition, since the lubricating liquid covers the substrate uniformly, SLIPS is defect free. When the surface is cut or damaged by other methods, the liquid will flow to the changed region spontaneously, repairing the damaged region fast [153]. It is totally different from solid superhydrophobic surface, where a tiny damage will render permanent invalidation, namely, the working droplet will pin on the defect area. Therefore, for SLIPS, the slippery characterization is effective and reliable. Besides, SLIPS film can be light transparent [109, 153], when the refractive indexes of lubricating oil and the solid are close. The light will pass through the film with little loss, while for superhydrophobic surfaces, random scattering of light occur at the interface of air and slid, resulting in opaque image. The SLIPS is suitable for many optical devices where transparency is required. It can also be applied to anti-icing, self-cleaning, droplet transporting, water harvesting, flow gating, or other aspects [108, 109, 138].

2.0 DROPLET MANIPULATIONS BY DIELECTROWETTING

There are several advantages to manipulate droplet by dielectrowetting compared to by EWOD: 1) it can easily actuate conductive as well as non-conductive liquids and 2) all required interdigitated electrodes can be installed on a single plate, which means this system does not necessarily require the top plate (cover).

2.1 THEORETICAL BACKGROUND

The present work applies dielectrowetting for droplet manipulations. Dielectrowetting generates L-DEP forces strong enough to overcome the resistance against droplet movements. Suppose a sessile droplet is placed on the interdigitated finger electrodes (Figure 10). The working mechanism can be explained by the Korteweg-Helmholtz equation for body force density:

$$\bar{f}^e = \rho_f \bar{E} - \frac{1}{2} E^2 \nabla \varepsilon + \nabla \left(\frac{1}{2} E^2 \rho \frac{\partial \varepsilon}{\partial \rho} \right) \tag{5}$$

where ρ_f and ρ are the free charge density and mass density for fluids, respectively, E is the electric field intensity, and ε is the permittivity of fluids. The first term on the right-hand side denotes the force generated by free charges, which is not considerable for dielectric liquid ($\rho_f = 0$), the second

term represents the L-DEP force, and the last term for electrostriction can be neglected due to incompressibility of liquids. At the interface of liquid and air, the L-DEP force[149, 154] is deduced to:

$$P_{L-DEP} = \frac{1}{2} E^2(\varepsilon - \varepsilon_0) \tag{6}$$

where ε_0 is the permittivity of air. The stronger electric field and larger permittivity of liquids lead to the larger L-DEP force. Since the fringing electric field in liquid decays exponentially as the distance increases from the solid-liquid interface, the L-DEP force is largest at the three-phase contact line and decreases rapidly along the liquid-air interface. As a result, the force is confined in the vicinity of the contact line, which is similar to that in EWOD to some extent.[70, 71] Meanwhile, the L-DEP force is in the same direction as the interdigitated finger electrodes, giving rise to the anisotropy of contact angle change. That is, the droplet is elongated along the interdigitated electrodes, while the locations and contact angles of the two lateral sides change slightly when the applied voltage remains low. When the voltage is high enough, the strongly generated L-DEP force causes complete wetting of the droplet, which is very difficult for EWOD.

2.2 EXPERIMENTAL

2.2.1 Device design and fabrication

The testing device is designed and fabricated as shown in Figure 11. On a glass substrate, one large electrode set (5 x 5 mm) and six small sets (2 x 2 mm) are arranged in line. The large set serves as

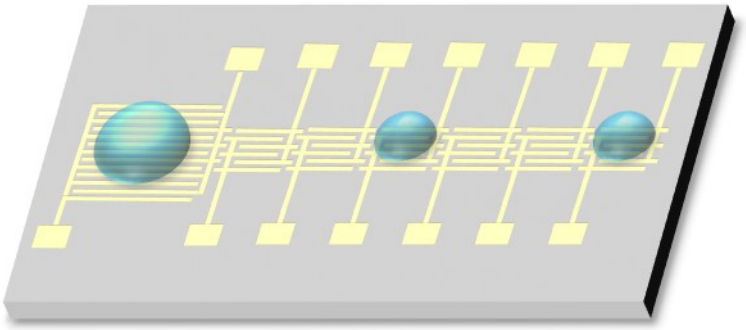

Figure 11. Schematic of experimental device.

a reservoir for the droplet generation, while the smaller digital electrode sets are used for droplet manipulations. Each electrode set consists of two interdigitated finger electrodes, one for signal and the other for ground. Both the finger width and spacing are 50 μm. A non-uniform electric field is generated between the fingers and pulls the three phase contact lines along the electrode fingers. Initially, a large droplet is placed on the reservoir, from which small droplets are created. During experiments, the reservoir droplet stays on the reservoir electrode set while the small droplets are generated, split, transported, and merged by the digital small electrode sets. In order to make droplets transiting smoothly between adjacent electrode sets, interlocking electrode fingers (150 μm long and 50 μm wide with identical spacing) are adopted.

The soda lime glass wafer for the substrate was purchased from UniversityWafer Inc., USA. The electrodes were patterned by standard photolithography. 5-nm Cr and 200-nm Ag layers were deposited by E-beam evaporation, followed by the lift-off process. To avoid any electrochemical reaction between the fluids and the electrodes, a 2-μm heavy Parylene C layer was deposited by a chemical vapor deposition (CVD) system (PDS 2010, Specialty Coating System). To increase the initial contact angles of droplets, the surface was treated with Teflon-AF (DuPont, USA) by dip coating and drying on a hotplate (55 ^{o}C, 10 min). Before this dip coating, the Teflon-

AF solution was diluted with Perfluoro-compound FC-40 (Sigma-Aldrich, USA) solvent to reach a 1% volume concentration.

2.2.2 Experimental setup

In this experiment, alternating current (AC) voltages were supplied to drive the droplets, which allow for deeper penetration of electric field into the liquids than DC voltage. A function generator (33220A, Agilent) generated a sinusoidal signal, which was amplified by an amplifier (PZD 700, Trek) and transmitted to the circuit. An oscilloscope (199C, Fluke) measured the output, up to several hundred volts, during the experiment. Note the voltages in this paper denote root-mean-square values. The real-time videos were recorded by a charge-coupled device (CCD) camera (CV S3200, JAI) paired with a microscope. The contact angles are measured by the Contact Angle plug-in in ImageJ software.

The testing fluid was propylene carbonate (Sigma-Aldrich, USA), a common, nontoxic solvent with low volatility (boiling point: 242 ^{o}C) and viscosity (0.0025 kg/(m-s)). The surface tension of propylene carbonate is 42 mN/m. As shown in Equation (6), the large permittivity of propylene carbonate ($\varepsilon = 65\,\varepsilon_0$) increases the L-DEP force. To broaden the application scope of the current dielectric operations, DI (deionized) water with and without surfactant (TWEEN®20, Sigma-Aldrich) were also tested. The surfactant was added to DI water to obtain a 1% (vol/vol) solution and mixed thoroughly to reduce the surface tension of the DI water.

2.3 RESULTS AND DISCUSSION

2.3.1 Droplet spreading

In the experiment, the L-DEP force is desired to be as large as possible. The force is sensitive to the frequency of voltage applied to propylene carbonate as shown in Figure 12. The contact angle change ($\Delta\theta$) is a good indicator of the L-DEP force. The contact angle at 0 V is 87.6^o. At a fixed voltage (175 V), as the frequency increases from 1 kHz to 10 kHz, $\Delta\theta$ increases from 16.2^o to 31.0^o. In the range of 20 kHz to 100 kHz, $\Delta\theta$ decreases to 14.0^o gradually. The optimal frequency occurs at 20 kHz as it induces the greatest contact angle change ($\Delta\theta$ = 32.7^o), meaning the largest L-DEP force is exerted on the droplet to cause spreading. Based on these results, 20 kHz was selected as the frequency for subsequent experiments of droplet manipulations using propylene carbonate.

To see how the magnitude of voltage influences the L-DEP force, and accordingly changes the contact angle, a set of experiments are carried out by changing the voltage. Figure 13 shows that with increasing the voltage, the contact angle decreases from 87.6^o (0 V) to 0^o (236 V). The relation between the contact angle change and the voltage can be predicted by the model[73]:

$$\cos\theta\,(\mathrm{V}) = \cos\theta_0 + (1 - \cos\theta_0)\left(\frac{V}{V_{Th}}\right)^2 \tag{7}$$

where θ_0 is the contact angle at V = 0 V and V_{Th} is the threshold voltage where the contact angle becomes 0^o, *i.e.*, complete wetting. The insets of Figure 13 show that the profile of the droplet deforms from a half circle, to a circular segment, and to a nearly flat shape at 0 V, 180 V and 236 V, respectively. As the voltage is further elevated, the flat film of the droplet becomes thinner due to the spreading of the droplet across the interdigitated fingers to increase the contact area. This

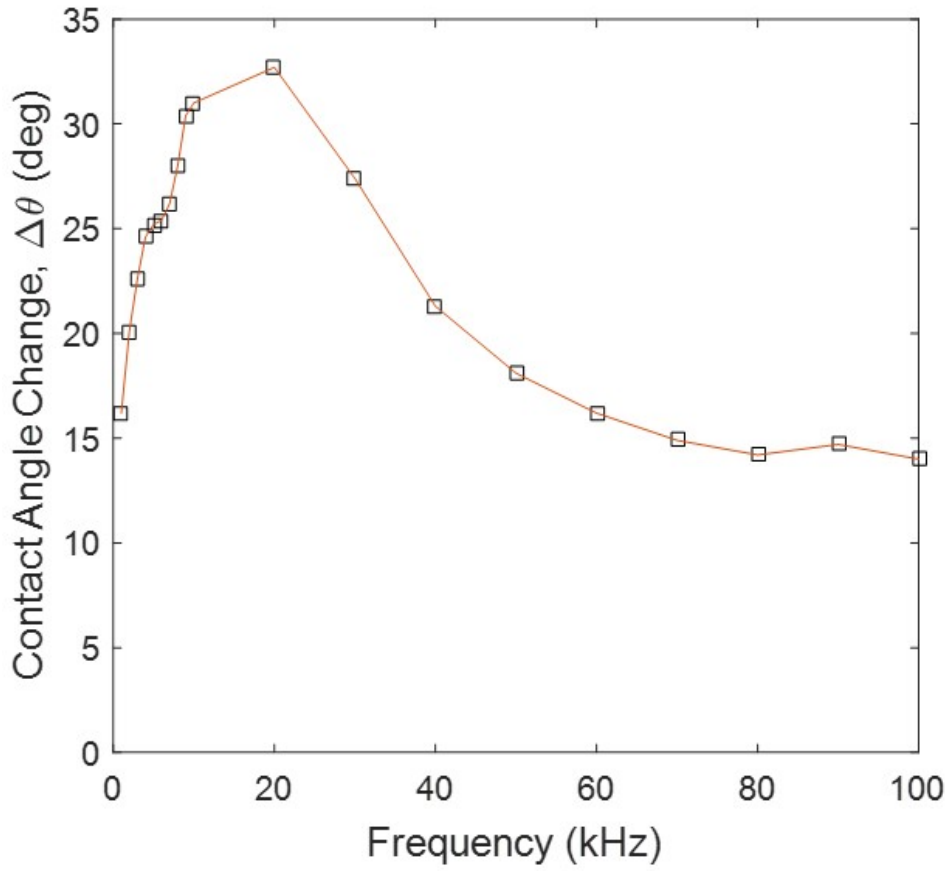

Figure 12. The effect of frequency on contact angle change of propylene carbonate. The contact angle at 0 V is 87.6º. The maximum change (32.7º) occurs at 20 kHz. The magnitude of voltage is set at 175 V.

phenomenon is also portrayed in Figure 14. A droplet (~1.5 µL) is placed at the center of the reservoir, after which the voltages of 180 V, 220 V, 240 V, 280 V, 320 V and 360 V are applied. In Figure 14(b) and (c), dielectrowetting elongates the droplet along the finger electrodes, while no change occurs in the perpendicular direction. Liquid is laterally bounded by the electrode edges and longitudinally pulled along the electrodes, as reported.[70] The contact angle decreases in the longitudinal view, while it remains nearly constant in the transverse view. When the voltage increases to 240 V, as shown in Figure 14(d), complete wetting occurs. The droplet spreads longitudinally to the left and right boundaries of the electrode pad and transversely crosses the

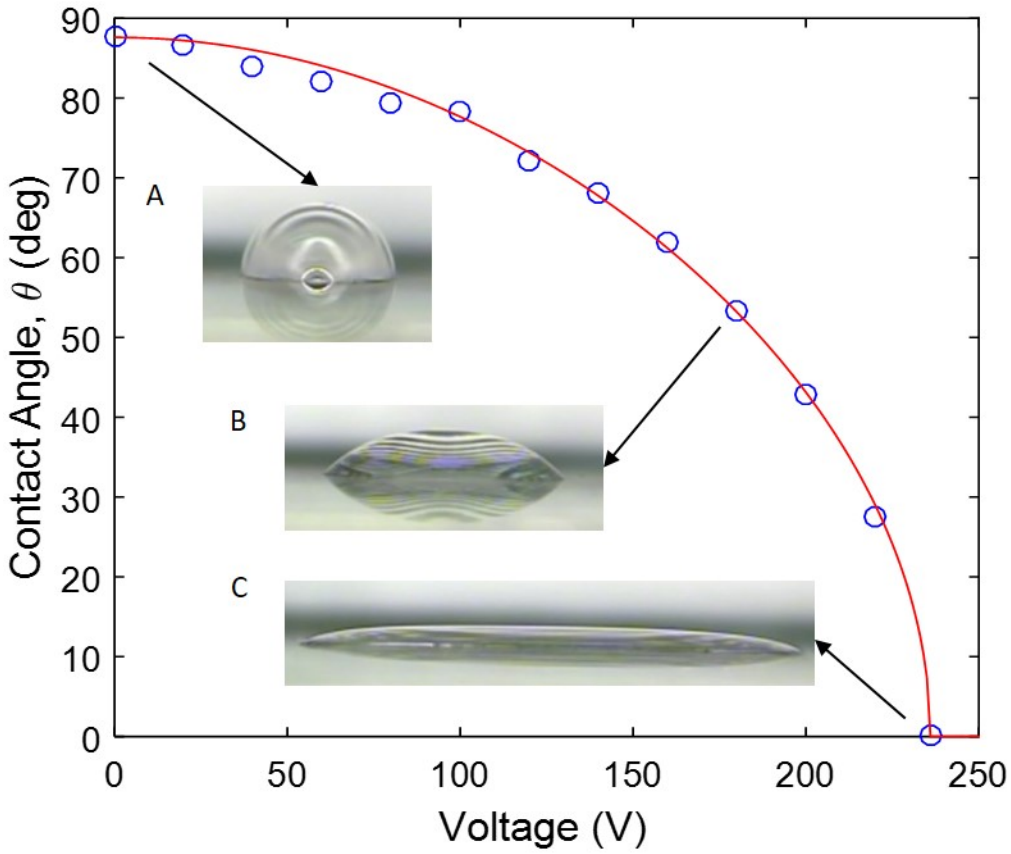

Figure 13. The effect of voltage on contact angle of propylene carbonate. The solid line from equation (1) fits the data points well. The inserts show the side views of droplet at (A) 0 V, (B) 180 V and (C) 236 V. The complete wetting is achieved at 236 V, where the top surface is flat, rather than arc. The frequency of voltages is 20 kHz.

fingers. The top surface of the droplet is flat and the contact angle is 0o when the voltage exceeds 236 V. Figures 14(e)-(g) show the spreading is further enhanced as the voltage is increased. The stronger DEP force broadens the contact area and makes the droplet lightner. Finally, in Figure 14(h) the droplet returns to the hemispherical shape after turning off the power, indicating the reversibility of dielectrowetting. Compared to EWOD using conductive liquids, dielectrowetting with dielectric liquids can stand up to much higher voltages of high frequency. The dielectric droplet has a wider range of contact angle change, even reaching complete wetting, which is almost

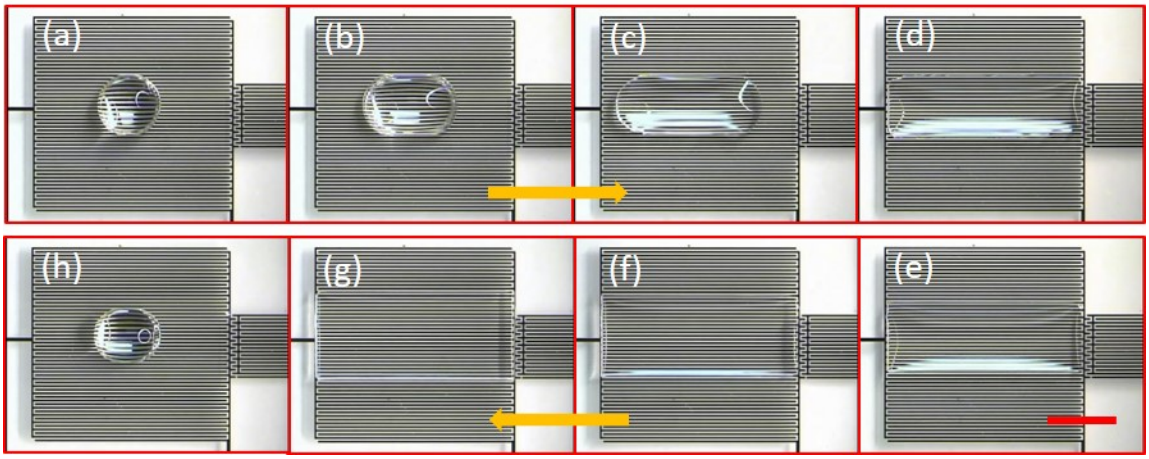

Figure 14. Top views of a droplet (~ 1.5 μL) spreading by dielectrowetting. (a)-(d) 0 V, 180 V, 220 V,240 V, (e)-(h) 280 V, 320 V, 360 V and back to 0 V. Starting at 240 V, complete wetting is achieved. Yellow arrows indicate the sequences of voltages. The frequency of voltages is 20 kHz. The scale bar is 2 mm

impossible for EWOD because of contact angle saturation. The strong DEP force renders the dielectric droplet to deform dramatically.

To further investigate the spreading behavior of dielectric fluids, experiments combining the reservoir and digital electrode pads were conducted. Figure 15(A) depicts the practicability of the device for droplet spreading. A large droplet (~65 μL) nearly covers the whole reservoir initially. All the electrode pads are connected to the same voltage source. The frequency is maintained at 20 kHz while the voltage is increased to spread the droplet to the small electrode pads. Figure 15(A2)-(A6) shows that the droplet can reach digital electrode pads No. 1, 2, 3, 4, and 6. The fluid exactly fills the footprints of the digital pads when spreading, except for No.1. Figure 15(B) summarizes the No. of electrode pads up to which the liquid front can arrive as a function of the voltage. At least 160 V is required for the droplet to spread to No.1 pad. When the voltage exceeds 353 V, the droplet can cover the entire area of electrodes. Increasing the voltage elevates the L-DEP force to drive the liquid front to a farther distance. Interestingly, reaching and

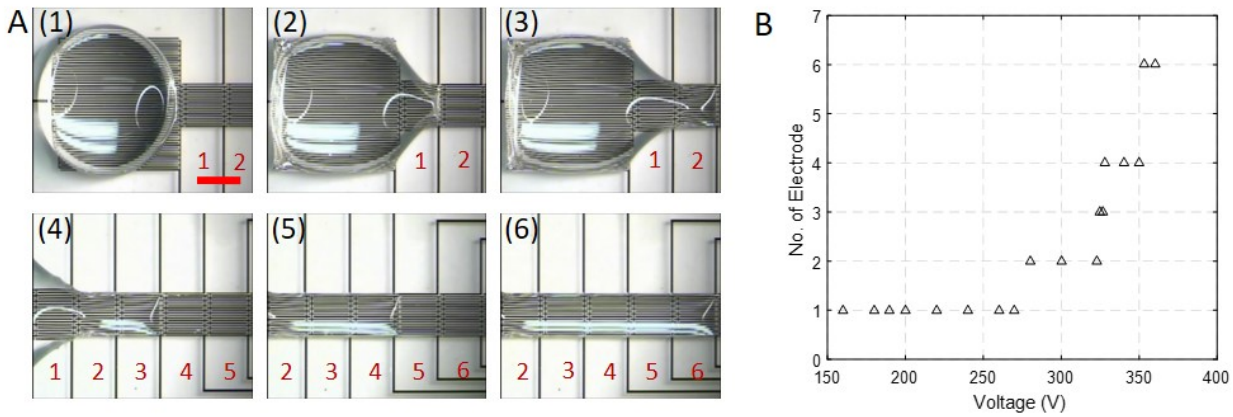

Figure 15. Droplet stretching along electrodes. (A) A large droplet (~ 65 μL) spreading from reservoir to digital electrode pads at different voltages (20 kHz): (1) 100 V, stay on reservoir; (2) 260 V, No. 1 electrode pad; (3) 280 V, No. 2 electrode pad; (4) 325 V, No. 3 electrode pad; (5) 340 V, No. 4 electrode pad; (6) 355 V, No. 6 electrode pad. Both the reservoir and the six digital electrode pads are energized simultaneously. The digital electrode pads are marked with numbers. (B) No. of electrode pad fluid can reach versus voltage applied. The scale bar is 2 mm.

staying on pad 5 was not observed for liquid front in this experiment. In fact, the voltage tolerance for each electrode pad is not constant. The interlocking patterns between two pads help to reduce the energy barriers at the boundaries and then facilitate the transition. When the voltage is high enough, the droplet can easily cross the boundaries of the digital electrode pads.

2.3.2 Droplet generating

Droplet generating is a fundamental operation for digital microfluidic manipulations. Given an excessive volume of testing fluid sample, it is indispensable to first extract a small metered amount from it for downstream analysis. The present device meets this demand by utilizing dielectrowetting, as shown in Figure 16. Based on the droplet spreading described above, droplet generation is accomplished at the voltage of 360 V (20 kHz). Figure 16(A) shows the process in 4

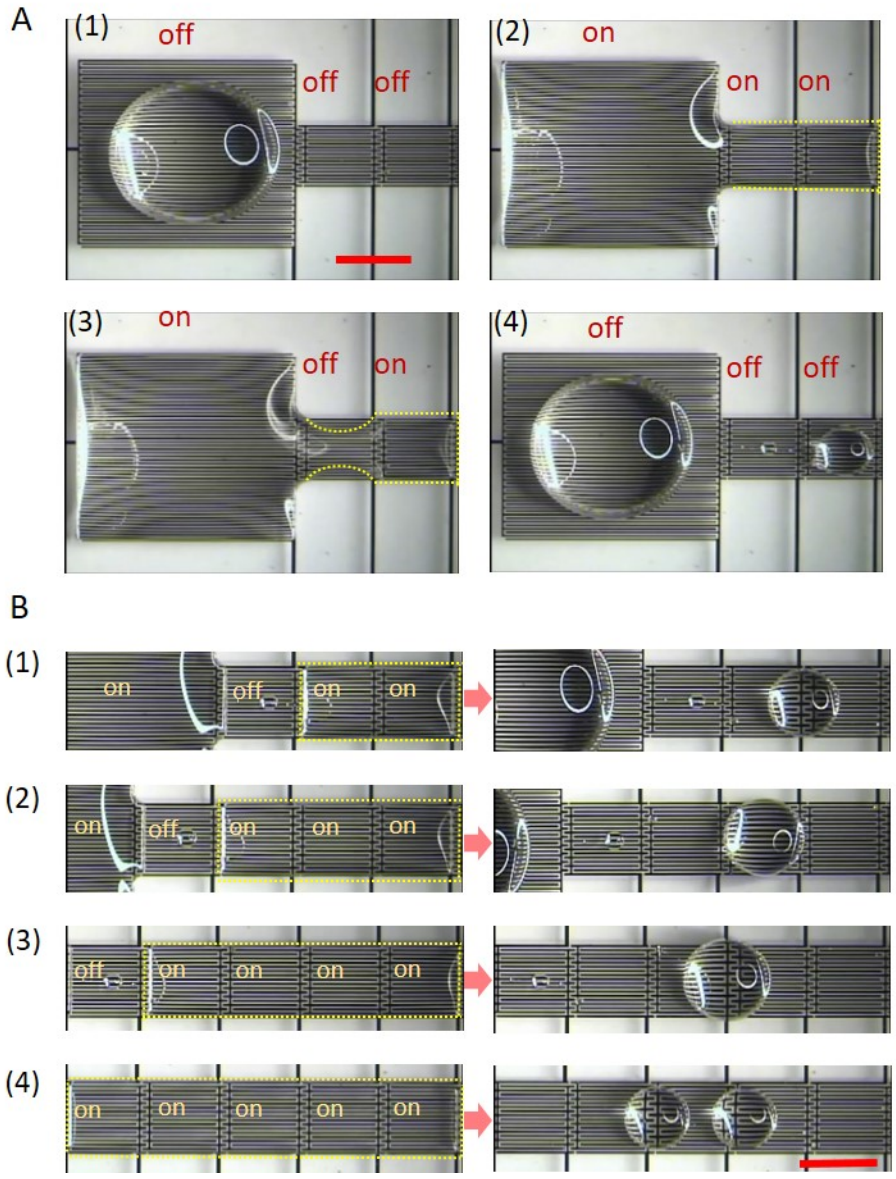

Figure 16. Droplet generating by dielectrowetting. (A) Four steps of droplet generating: (A1) place a droplet (~ 22 μL) of propylene carbonate on the reservoir pad; (A2) turn on the three electrode pads (360 V, 20 kHz) to spread the fluid on them; (A3) turn off the middle one to neck and cut the droplet; (A4) turn off all the pads to attain the small droplet (~0.9 μL) on the right. (B) Generating droplets by activating different numbers of electrode pads (after powering off the first one) at same conditions: (B1) 1.6 μL, 2 pads; (B2) 2.6 μL, 3 pads; (B3) 3.2 μL, 4 pads; (B4) two 1.5 μL droplets, 5 pads. Yellow dashed lines are used to highlight the boundaries of fluid. Scale bars are 2 mm.

steps: first, a droplet (~22 µL) as the source, or mother droplet, is dispensed on the reservoir electrode pad with all pads off; secondly, the large pad and digital pads 1 and 2 are turned on to spread the droplet over the entire activated area; thirdly, digital pad 1 is turned off to neck and cut the droplet; finally, all the pads are turned off to attain a small droplet (~0.9 µL) on digital pad 2. When powering off pad 1, the liquid on it contracts to a neck due to surface tension, and eventually narrows to separate the small daughter droplet from the source droplet. The cutting is achieved almost immediately after digital pad 1 is turned off. In Figure 16(B), using similar principles, different droplet volumes (~1.6 µL, 2.6 µL and 3.2 µL) are generated by changing the numbers of activated pads from 2 to 3 and 4. Energizing more pads increases the volume of the created droplet. Meanwhile, after activating 5 pads, two individual droplets are formed because of the hydrodynamic instability of the long liquid thread. For the same reason, tiny satellite droplets are left on digital pad 1 after each trial, as observed in other cutting experiments.[150] All the generated droplets deform rapidly from a light film to a spherical cap after powering off the electrodes to reach the minimum energy equilibrium. In addition, the created droplets are located in the middle of the activated area.

2.3.3 Droplet splitting, transporting and merging

More droplet manipulations are achieved on the present digital microfluidics, including splitting, transporting, and merging. These operations are carried out under the same conditions: 360 V, 20 kHz. In Figure 17 (a)-(d), a single droplet (~2.3 µL) is split into two equal smaller droplets by dielectrowetting. The mother droplet is stretched to a film when activating the three electrode pads in the middle of the pad array. By powering off the middle pad, two daughter droplets are separated from each other. The remaining electrode pads are turned off to complete the splitting process. The

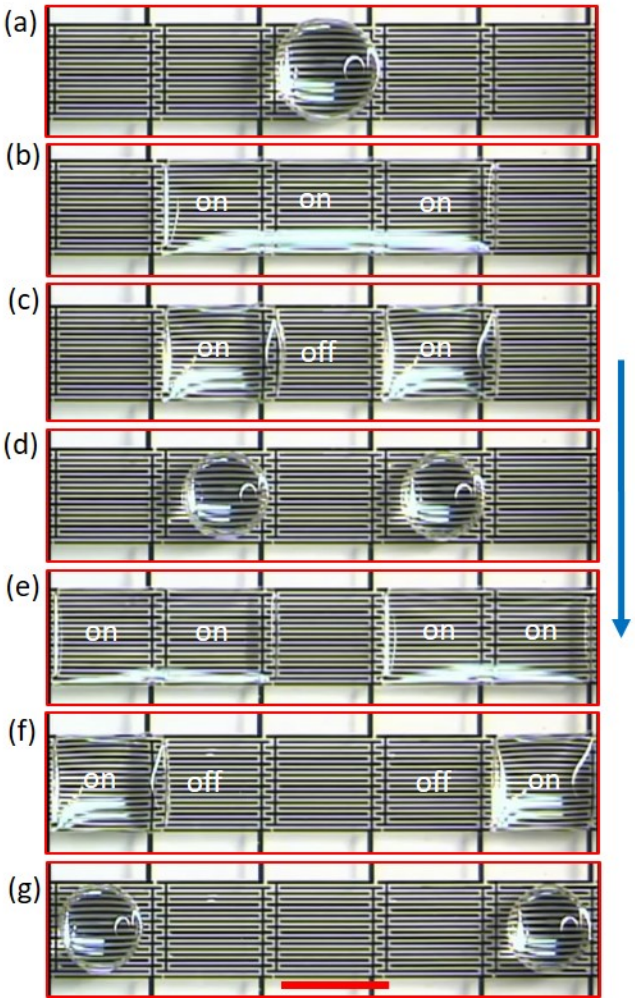

Figure 17. Droplet splitting and transporting (360 V, 20 kHz). (a)-(d) ~2.3 μL droplet split by powering on three pads and then turning off the middle one. (e)-(g) droplet transported by powering on two pads and then turning off one. The blue arrow shows the time sequence. Scale bar is 2 mm.

present splitting procedure is different from that in EWOD. Most importantly, the present splitting does not need the top plate that is in contact with the mother droplet. Namely, splitting can be done in an open environment while splitting by EWOD works only with pancake-shaped droplets (the mother droplet should be sandwiched between two plates within a critical gap as studied in detail).[60] In addition, for EWOD, the mother droplet should be initially centred on the electrode where no electric potential is applied. Then it is pulled by the two adjacent electrode pads by

changing the contact angles, resulting in neck formation and separation. In this case, the initial position of the mother droplet is critically important to keep the force balance during splitting and to evenly split. Otherwise, the mother droplet would split into daughter droplets with uneven volumes or simply move to the adjacent electrode pad without splitting. In EWOD, another precondition for successful splitting is that the droplet footprint should be overlapped with some portion of the adjacent electrodes to stretch the mother droplet. Such requirements make the operation delicate and laborious in addition to the complicated fabrication and packaging. More importantly, the two-plate configuration limits the volume of the working fluid due to the small gap between the plates. For the present dielectrowetting device, these issues do not exist when complete wetting is applied to a single mother droplet. The mother droplet footprint does not need to be in contact with the adjacent electrodes. The intermediately formed light film is spontaneously split by surface tension in an open space after turning off the middle electrode pad.

Similarly, the split droplets can be transported to other positions, as shown in Figure 17(d)-(g). First, two electrodes are turned on so that the droplet spreads over both (one is the electrode on which the droplet currently sits and the other is the electrode adjacent to where the drop currently sits but where it will move towards). Next, the electrode on which the droplet initially sits is powered off while the adjacent electrode remains activated. The entire volume of the droplet moves to the adjacent electrode. All the electrodes are powered off to complete the droplet transportation.

In EWOD, it is very difficult to split one droplet into more than two new droplets due to the limitation explained above. However, the present dielectrowetting method overcomes this difficulty, as depicted in Figure 18 (a)-(d). One droplet (~3.4 μL) covers the entire area of five electrode pads when activating them at the same time. The multiple splitting is realized by turning

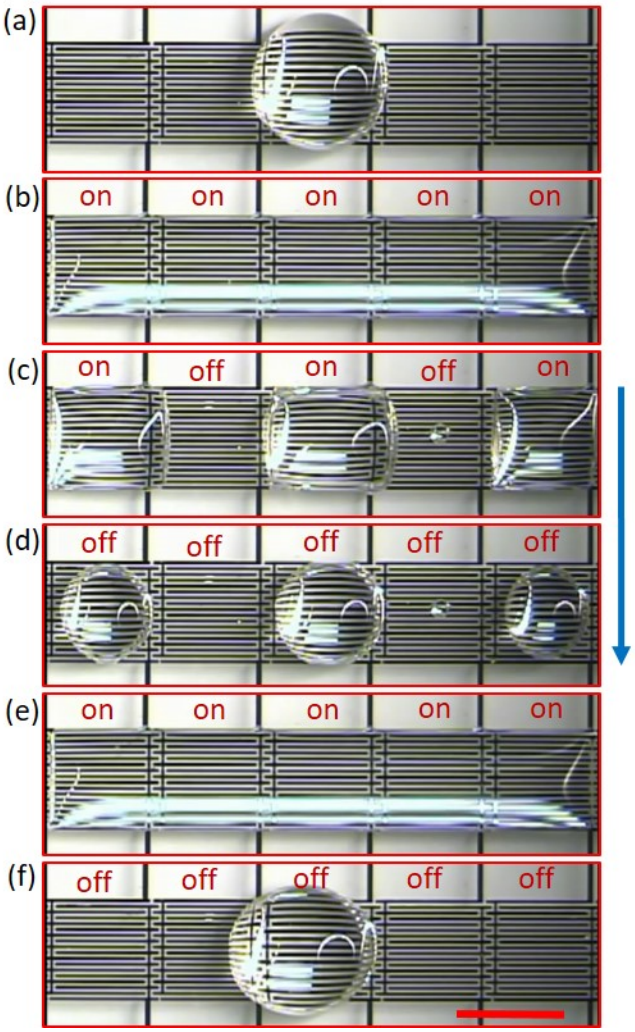

Figure 18. Multiple splitting and merging (360 V, 20 kHz). (a)-(d) ~3.4 μL droplet is multi-split by powering on five pads and then turning off the alternating pads. (e)-(f) three droplets are merged by powering on 5 pads and then turning them off. The blue arrow shows the time sequence. Scale bar is 2 mm.

off the alternating electrode pads, followed by turning off the remaining pads. The three discrete droplets after splitting can be reunited by powering on five pads and then turning them off, as shown in Figure 18(e) and (f). This demonstrates the ability to merge several droplets to a single droplet by one-shot activation.

2.3.4 Manipulations for aqueous liquids

In theory, the liquid used for EWOD should be conductive (aqueous) and performs like dielectric fluid if the applied frequency is high enough.[70, 155] This indicates that aqueous liquid can be actuated by the present electrode design. The co-planar electrodes were previously used to actuate aqueous droplets but did not complete the droplet operations (especially droplet splitting in an open environment).[46, 147] In this study, in addition to the propylene carbonate, the aqueous liquids, i.e., DI water with and without surfactant, were also tested for droplet splitting and transporting using the present dielectrowetting system. All experiments in this section are performed at high frequency (55 kHz). Figure 19 shows the dependence of the contact angle on the voltage applied for the two liquids. The contact angle of DI water drops from 120^o (0 V) to 61^o (340 V) and then reaches contact angle saturation; the change is 59^o, while the typical change for EWOD is only 40^o. Upon addition of 1% surfactant, the contact angle changes from 80^o (0 V) to 36^o (340 V) with 44^o span. The results illustrate that the interdigitated electrode structure is more effective to change the contact angles of aqueous liquids than solid electrodes in EWOD. Similar to the dielectric liquid case, the contact angles were measured from the longitudinal view of droplets. To test whether the L-DEP forces for aqueous liquids are applicable for droplet manipulations in an open space, additional experiments were carried out. Figure 20 shows successful transporting and splitting of DI water droplets. Adding 1% surfactant produces the nearly same results (images not shown). Since complete wetting is not achieved for aqueous liquids, the mechanisms of moving and cutting are far from the dielectric fluid cases but more similar to those in EWOD. In Figure 20(A), the droplet (~10.8 μL) needs to contact part of the adjacent electrode pad. By applying 340 V to the adjacent pad only, the droplet is transported to the right. Figure 20(B) shows the process of water droplet cutting. The droplet (~7.2 μL) is in

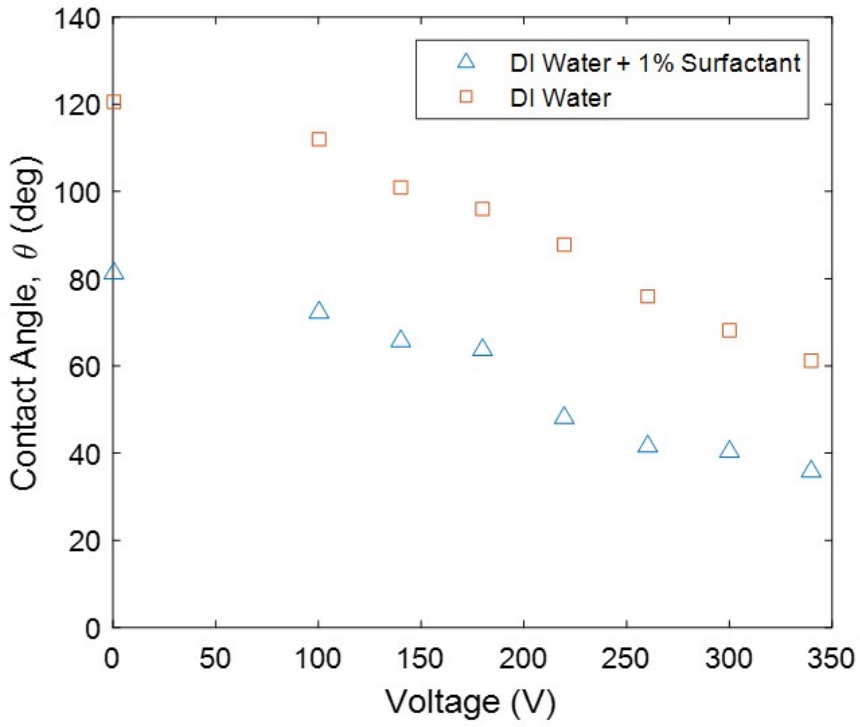

Figure 19. Contact angle versus voltage for DI water with and without surfactant.

contact with two adjacent pads which are then activated by providing voltage (340 V) to them simultaneously. Necking appears in the middle and eventually breaks to produce two small droplets. It is found that increasing the longitudinal length of the electrodes (1.8 x 2.7 mm, with 2 mm spacing in the middle section) facilitates the splitting process by further stretching the droplet. Again note that there is no top plate; the droplet is on a single bottom plate in an open environment. Finally, volume effects on splitting results were investigated, as depicted in Figure 20(C). At 340 V (55 kHz), the three fluids (propylene carbonate, DI water with and without surfactant) show that threshold volumes exist for splitting. If the volumes exceed the critical values, the droplets are merely elongated and do not split. The threshold volumes are about 4.5 µL, 5.8 µL, and 8.2 µL for DI water with surfactant, propylene carbonate, and DI water without surfactant, respectively. The

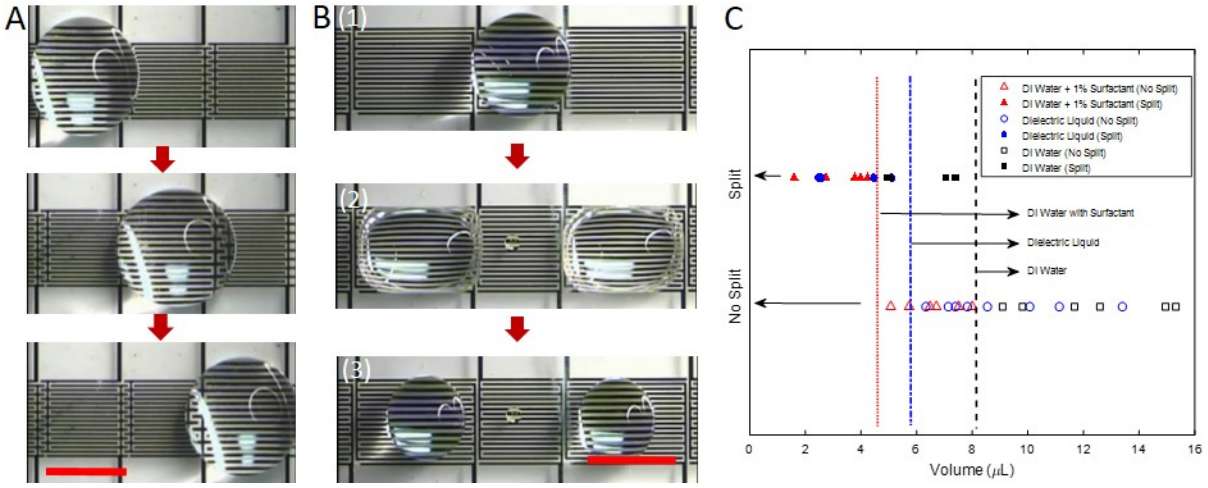

Figure 20. DI water droplet manipulations by dielectrowetting. (A) Water droplet (~10.8 μL) transporting from left to right. (B) water droplet (~7.2 μL) splitting sequential procedure. (C) Volume effect on splitting for three liquids: propylene carbonate, DI water with and without surfactant. The three broken lines from left to right show the threshold volumes where splitting occurs for different liquids. All the manipulations are carried out at 340 V, 55 kHz without top cover plate. Scale bars are 2 mm.

threshold volumes seem to depend on the initial contact angles, contact angle changes of the fluids, and surface tension but a more in-depth study is required to understand this phenomenon better.

In the current study, all droplet operations are performed in the air surroundings. It would be a next step to study that the present droplet operations are applied to the droplets immersed in a second liquid (oil), as droplet spreading in the second liquid has been studied previously.[72] Such liquid environments are useful for many digital microfluidic applications. Another interesting topic would be to develop control schemes and systems to manipulate a large number of droplets on a 2-D plane. Like EWOD [42-45, 156-158], the present method can be extended to a variety of applications.

2.4 CONCLUSION

This paper describes a novel digital microfluidic circuit based on dielectrowetting. In order to manipulate (create, transport, split, and merge) droplets, an individually addressable interdigitated electrode array is designed to generate non-uniform electric fields, which is essential to generate strong L-DEP forces. The L-DEP force is a driving force in dielectrowetting that changes the contact angle even down to 0o at a high voltage. This dielectrowetting actuation is utilized for droplet generating, splitting, transporting, and merging. First, the contact angle change, $\Delta\theta$, versus voltage and frequency was investigated for dielectric fluid (propylene carbonate). $\Delta\theta$ responds most notably at 20 kHz for propylene carbonate, which is chosen as the operating frequency for the following experiments. The contact angle as a function of voltage is depicted from 87.6^{o} to 0^{o}, and is in good agreement with the given model. Complete wetting occurs when the voltage is elevated to more than 236 V. A single droplet is stretched along the electrodes, without crossing the finger electrode edges. Over the threshold voltage, it starts to spread laterally to the electrodes, resulting in a light film. The DEP force is large enough to drive the droplet to cross the boundaries between two electrode pads.

Droplet generation with several different volumes is achieved by activating multiple electrodes. The procedure is to pull the liquid from the reservoir to the linear array of digital electrode pads, followed by powering off the first electrode adjacent the reservoir. The surface tension contracts the droplet to neck and eventually break it into a small droplet. Similarly, splitting and transporting are achieved by spreading and turning off the involved electrode pads. Splitting and merging of *multiple* droplets are achieved easily in the present device. To prove the above droplet operations with aqueous (conductive) fluid, DI water with and without surfactant are actuated by the same electrode design. The contact angle of water changes significantly more

(from 120^o to 61^o without surfactant and from 80^o to 36^o with surfactant), compared to the typical 40^o change for water without surfactant in the conventional EWOD. Transporting and splitting for both water fluids are realized. The initial droplet volume effect on splitting is also studied. It should be emphasized that all these droplet operations are achieved in an open environment without the top plate covered.

3.0 ANTI-BIOFOULING DIGITAL MICROFLUIDICS

Digital microfluidics owns many advantages compared to conventional channel-based microfluidics. First, it is highly flexible and reconfigurable. Secondly, no mechanical components are required, like pump, tube, valve or connector. Thirdly, cannel-based microfluidics is totally avoided. Despite of the above advantages, the applications of digital microfluidics are still not wide. The key problem is the biofouling, when the droplets are bio-solutions. For example, the protein droplet is very difficult to actuate, because the protein tends to adhere to the hydrophobic surface, rendering a large contact angle hysteresis. Currently, the most popular method to reduce the biofouling is to immerse the digital microfluidic device into silicone oil, where a light oil layer will separate the droplet and the solid hydrophobic surface to avoid direct contact. However, the drawbacks of such method are obvious: the device should be integrated with oil phase, complicating the structure and operation; the droplet is totally capsulated with oil, preventing the direct contact with air, which also weakens the advantage of digital microfluidics.

To solve the biofouling issue thoroughly, a more applicable and simple way is required. In this chapter, a novel method is reported to meet the demand of anti-biofouling on digital microfluidics. The fundamental principle of this method is adopting an anti-biofouling surface to add to the current device. The surface should be robust to avoid biofouling, including wide range of concentrations of bio-solutions, as well as working long time under actuating voltages. It turns out that the slippery liquid infused porous surface (SLIPS) is an ideal choice as the anti-biofouling

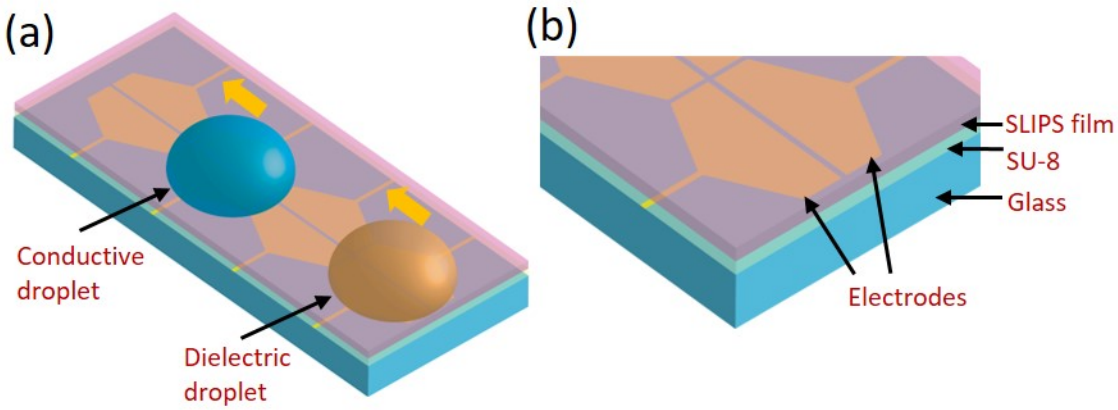

Figure 21. Schematic of experimental device. (a) an array of hexagonal electrode couples are fabricated on the substrate, as the transporting pathway of the droplets. Two kinds of droplets can be moved on the top surface of the device. The blue one denotes the conductive droplet, while the brown represents the dielectric droplet. The yellow arrows show the moving directions of the droplets, when sequentially powering on the first and the third electrode couples. (b) Zoomed view of the device. From the top to bottom: SLIPS film (4.2μm thick), SU-8 (2 μm thick), electrodes (10 nm Cr + 100 nm Au), and glass substrate. The gaps between each two electrodes are 50 μm.

surface. After integrating the surface with conventional digital microfluidic device, the droplet will be separated from the solid surface of the device. Instead, it directly contacts with SLIPS, or more specifically, the lubricating oil of SLIPS. The SLIPS is not a solid surface, but a liquid surface while keeping the solid structure by the porous film. It combines the advantage of liquid surface to overcome biofouling issue, and that of solid structure to hold the liquid in a uniform film, making it robust even under electrowetting force. In this chapter, the fabrication of the anti-biofouling digital microfluidic device will be introduced first, followed by the results and discussion, and the final part is conclusion.

3.1 EXPERIMENTAL

3.1.1 Device structure

Compared to conventional digital microfluidic device, the SLIPS film is added to the top surface as the anti-biofouling component. As shown in Figure 1, an array of hexagonal electrode couples are fabricated on the glass substrate. When it works, the voltage can be applied to different couples to selectively actuate the droplet on the top surface. Such voltage can be controlled by computer program, making it highly reconfigurable. The array of electrodes can be treated as the channel of conventional microfluidics, since it determines the transporting pathway of the droplets. Two kinds of droplets can be actuated on this device, either conductive or dielectric. The working principles are electrowetting for conductive droplet and liquid dielectrophoresis for nonconductive droplet. The blue droplet denotes the conductive droplet, while the brown represents the dielectric one. It means the platform is a versatile device for real applications, with wide range of droplets can be transported. From the zoomed view of Figure 21, different layers are shown clearly. The electrodes are fabricated on the glass substrate. Each two electrode couples are independent, as well as the two electrodes in one couple. The narrow gaps are all 50 μm, and the length of the electrode is 1.5 mm. The SU-8 layer is coated to the substrate as the dielectric layer for electrowetting. Finally, the SLIPS film is attached to the top surface to prevent biofouling.

3.1.2 Fabrication process

As shown in Figure 22-24, a clean glass wafer is prepared first. The metal layers (10 nm Cr and 100 nm Au) are deposited by electron-beam evaporation. The electrode pattern is fabricated by

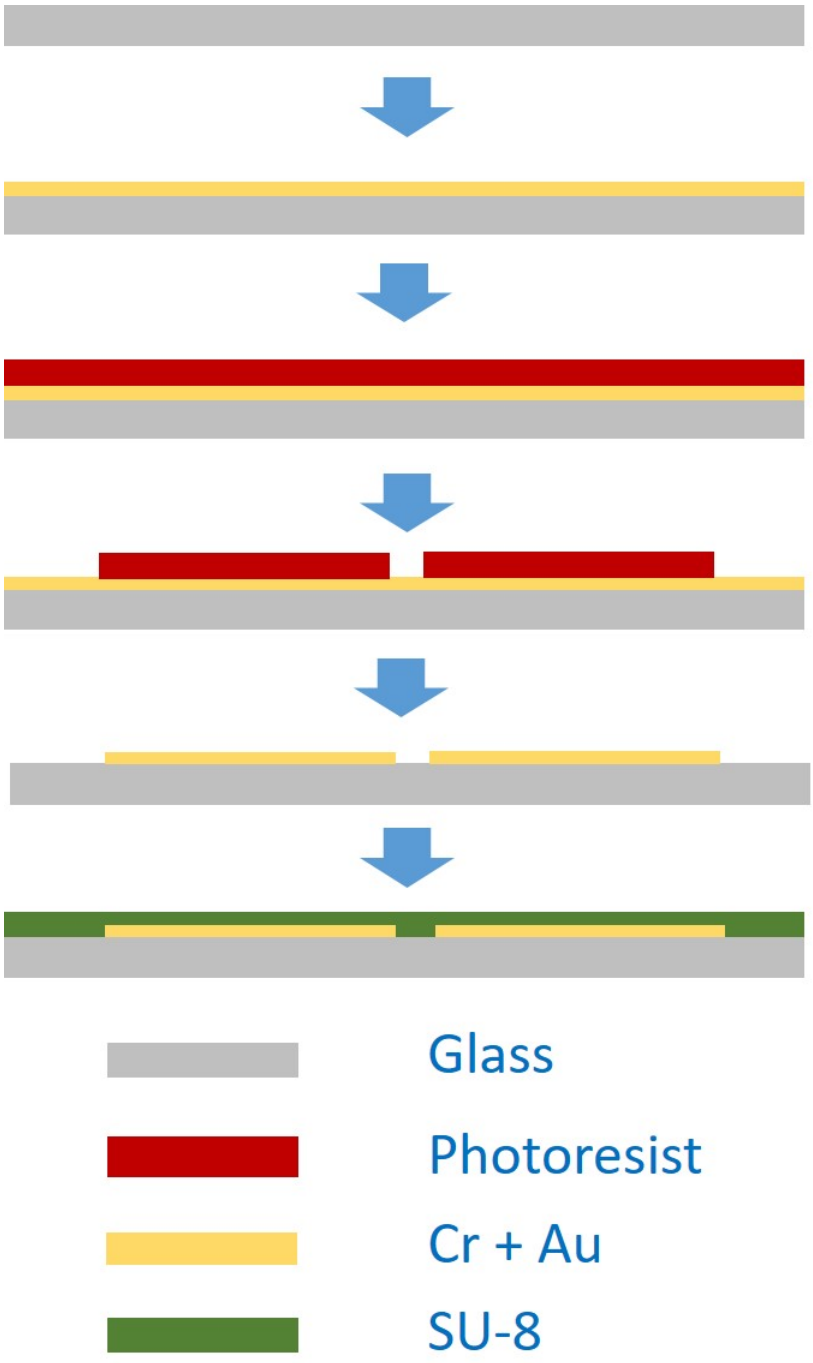

Figure 22. Fabrication process of the digital microfluidic device. The AZ 4210 photoresist is spin coated on the glass wafer. The photoresist is patterned by conventional photolithography and development. After thorough drying, the Cr and Au thin films are deposited by electron-beam evaporation. The metal pattern is achieved by lift-off process, which is covered by spin coating a thin SU-8 film.

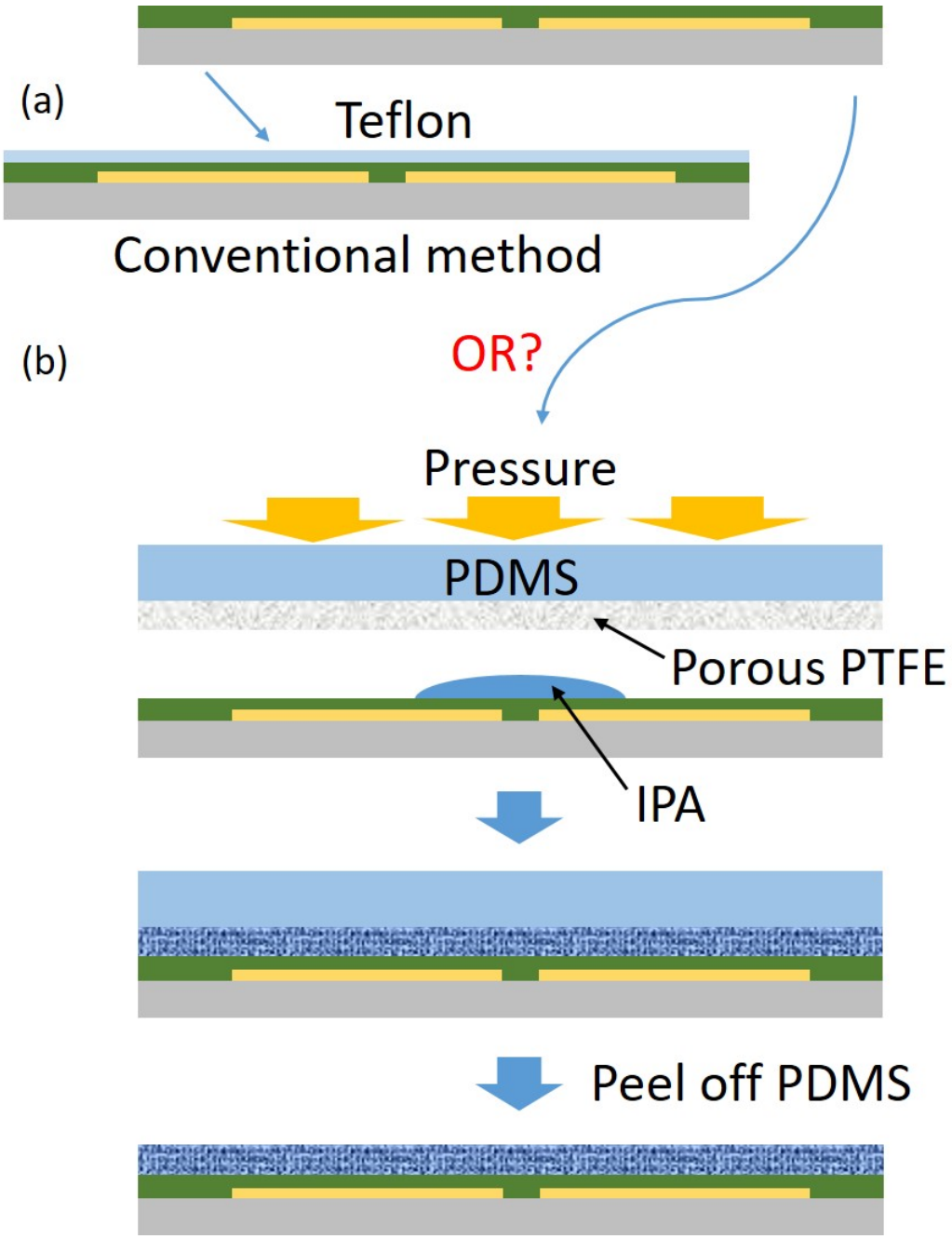

Figure 23. Continuous fabrication process. (a) Conventional digital microfluidic device with a thin hydrophobic Teflon layer coated on the surface. (b) Steps to fabricate the novel device with SLIPS on the top surface. The porous PTFE film (4.2 μm) is attached on the thin PDMS slab, followed by pressing them to the SU-8 surface. To keep the uniformity and improve the adhesion between PTFE and SU-8, a droplet of IPA is placed on the SU-8 first, which will saturate the porous film by capillarity. After that, peel off PDMS, leaving the PTFE film on the device.

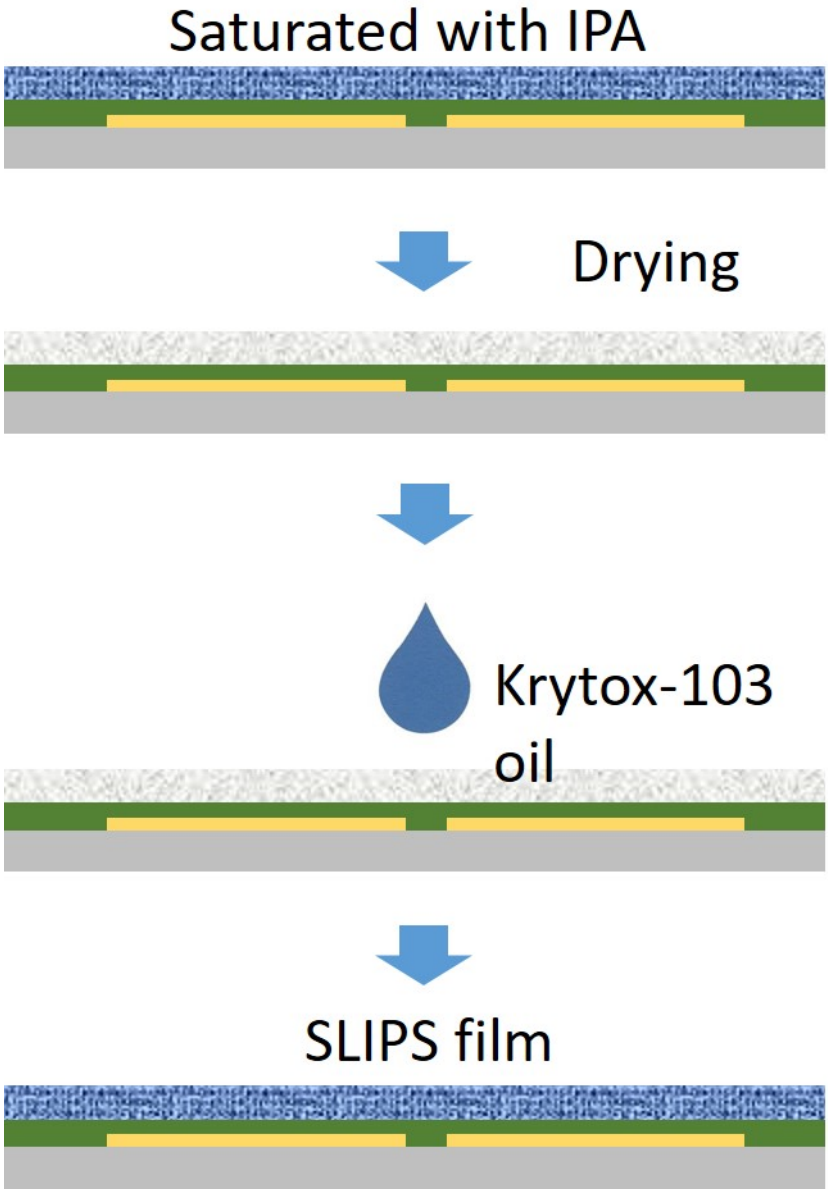

Figure 24. Final fabrication process. The saturated PTFE film dries in several seconds, due to the fast evaporation of IPA. Finally, the SLIPS is achieved by dropping Krytox-103 oil to the porous surface, and removing the excess liquid by gravity.

photoresist first through conventional photolithography, followed by wet etching, using Au etchant and Cr etchant in sequence. After that, a 2-μm SU-8 layer is spin coated at 3000 rpm, and exposed to ultraviolet light to strengthen the layer. Next, two options are applied to the SU-8 surface. One

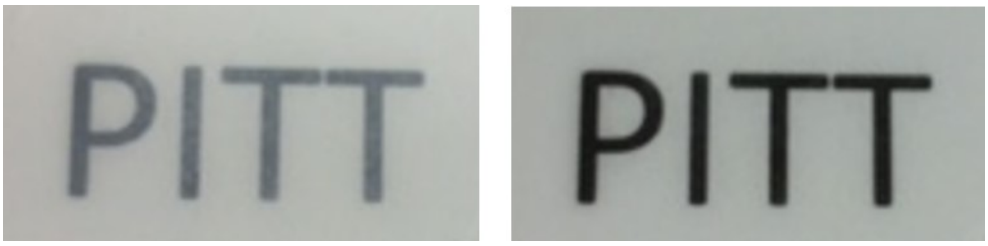

Figure 25. Change of the opacity of the PTFE film. The film is attached onto the plastic surface with black word. Before infusing Krytox-103 oil, the word is blurred, since the nanoporous film reflect light diffusively. In comparison, after infusing oil, the layer becomes transparent, showing the word clearly.

is conventional method by dip coating a light Teflon layer onto the surface, which will serve as the reference sample. The second choice is adding SLIPS to SU-8 surface. The porous PTFE film (4.2 μm heavy) is attached on a light PDMS slab, followed by pressing them to the SU-8 surface. To keep the uniformity and improve the adhesion between PTFE and SU-8, a droplet of IPA is placed on the SU-8 first, which will infuse the porous film by strong capillary force. After that, the PDMS slab is peeled off, leaving the PTFE film on the device. Several seconds later, the saturated PTFE film dries at room temperature. Finally, the SLIPS is achieved by dropping Krytox-103 oil to the porous surface, and removing the excess liquid by gravity for several hours.

Figure 25 shows the difference before and after dropping lubricant oil. Before infusing the oil, the porous light film shows semi-transparent white, blurring the black word “PITT” underneath. However, after infusing the oil, it becomes transparent because of the similar refractive indexes of the oil and film.

3.2 RESULTS AND DISCUSSION

3.2.1 Different types of droplets transporting

The lubricating oil is immiscible to aqueous and hydrocarbon liquids, compatible with a variety of working liquids. In addition, the electrodes can actuate both conductive and dielectric droplets. The above conditions determine the wide applications of the digital microfluidic device, not only anti-biofouling performance.

In Figure 26, different conductive droplets are transported by sequentially powering on the electrode couples from right to left. Figure 26(a) shows the DI water transporting at 350 V. Figure 26(b) shows the 1 mg/mL protein solution transporting at 350 V. Figure 26 (c) shows the transporting of a highly conductive liquid, saline at 350 V. And Figure 26(d) shows the ionic liquid transporting at 275 V. All the working frequencies are 1 kHz in this chapter.

In Figure 27, some complex conductive droplets are transported. In Figure 27(a), the sheep blood can be transported at 300 V. Figure 27(b) shows the transporting of whole milk at 350 V. Figure 27(c) shows the DNA solution transporting at 350 V. Figure 27(d) shows the honey transporting at 450 V. This group shows the good performance of anti-biofouling on the device. All the solutions can be stuck to conventional surfaces easily, making it impossible to move them by electrowetting. However, due to the SLIPS, the adhesion forces between the surface and the complex liquids are small enough to be overcome by electrowetting forces.

In Figure 28, different dielectric droplets are transported by the electrode couples. Figure 8(a) shows the light crude oil can be transported at 250 V. Figure 28(b) and (c) show the transporting of propylene carbonate and IPA at 200 V. This group can be explained by the liquid

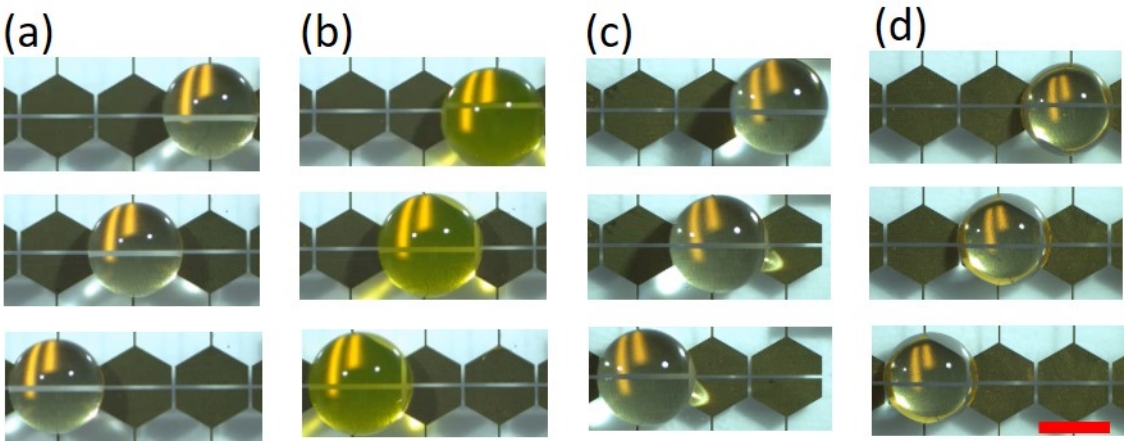

Figure 26. Transporting of conductive droplets. (a) DI water, 350 V. (b) 1 mg/mL protein solution, 350 V. (C) Saline, 350 V. (d) Butyltrimethylammonium (ionic liquid), 275 V. All signal frequencies are at 1 kHz. Scale bar: 1.5 mm.

dielectrophoresis, not electrowetting. As long as the dielectric constants are large enough, the droplets can be moved on the digital microfluidic device.

The mechanism of easy transporting on SLIPS is attributed to the low contact angle hysteresis. No matter what types of liquids are used, they can be moved with large enough eternal forces. As for this device, the forces are provided by applying voltage.

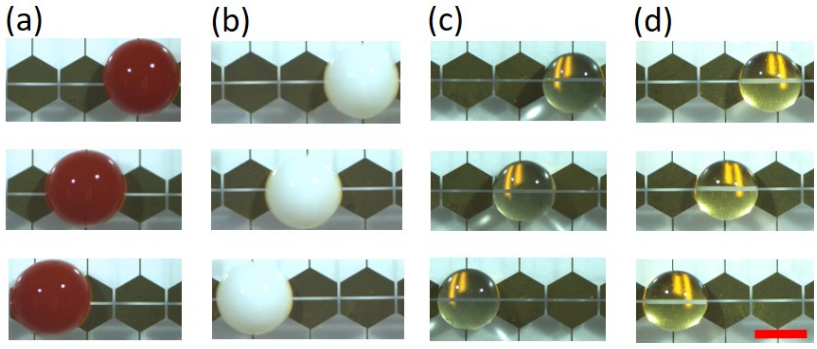

Figure 27. Transporting of complex fluids. (a) Sheep blood, 300 V. (b) Whole milk, 350 V. (C) DNA solution, 350 V. (d) Honey, 450 V. All signal frequencies are at 1 kHz. Scale bar: 1.5 mm.

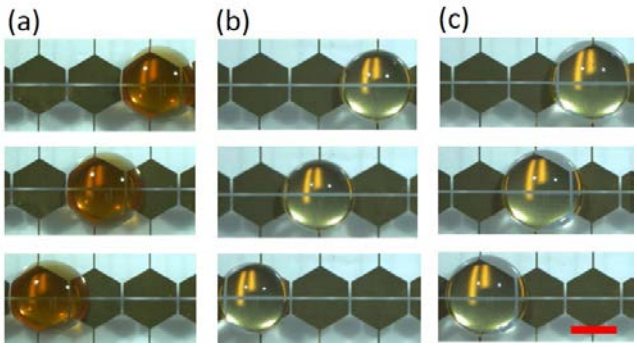

Figure 28. Transporting of dielectric fluids (a) Light crude oil, 250 V. (b) Propylene carbonate, 200 V. (C) IPA, 200V. All signal frequencies are at 1 kHz. Scale bar: 1.5 mm.

Figure 29 shows the contact angles of different liquids on the SLIPS film. From Figure 29(a) to (c), they are sheep blood, whole milk and honey, with contact angle 105.3^{o}, 96.4^{o} and 113.6^{o}, respectively. From Figure 29(d) to (f), they are IPA, propylene carbonate and light crude oil, with contact angle 59.8^{o}, 87.9^{o} and 65^{o}. Although the contact angles are different, the hysteresis for them are small, owing to the SLIPS.

To demonstrate the difference between electrowetting and liquid dielectrophoresis, the voltage is applied to the droplet and the electrode underneath the SU-8 layer. Figure 30 shows the

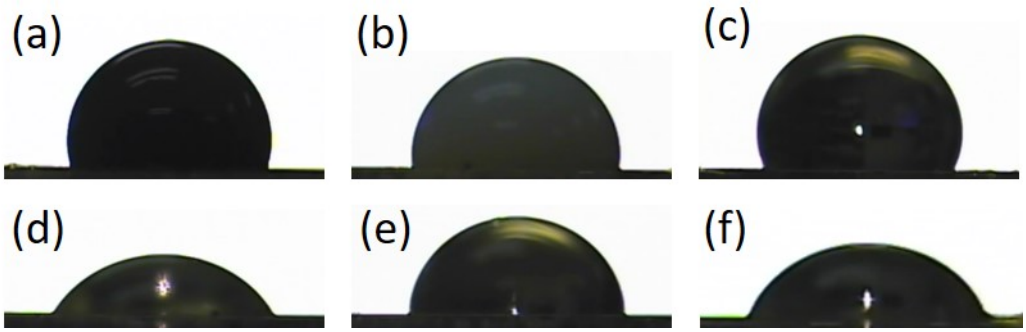

Figure 29. Contact angles for light crude oil and DI water on the SLIPS film. Thin crude oil: (a) 0 V, 64.7^{o}. (b) 175 V, 65.4^{o}. (c) 275 V, 64.8^{o}. DI water: (d) 0 V, 113^{o}. (e) 175 V, 90.8^{o}. (f) 275 V, 62.5^{o}.

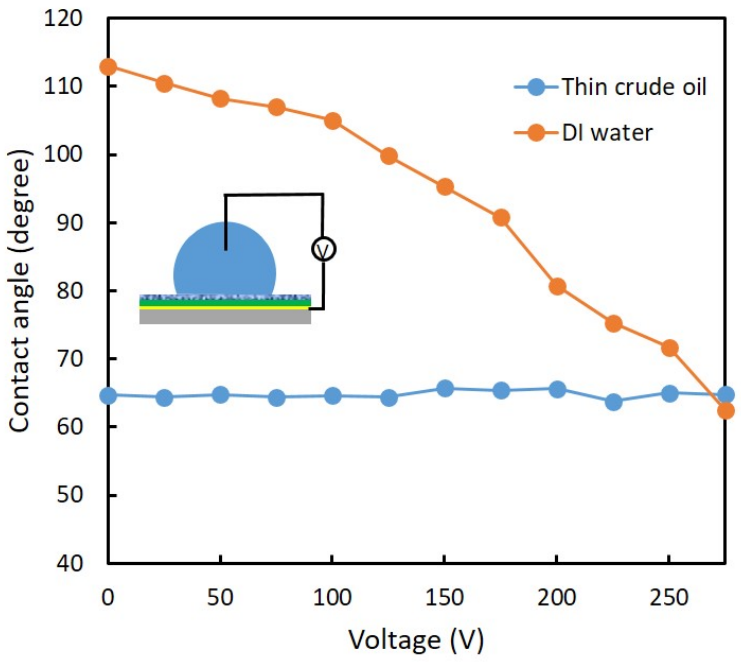

Figure 30. Contact angles of different liquids on the SLIPS film under voltage. For DI water, the contact angle decreases from 113º to 62.5º, when the voltage is applied from 0 to 275 V, which can be explained by electrowetting. For thin crude oil, however, the contact angle remains almost same, 65º. Due to the non-conductive nature, electrowetting does not work. The inserted picture shows the experimental schematic.

contact angles of conductive and dielectric liquids on the SLIPS film under voltage. For DI water, the contact angle decreases from 113º to 62.5º, as the voltage increases from 0 to 275 V. It is the result of electrowetting on dielectric. However, for light crude oil, the contact angle remains almost same at the same voltage range. Since it is dielectric liquid, the voltage has no influence on the contact angle change. Therefore, the transporting of dielectric liquids should be explained by the liquid-dielectrophoresis. Figure 31 shows the side views of light crude oil and DI water under voltage. The contact angle of the oil is always 65º, no matter how large the voltage is. However, there is a big difference for water at high voltage.

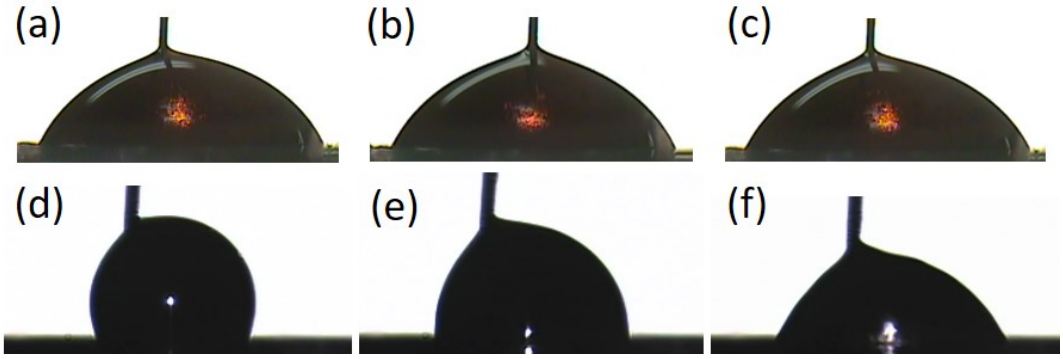

Figure 31. Contact angles for light crude oil and DI water on the SLIPS film**.** Thin crude oil: (a) 0 V, 64.7º. (b) 175 V, 65.4º. (c) 275 V, 64.8º. DI water: (d) 0 V, 113º. (e) 175 V, 90.8º. (f) 275 V, 62.5º.

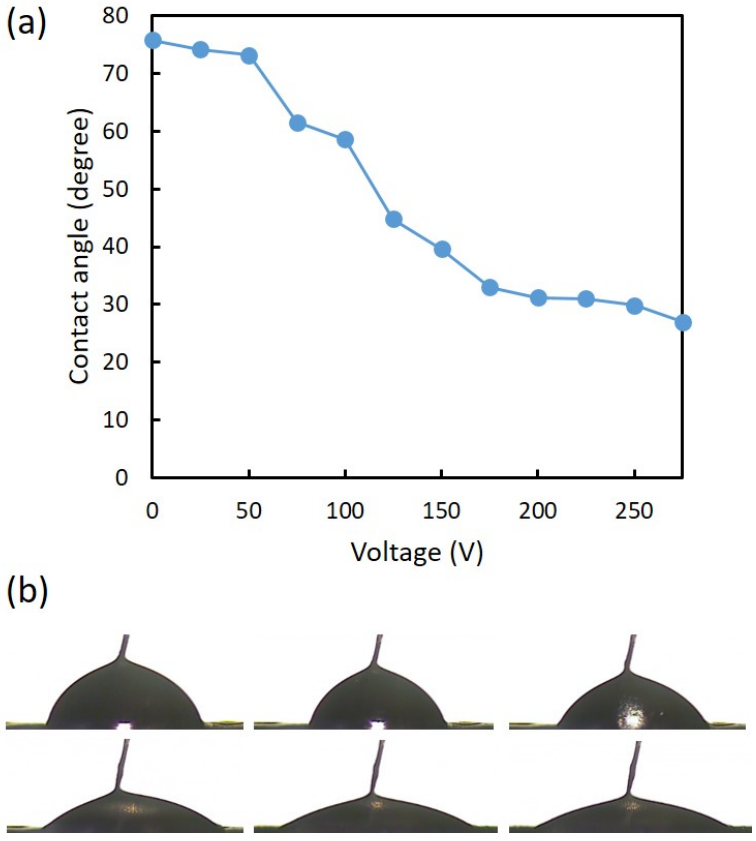

Figure 32. Contact angle measurement of ionic liquid on the SLIPS film. (a) With voltage from 0 to 275 V, the contact angle of ionic liquid decreases from 75.8º to 27º, which is much lower than water. (b) The contact angles at 0 V, 50 V, 100 V, 150 V, 200 V, and 250 V are 75.8º, 73.2º, 58.6º, 39.6º, 31.2º, and 29.8º.

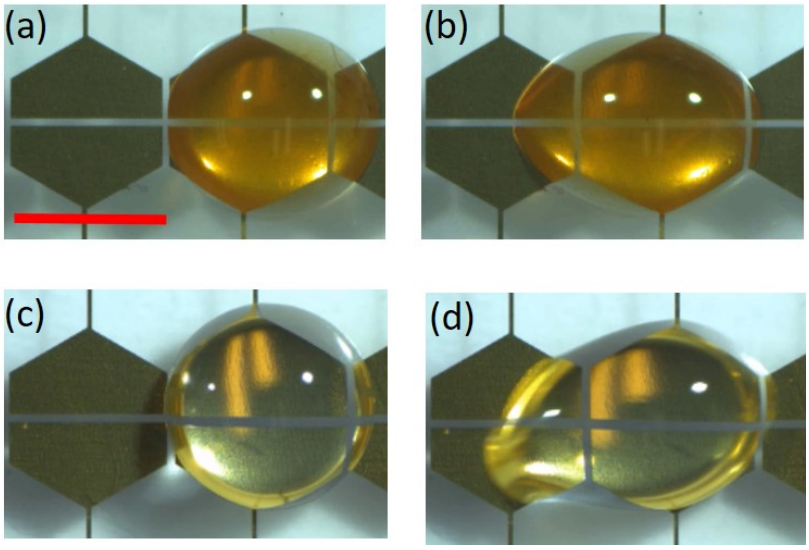

Figure 33. Different mechanisms for the transporting of dielectric and conductive droplets. For (a) and (b), the dielectrophoretic force is maximum at the gap region at 300 V. For (c) and (d), the ionic liquid spread in the electrode region, at 275 V. Scale bar: 1.5 mm.

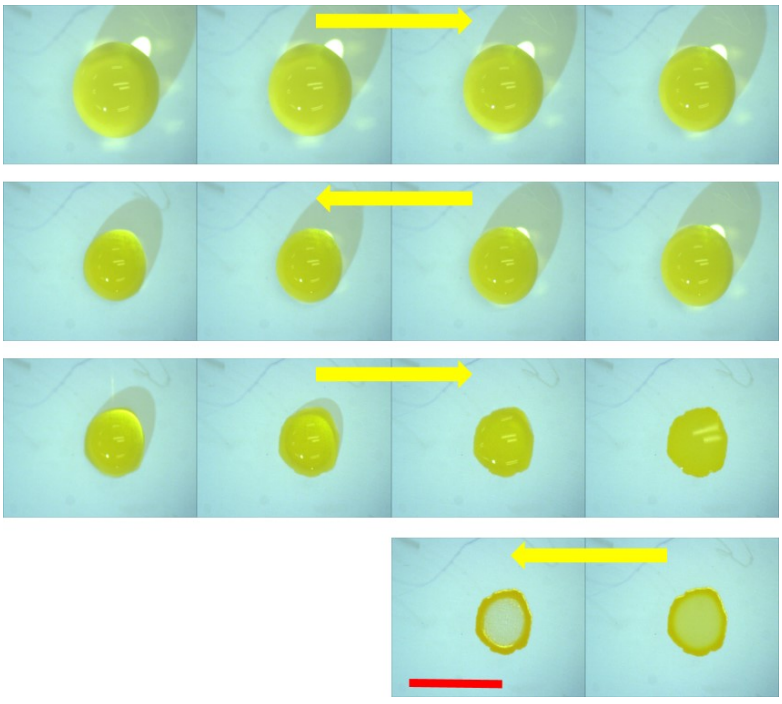

Figure 34. Evaporation of 1 mg/mL protein droplet on porous PTFE surface. 1.5 µL of protein is placed on the surface at room temperature with taking snapshot every 2 min, except the last three (1 min). The yellow arrows denote the time line. Finally, the dried protein pattern is coffee-ring shape. Scale bar: 1.5 mm.

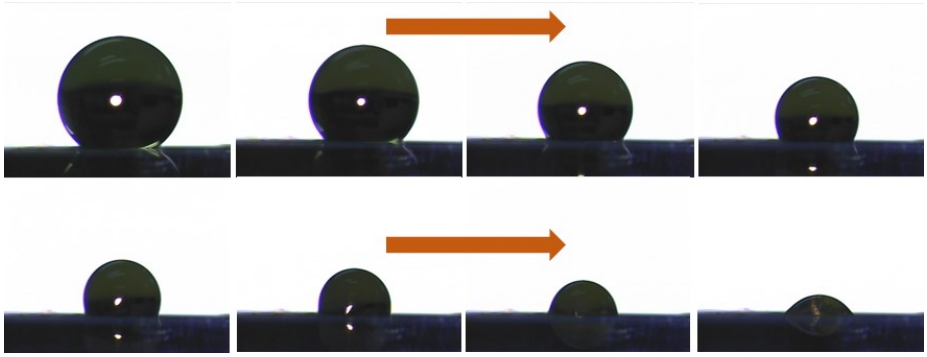

Figure 35. Side views of evaporation of 1 mg/mL protein droplet on porous PTFE surface. The images are taken at 0 min, 6 min, 12 min, 14 min, 16 min, 18 min, 20 min and 23 min. The contact angle decreases gradually. The arrows denote the time line.

In addition to aqueous liquids, ionic liquid is also tested successfully. As shown in Figure 32(a), with voltage from 0 to 275 V, the contact angle decreases from 75.8º to 27º, which is much lower than water due to the low surface tension. Figure 32(b) shows the side views of the contact angle at 0 V, 50 V, 100 V, 150 V, 200 V and 200 V. The contact angle reduces gradually.

Since the force sources of electrowetting and dielectrophoresis are different, the phenomena of transporting are distinctive. As shown in Figure 33 (a) and (b), for the light crude oil, the droplet is stretched along the electrode gap when the voltage is applied. It can be explained by the strong dielectric force generated by the fringing field around the gap. The other electrode area seems not significant, because there is not contact angle change on such region. However, if the droplet is conductive, the shape is different. In Figure 33(c) and (d), ionic liquid is transported, and the droplet tends to spread on the whole electrode area. Due to electrowetting, the contact angle changes on the electrode region to actuate the droplet. This experiment demonstrates the different forces for conductive and dielectric liquids.

3.2.2 Protein droplets evaporation on different surfaces

To better understand the anti-biofouling performance of SLIPS, it is necessary to compare it with other common surfaces, including superhydrophobic and hydrophobic solid surfaces. The porous PTFE can serve as superhydrophobic surface due to its highly porous surface. Teflon surface is another hydrophobic surface, which is widely used in conventional digital microfluidics. The anti-biofouling property means the adhesion of the surface and the bio-solution is very small. Therefore, the solutes are not able to attach to the surface easily, and can be removed without much effort. Here, the evaporation process is chosen as the index to demonstrate the biofouling problem on conventional surfaces, as well as the anti-biofouling on SLIPS.

Figure 34 shows the process of 1 mg/mL protein evaporation on porous PTFE. The droplet is at room temperature and observed every two minutes. It takes more than 20 min to become totally dry. The final dried protein pattern is coffee-ring shape, which is due to the biofouling. As the evaporation process goes on, the bottom area of the droplet remains same, with only decreasing volume of droplet. It means the droplet is pinned to the specific region, because of protein adsorption onto the surface. The protein tends to accumulate to the edge of the droplet, leaving very small amount of protein in the central area. Figure 35 shows the side views at different time points. The contact angle decreases with time, but the contacting area almost does not change. Protein can contaminate the surface easily, and the biofouling problem cannot be avoided. Washing with water is not helpful to eliminate the problem.

Figure 36 shows the evaporation process on Teflon surface. The droplet forms a uniform protein film at last, and the area is smaller than that on the porous PTFE. The small shrinking of the contacting area means the adhesion between the protein and solid surface is smaller than that on superhydrophobic surface. However, the biofouling issue is still considerable, and not

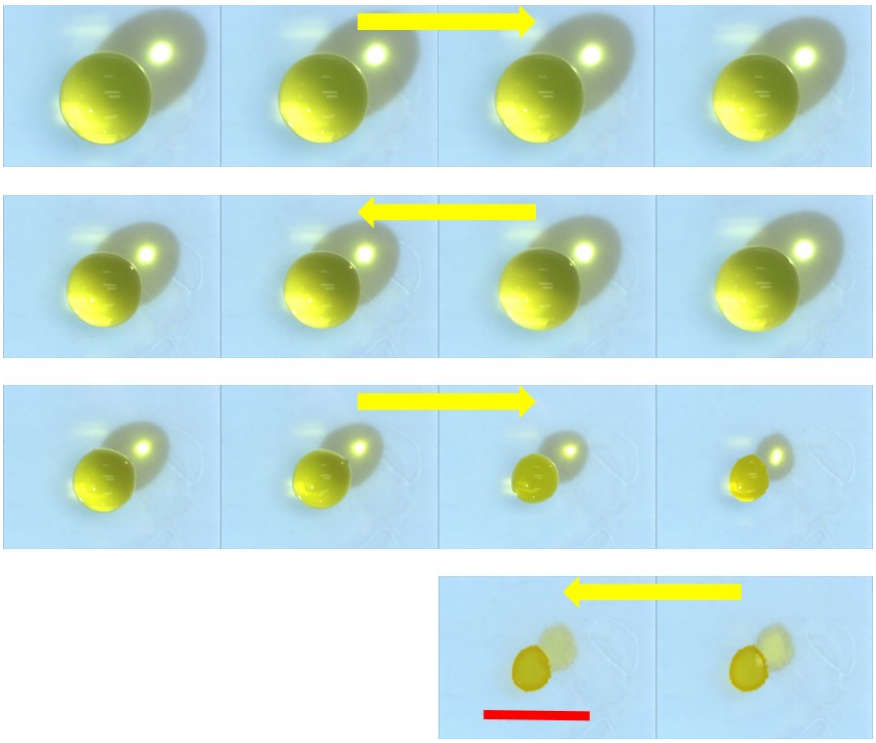

Figure 36. Evaporation of 1 mg/mL protein droplet on Teflon surface. 1.5 µL of protein is placed on the surface at room temperature with taking snapshot every 2 min, except the last three (1 min). The yellow arrows denote the time line. Finally, the dried protein pattern is a uniform film. Scale bar: 1.5 mm.

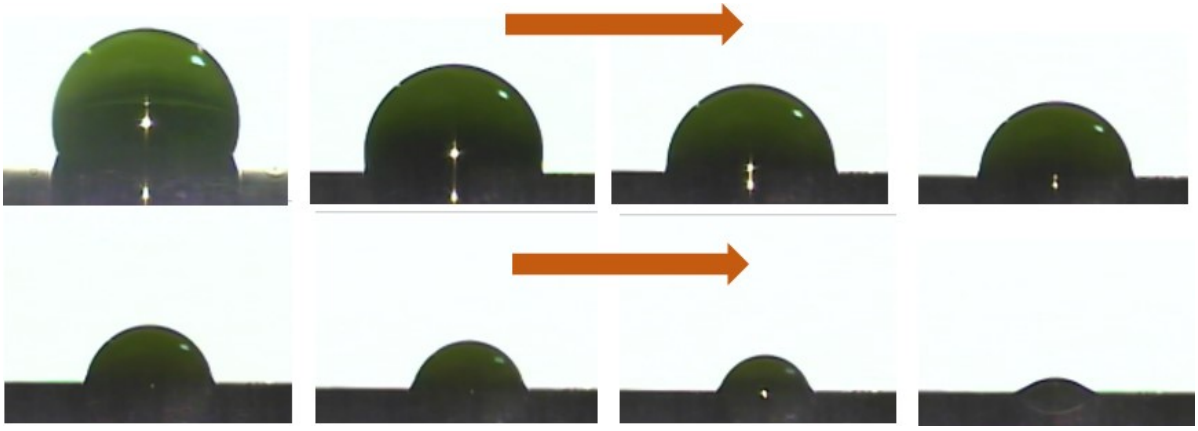

Figure 37. Side views of evaporation of 1 mg/mL protein droplet on Teflon surface. The images are taken at 0 min, 6 min, 10 min, 14 min, 18 min, 20 min, 22 min and 24 min. The contact angle decreases gradually. The arrows denote the time line.

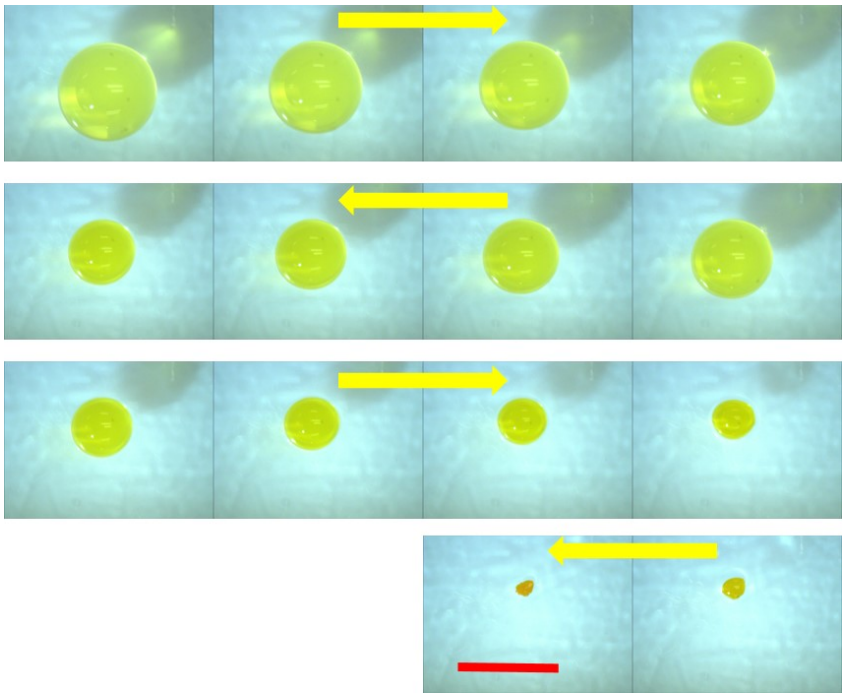

Figure 38. Evaporation of 1 mg/mL protein droplet on SLIPS. 1.5 µL of protein is placed on the surface at room temperature with taking snapshot every 2 min, except the last three (1 min). The yellow arrows denote the time line. Finally, the dried protein pattern is a tiny dot. Scale bar: 1.5 mm.

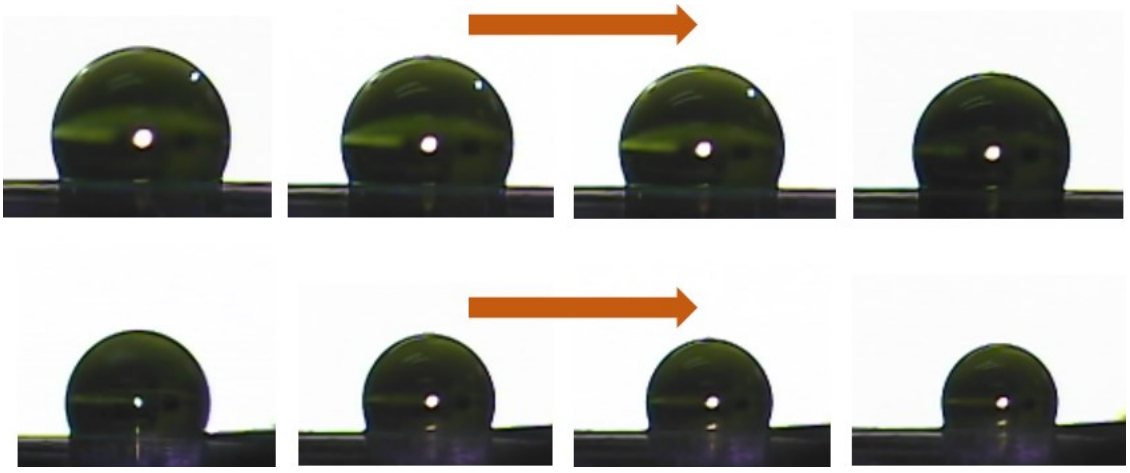

Figure 39. Side views of evaporation of 1 mg/mL protein droplet on SLIPS. The images are taken at 0 min, 2 min, 4 min, 6 min, 8 min, 10 min, 12 min and 14 min. The contact angle almost remains same. The arrows denote the time line.

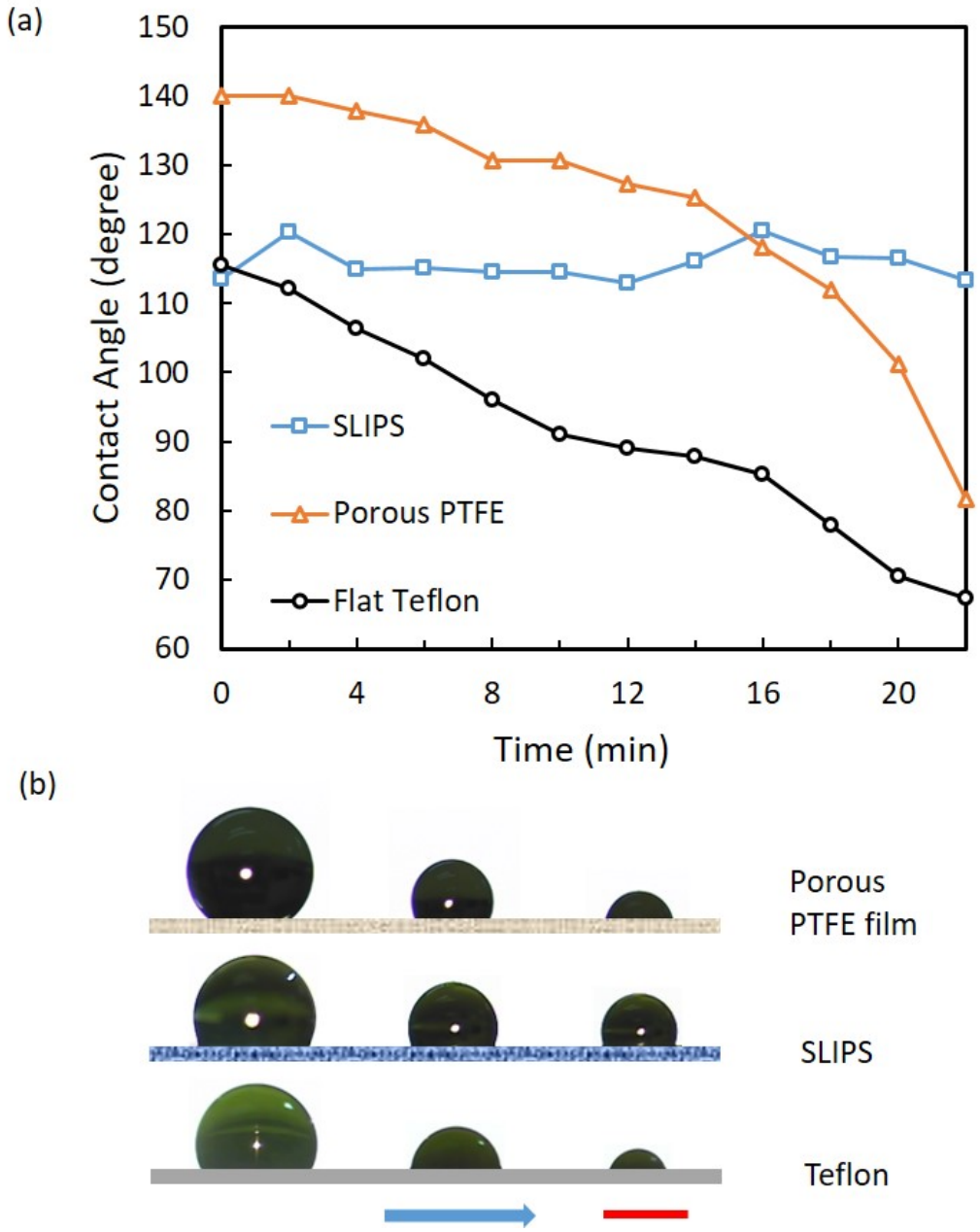

Figure 40. Evaporation of 1.5 µL 1 mg/mL protein droplet on different surfaces. (a) On the porous PTFE film, the contact angle (140º) is largest at the beginning, but decreases rapidly. At 22 min, the contact angle is only 81.6º. On the SLIPS, the contact angle almost remains 115º in 22 min. As for the Teflon surface, the initial contact angle (115.6º) is close to that on SLIPS, but decreases to 67.2º at 22 min. (b) Side views of the contact angle change on different surfaces. The time points selected are 0 min, 16 min and 22 min. The arrows denote the time line. Scale bar: 1.5 min.

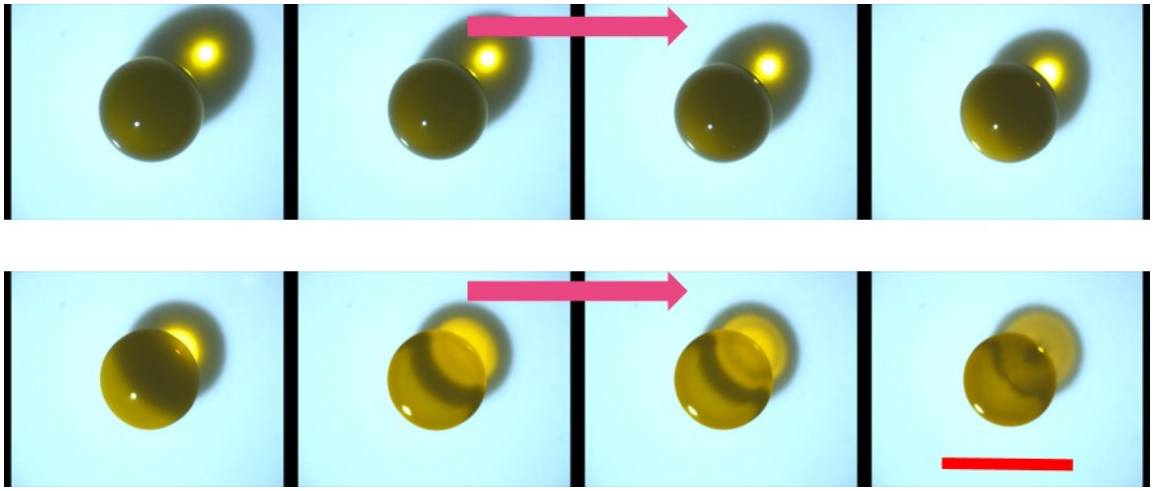

Figure 41. Evaporation of 50 mg/mL protein droplet on Teflon surface. 1 μL of protein is placed on the surface at room temperature with taking snapshot every 2 min. The arrows denote the time line. Finally, the dried protein pattern is a uniform circular film. Scale bar: 1.5 mm.

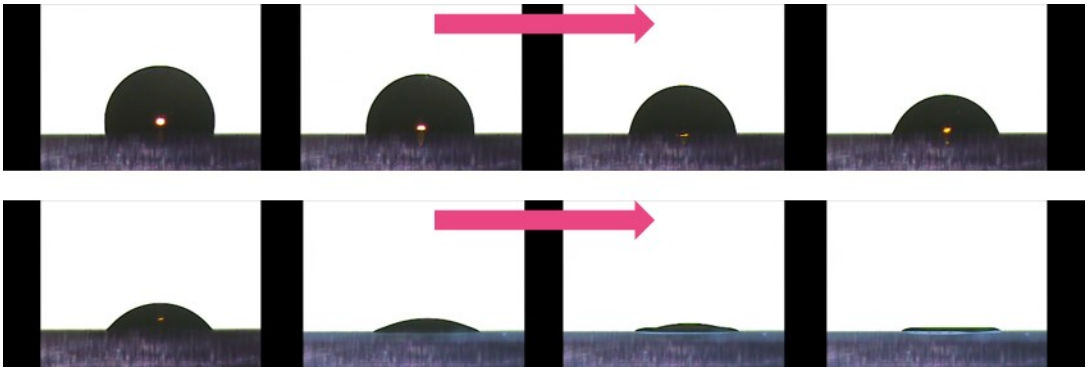

Figure 42. Side views of evaporation of 50 mg/mL protein droplet on Teflon surface. The images are taken every two minutes. The contact angle decreases gradually. Finally, the protein becomes a thin film. The arrows denote the time line.

reversible. Figure 37 shows the side views of the evaporation, the contact angle is still decreasing, but the contact area is also decrease to some extent.

To test the anti-biofouling performance of SLIPS, a same volume of protein droplet is placed on the surface, as shown in Figure 38. The volume of the droplet decreases gradually, as

well as the contacting area. As a result, the final dried protein pattern is a tiny dot. Figure 39 shows the side views. The surface behaves hydrophobic, and the volume is decreasing with time, but the contact angle almost does not change during the evaporation process. The droplet is not pinned to the surface, and the three phase line can move freely even under the small force generated by the surface tension during the evaporation. It is a key performance of anti-biofouling. The tiny dot can be washed away easily.

In summary, Figure 40(a) shows the contact angle change on different surfaces. On the porous PTFE film, the initial contact angle (140^o) is largest, but reduces rapidly. At 22 min, the contact angle becomes only 81.6^o. On Teflon surface, the initial angle is 115.6^o, while after 22 min, the contact angle is 67.2^o. Both on porous PTFE and Teflon surfaces, the contact angle changes are very large. In comparison, there is almost not contact angle change in 22 min for SLIPS. Figure 40(b) depicts the difference of contact angle at 0 min, 16 min and 22 min. At the beginning, the contact angle on SLIPS is around 115^o, similar to the initial contact angle on Teflon, much smaller than that on porous PTFE. At 16 min, the contact angles on SLIPS and porous PTFE are close, much larger than that on Teflon. At 22 min, only on SLIPS, the contact angle is still large. The solid surfaces, like porous PTFE and Teflon, are contaminated by the protein, but the liquid surface, namely, SLIPS, is owning anti-biofouling property.

To find out whether SLIPS works for high concentrated bio-solutions, another experiment is carried out to compare the difference between Teflon surface and SLIPS. In Figure 41, 50 mg/mL protein is placed on Teflon surface. After 14 min, the final pattern is circular film. Figure 42 shows the side views of the same droplet. The contact angle decreases fast, and finally, the protein film is visible on the surface. The area of the protein film is same as the contacting area at

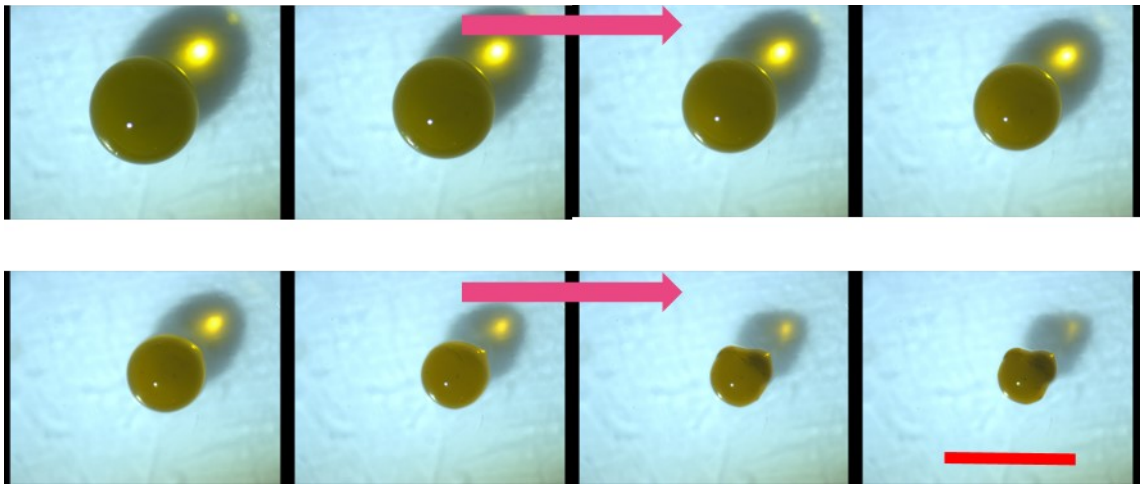

Figure 43. Evaporation of 50 mg/mL protein droplet on SLIPS. 1 µL of protein is placed on the surface at room temperature with taking snapshot every 2 min. The arrows denote the time line. Finally, the dried protein is concentrated to a dot. Scale bar: 1.5 mm.

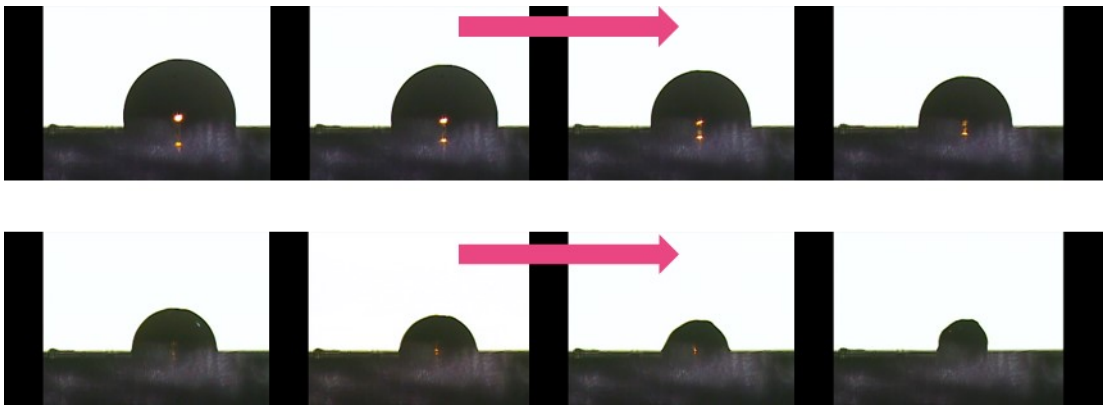

Figure 44. Side views of evaporation of 50 mg/mL protein droplet on SLIPS. The images are taken every two minutes. The contact angle decreases a little. Finally, the protein concentrates to a small island. The arrows denote the time line.

the beginning. Therefore, with high concentration, the protein adheres to the Teflon surface strongly, even from the very beginning.

On SLIPS, the situation is totally different, as shown in Figure 43. The final dried protein is larger the dot formed by 1 mg/mL protein, but still much smaller than that on Teflon. Figure 44

shows the side views of the evaporation process. The contact angle changes not much. The final pattern of the protein looks like a small island, meaning the protein accumulates to the central point during the evaporation. Therefore, the SLIPS works well for high concentrated protein solution, showing the robust anti-biofouling behavior.

3.2.3 Contact angle hysteresis of protein droplet

Contact angle hysteresis is a dynamic parameter to evaluate the adhesion between liquid and the contacting surface. Hydrophobic or hydrophilic are termed to show the sessile droplet behaviors on different surfaces, but when the three phase line is moving, contact angle hysteresis must be taken into consideration. Typically, if the line is moving to the dry surface, the contact angle will become larger than the equilibrium contact angle, which is called advancing contact angle. If the line is leaving the wetted zone, the contact angle will be smaller than the equilibrium one, which is called receding contact angle. The contact angle hysteresis is the difference between the two values. The larger the hysteresis, the more difficult to move the droplet. As for the transporting, hysteresis is more important than the equilibrium contact angle. It can even say that the contact angle hysteresis can be seen as the index of biofouling for bio-droplet. When biofouling occurs, the hysteresis is very large and the droplet is stuck on the surface. While if the surface is anti-biofouling one, the contact angle hysteresis should be very small to remove the bio-droplet.

Two methods can be utilized to calculate the hysteresis. One is increasing and decreasing the volume of one droplet to see the contact angles during the two processes. The other method is trying to move the droplet slowly and measuring the front and back contact angle. Both of them are tested in the experiment.

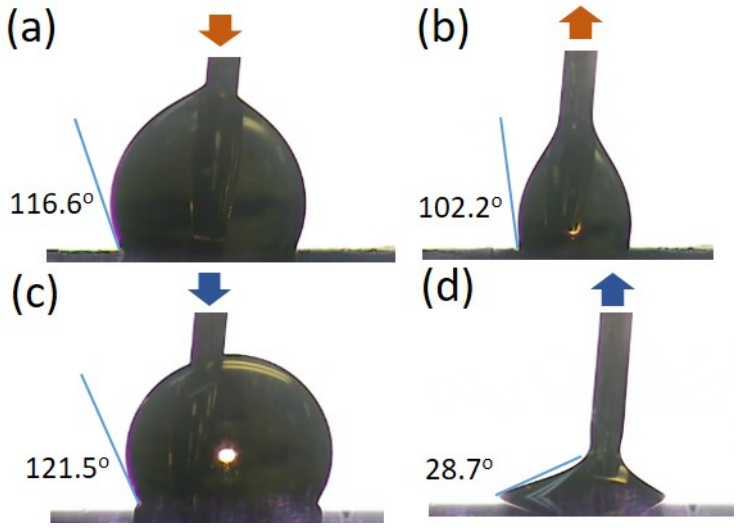

Figure 45. Advancing and receding contact angles on SLIPS and Teflon surface. (a) When infusing 1 mg/mL protein on SLIPS, the advancing contact angle is 116.6°. (b) When pumping out on SLIPS, the receding contact angle is 102.2°. (c) When infusing on Teflon surface, the advancing contact angle is 121.5°. (d) When pumping out on Teflon, the receding contact angle is 28.7°.

In Figure 45, the advancing and receding contact angles are measured on Teflon surface and SLIPS. When infusing 1 mg/mL protein on SLIPS, the advancing angle is 116.6°. When pumping out the solution from the droplet, the receding contact angle is 102.2°. The difference is 14.4° on SLIPS. The situation is different on Teflon, as shown in Figure 45(c) and (d). The advancing contact angle is 121.5°, while the receding contact angle is 28.7°. As a result, the hysteresis is 92.8°, which is much larger than that on SLIPS.

In Figure 46, the droplets on different surfaces are transported by hand. During the transporting process on SLIPS, the advancing contact angle is 111.1°, and the receding one is 101.1°. The contact angle hysteresis on SLIPS is 10°. In comparison, the advancing contact angle on Teflon is 135°, and the receding contact angle is 58.7°. The contact angle hysteresis is 76.3°, which is much larger than that on SLIPS. The protein droplet is very hard to move on Teflon

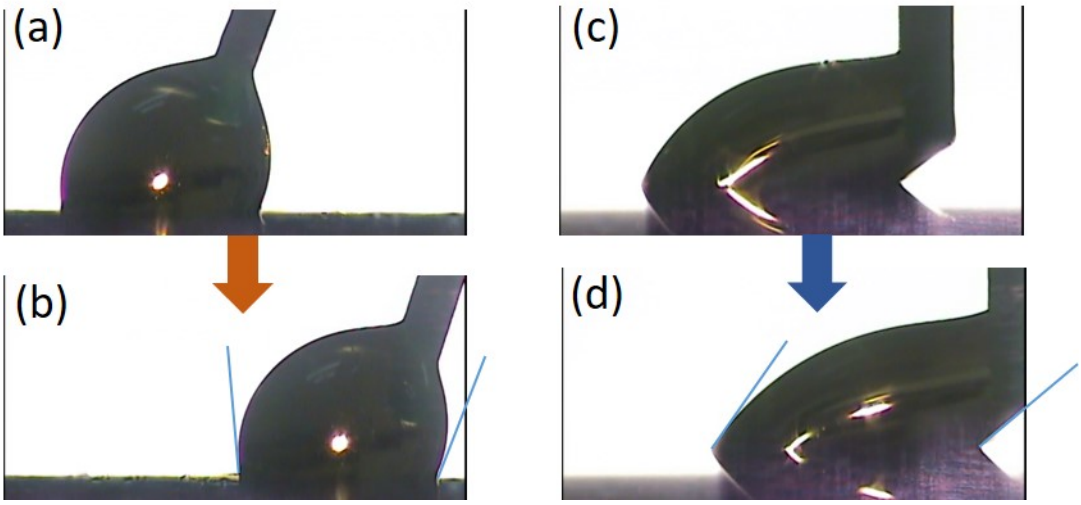

Figure 46. Advancing and receding contact angles when transporting. (a) and (b) show the transporting of 1 mg/mL protein droplet on SLIPS. The advancing contact angle is 111.1°, and the receding contact angle is 101.1°. The contact angle hysteresis is 10°. (c) and (d) show the transporting on Teflon Surface. The advancing contact angle is 135°, and the receding contact angle is 58.7°. The contact angle hysteresis is 76.3°.

surface than on SLIPS. It explains the reason that the protein droplet is not movable on conventional digital microfluidic device: the electrowetting force is not large enough to overcome the pinning force by contact angle hysteresis. However, on SLIPS, the force required to actuate droplet is much lower due to the low hysteresis.

3.2.4 Protein droplet electrowetting on different surfaces

Not only spontaneous biofouling, the electrowetting effect may also deteriorate the problem, rendering it more challenging to transport droplet on digital microfluidics. Therefore, the reversible contact angle change under electrowetting is essential for real applications. In figure 47, electrowetting on Teflon and SLIPS are tested. The protein on SLIPS is at 175 V, while on Teflon is at 75 V, making their contact angle change is close at the beginning.

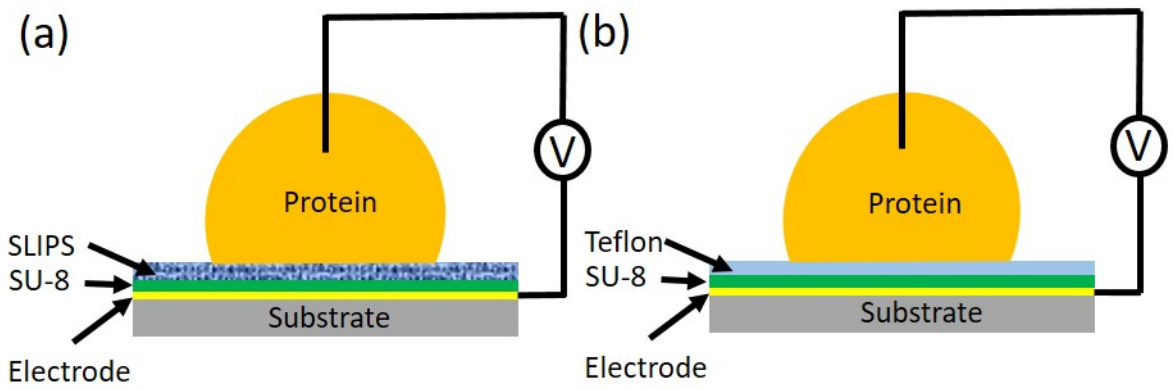

Figure 47. Electrowetting on different surfaces. (a) 1 mg/mL protein on SLIPS with 175 V. (b) 1 mg/mL protein on Teflon surface with 75 V.

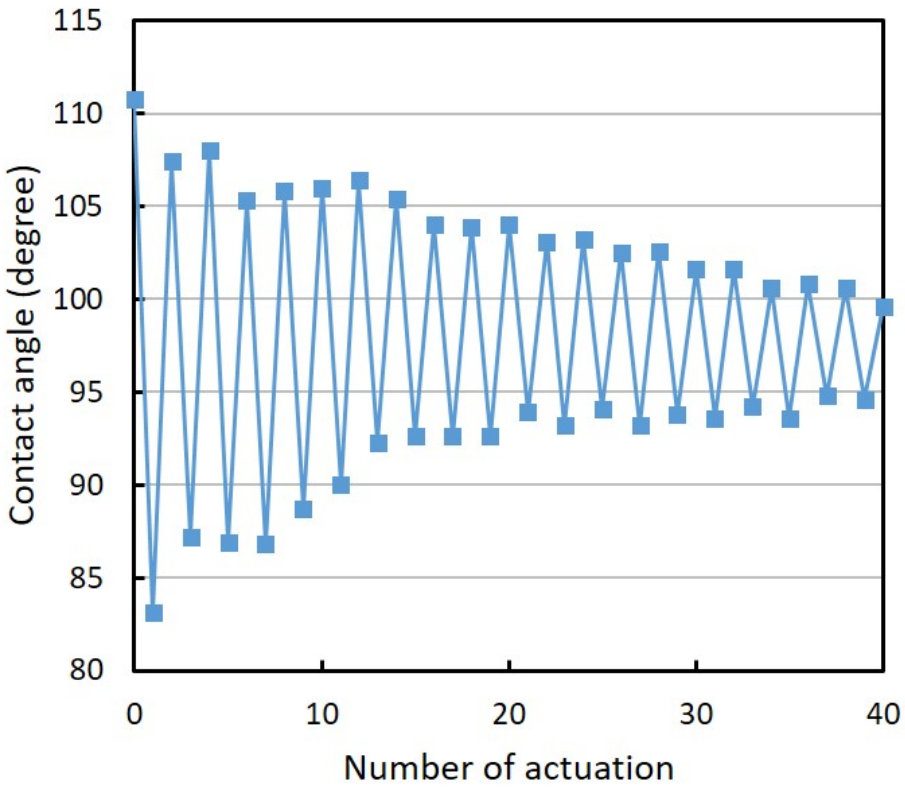

Figure 48. Electrowetting on Teflon surface with 75 V applied. Every cycle is 3s, and the actuation time is 1s in each cycle. After 40 actuations, the contact angle change is only 5º, while at the beginning it is 27.6º.

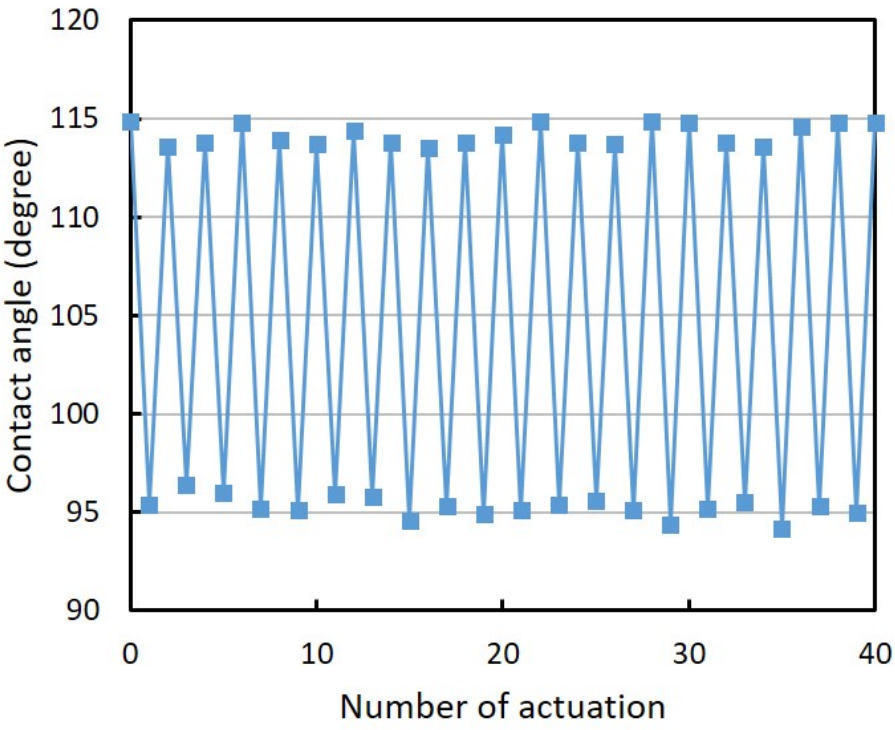

Figure 49. Electrowetting on SLIPS with 175 V applied. Every cycle is 3s, and the actuation time is 1s in each cycle. After 40 actuations, the contact angle change is same that at the beginning, about 20°.

Figure 48 shows the electrowetting on Teflon. The actuation cycle is 3s, with powering on 1s and off 2s. At the first cycle, the contact angle change is 27.6°. However, the change is decreasing as time becomes longer. Finally, after 40 cycles, the contact angle change is only 5°. Figure 49 shows the electrowetting on SLIPS. The contact angle change almost remain same, about 20°. No decreasing trend for the contact angle change, meaning the good reversibility.

Figure 50 shows the first cycle and the 40th cycle on Teflon. At the beginning, the contact angle is 110.8° without voltage applied, and 83.1° at 75 V. After 40 actuations, the contact angle is 99.6° at 0 V and 94.6° at 75 V. Therefore, the surface is more contaminated under the electric field. The biofouling issue is more serious with more voltage cycles. Figure 51 shows the results on SLIPS. At the beginning, the contact angle is 114.9° at 0 V, and 95.4° at 175 V. After 40 cycles,

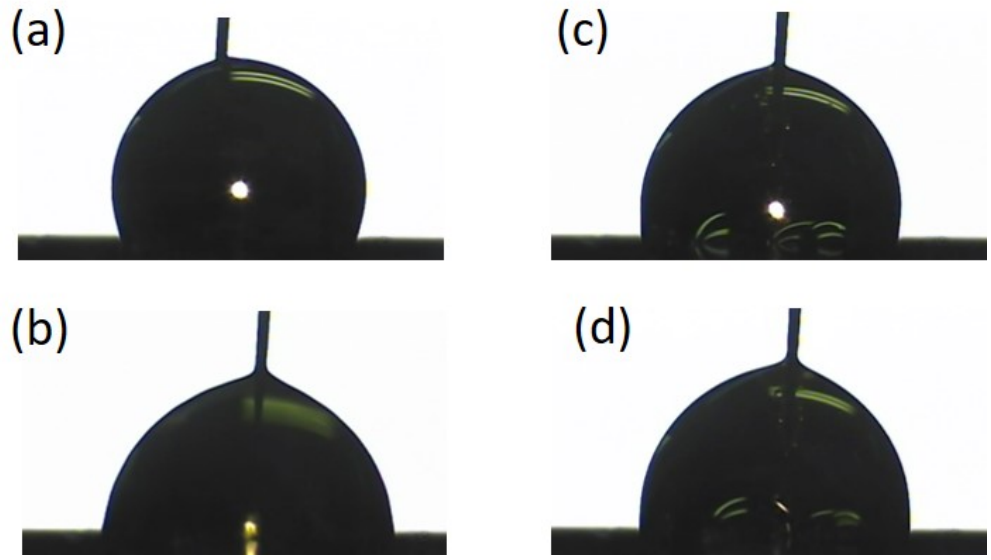

Figure 50. Contact angles with and without applying 75 V on Teflon. At the beginning, the contact angle is (a) 110.8º with 0 V, and (b) 83.1º with 75 V. After 40 actuations, the contact angle is (c) 99.6º with 0 V and (d) 94.6º with 75 V.

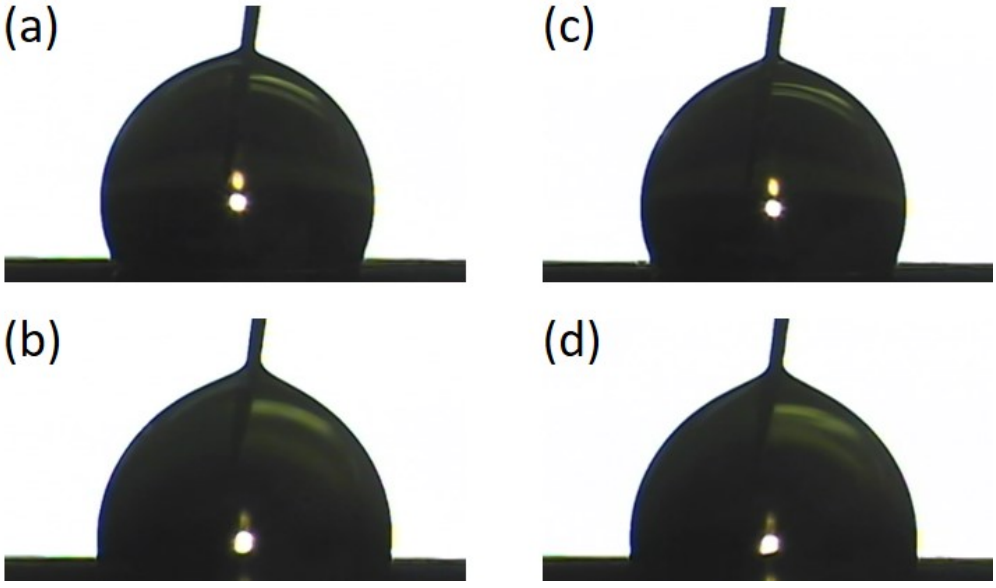

Figure 51. Contact angles with and without applying 175 V on SLIPS. At the beginning, the contact angle is (a) 114.9º with 0 V, and (b) 95.4º with 175 V. After 40 actuations, the contact angle is (c) 114.8º with 0 V and (d) 95º with 175 V.

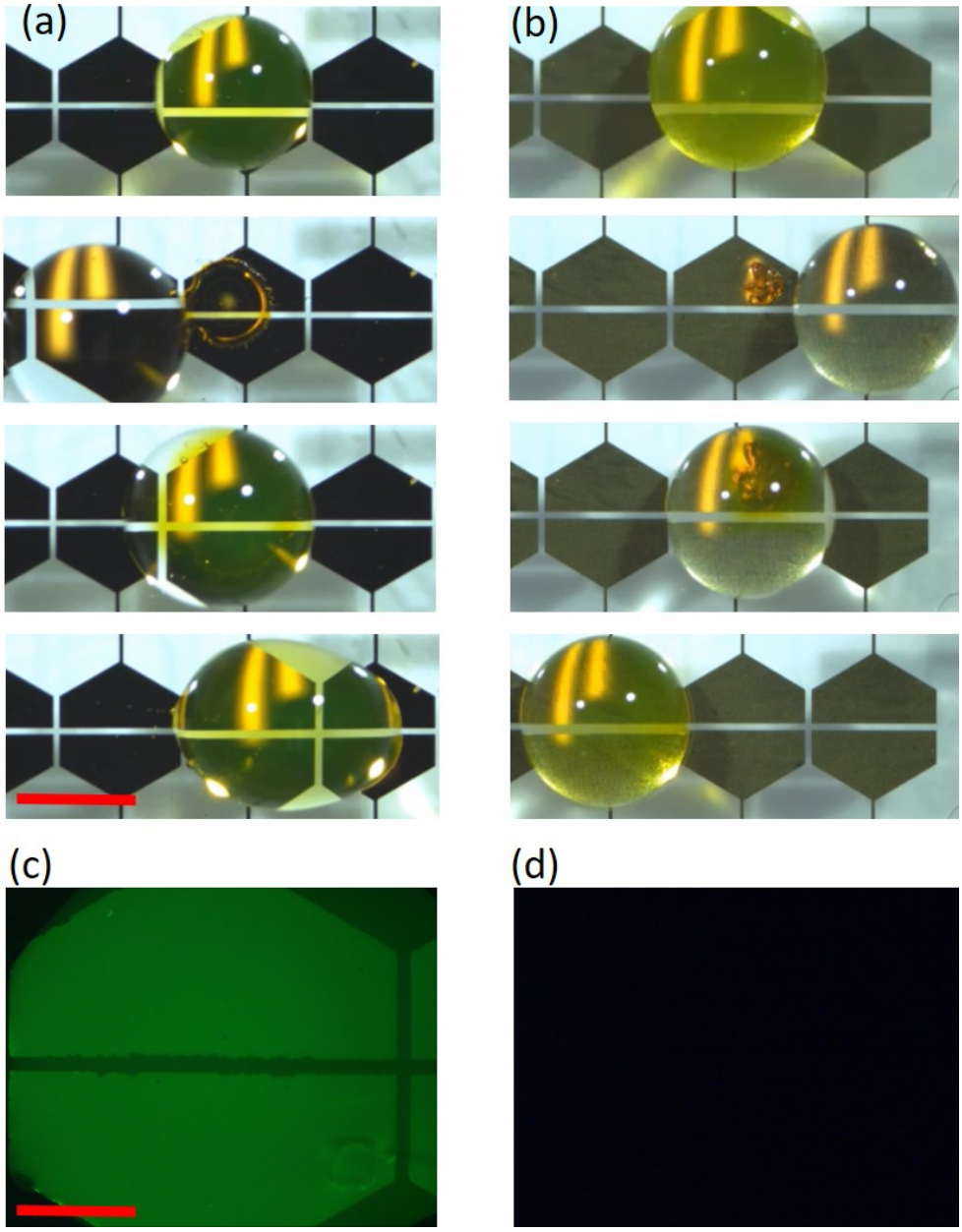

Figure 52. Biofouling issue on Teflon and anti-biofouling performance on SLIPS. (a) On Teflon surface, after drying 1 mg/mL protein, another DI water droplet is transported from left to dissolve the protein. However, it cannot be moved to the right side because of the biofouling problem. (b) On SLIPS, DI water is moved from right to dissolve the dried protein (from 1 mg/mL droplet), and can be transported to the left smoothly, showing the anti-biofouling performance. (c) and (d) Fluorescent images of the central electrode couple region on Teflon and that on SLIPS. Scale bar for (a) and (b): 1.5 mm. Scale bar for (c) and (d): 0.5 mm.

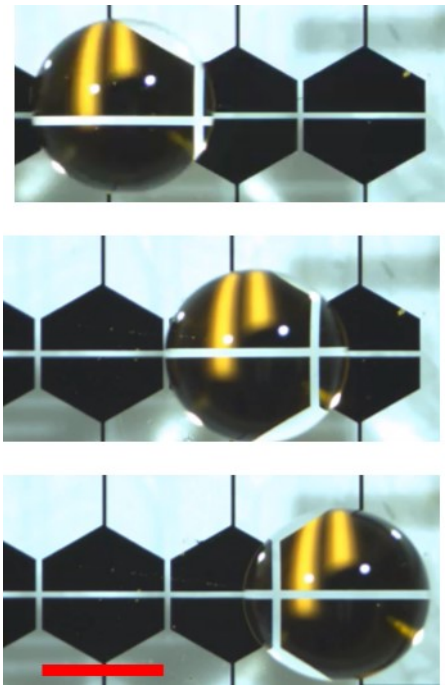

Figure 53. DI water transporting on Teflone.

the contact angles become 114.8^{o} and 95^{o}. No biofouling occurs on the SLIPS under the voltage cycles applied, meaning SLIPS is compatible with electrowetting.

3.2.5 Protein transporting on different surfaces

Figure 52 shows the protein contaminations after drying on Teflon and SLIPS. In Figure 52(a), after the drying, a DI water droplet is transported to dissolve the protein again, followed by actuating the third electrode couple to transport the droplet. However, the droplet is only stretched, without moving to the right position at 150 V. In Figure 52(b), after the DI water dissolves the protein, it can be moved to the third electrode couple on SLIPS at 300 V. The biofouling issue is overcome simply on SLIPS, while it is serious on Teflon. Figure 52(c) and (d) show the corresponding fluorescent images for the middle electrode couples on Teflon and on SLIPS.

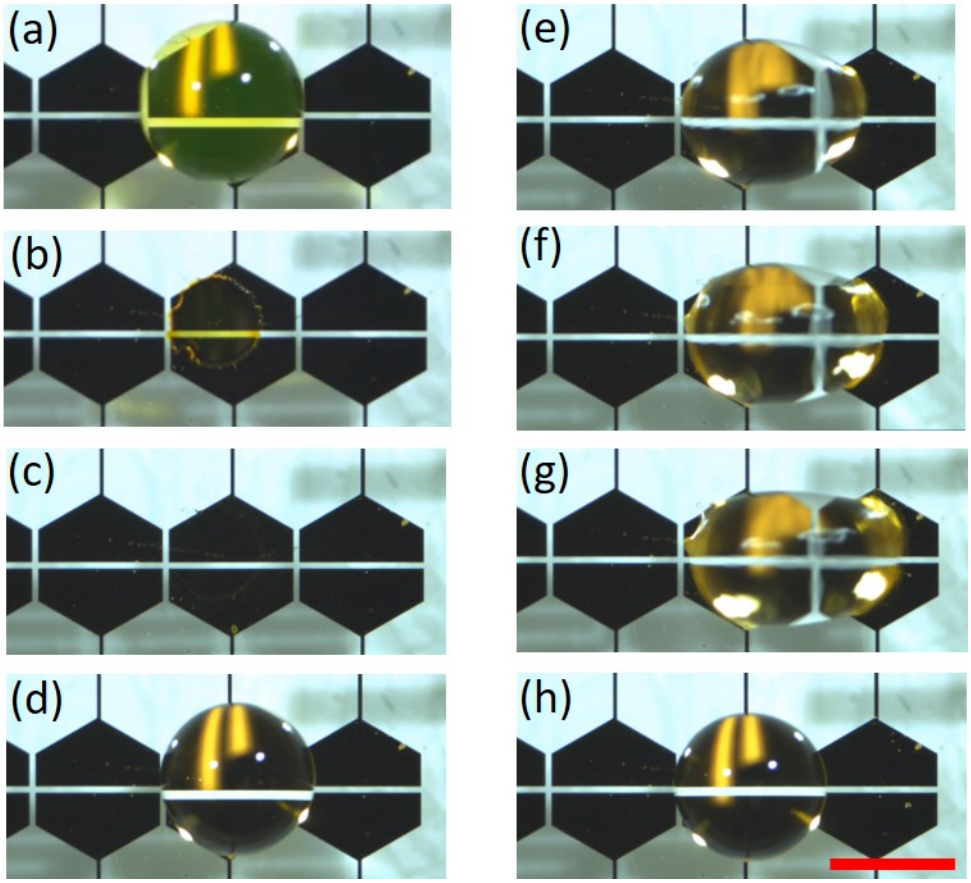

Figure 54. DI water transporting after removing the dried protein on Teflon. (a) and (b) Drying 1 mg/mL protein on Teflon surface. (c) Removing the dried protein with DI water. (d) Transporting another DI water droplet to the central electrode couple. (e) Applying 150 V to the couple on the right, the droplet is pinning in the middle. (f) Increasing to 200 V, pinning. (g) Increasing to 250 V, still pinning. (h) Turning off the power, the droplet returns to the central region again. Scale bar: 1.5 mm.

Even removing the protein on Teflon surface, the surface is still damaged. Figure 53 shows the water droplet can transport on clean Teflon surface at 150 V easily. After the protein drying and dissolving on Teflon, the protein is removed and a new water droplet is added to the central electrode couple, as shown in Figure 54. When applying 150 V, 200 V and 250 V to the third electrode couple, the droplet is only stretched more and more, without droplet transporting. After powering off the voltage, the water droplet go back to the initial position. The Teflon surface

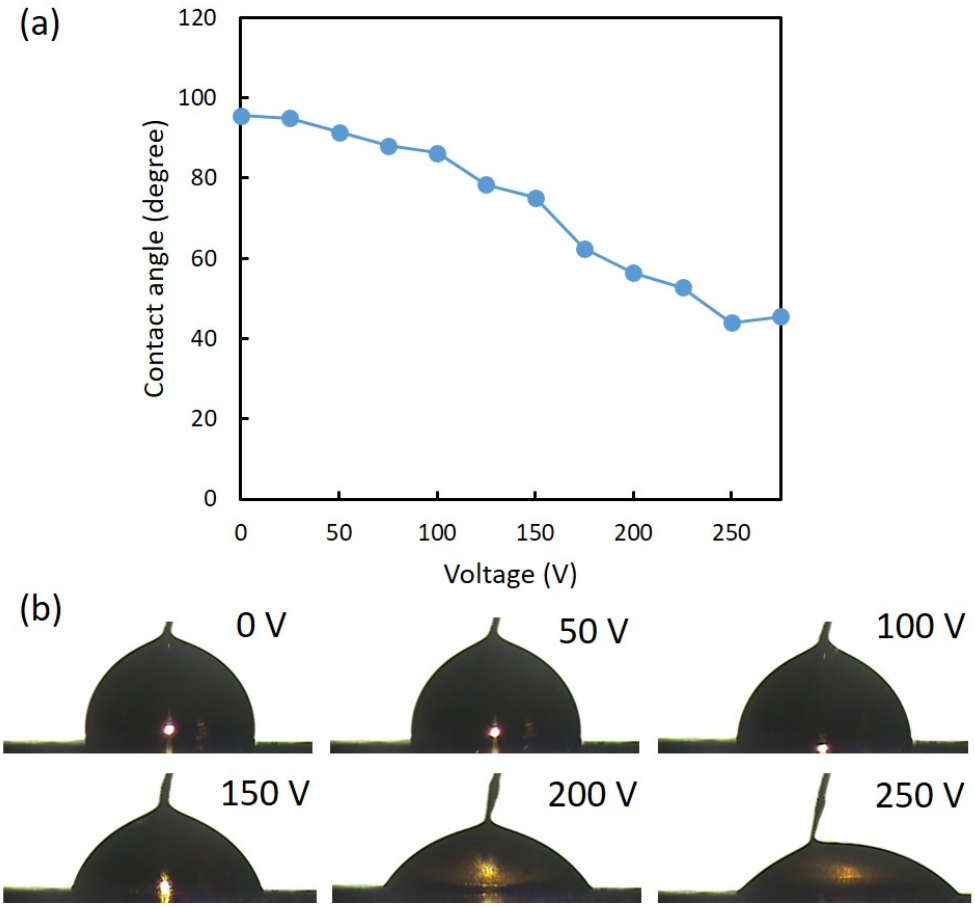

Figure 55. Electrowetting of 50 mg/mL protein droplet on SLIPS. (a) As the voltage increases from 0 to 275 V, the contact angle decreases from 95.6° to 45.5°. (b) Side views of the droplet with different voltages applied.

encounters unrecoverable damage by the biofouling, resulting in the failure of droplet transporting. The DI water is pinned at the contaminated area.

3.2.6 Electrowetting for high concentrated protein solution

Extreme situation for digital microfluidics is the high concentrated bio-solution. For conventional digital microfluidic device, it is never successful for such situation. Therefore, it is necessary to see whether the novel device is working to such extreme case, like high concentrated protein

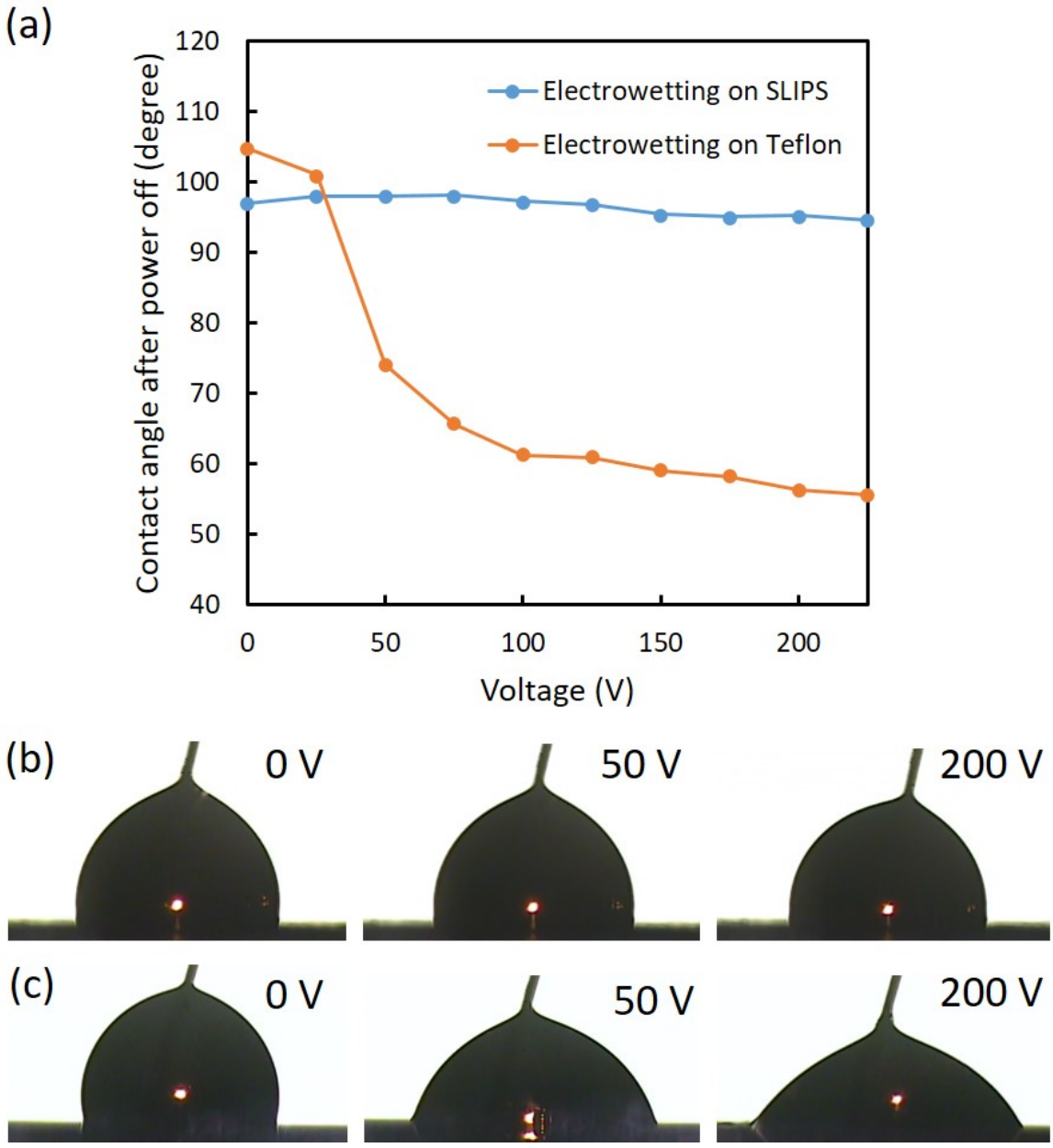

Figure 56. Electrowetting recovery properties of 50 mg/mL protein droplet. (a) Apply voltage to the droplet, and turn off to see the contact angle. On the SLIPS, as the voltage increases from 0 to 225 V, the contact angles remain almost same. However, on the Teflon, after powering off, the contact angles are not able to return to the initial state. With higher voltage, the contact angle is smaller. (b) Side views of the droplets on SLIPS after powering off the voltage, showing good anti-biofouling property. (c) Side views of the droplets on Teflon after powering off the voltage, showing the biofouling issue rendering the unrecoverable contact angle decrease.

solution. In figure 55(a), 50 mg/mL protein droplet is tested on SLIPS with different voltages applied. The contact angle decreases from 95.6º to 45.5º with voltage from 0 V to 275 V. Figure 55(b) shows the side views at different voltages.

To evaluate the recoverability of high concentrated protein on different surfaces, another experiment is carried out. As shown in Figure 56(a), when applying voltage and powering off, the droplet on Teflon cannot return the initial state even after one trial. The contact angles on Teflon decrease from 105º to 55.5º with voltage increasing to 225 V. The droplets are firmly pinned on Teflon. However, on SLIPS, the contact angle can go back to the initial value after powering off the voltage. Five actuations are conducted for each voltage. Figure 56(b) shows the side views on SLIPS after powering off. The contact angles are same at different voltages. Figure 56(c) shows the side views on Teflon after powering off. The contact angles decrease with large range, demonstrating the biofouling issue rendering the unrecoverable pinning.

3.2.7 Protein droplet transporting on different surfaces

To elucidate the biofouling performance of the digital microfluidic device with SLIPS, it is necessary to compare it with conventional one. The evaluating index used here is the transporting steps. Every two seconds, activating one electrode couple and the adjacent one by sequence to count how many steps the protein droplet can move. Different concentrations are adopted here to broaden the application range.

In Figure 57, 20 μg/mL protein droplet is transported on Teflon surface. At the beginning, it can be moved easily at 125 V. However, after 80s, it is pinned to the surface without moving. The conventional digital microfluidic device is not working well even for low concentration bio-solution. In Figure 58, 1 mg/mL protein is tested on Teflon surface and SLIPS. It cannot be

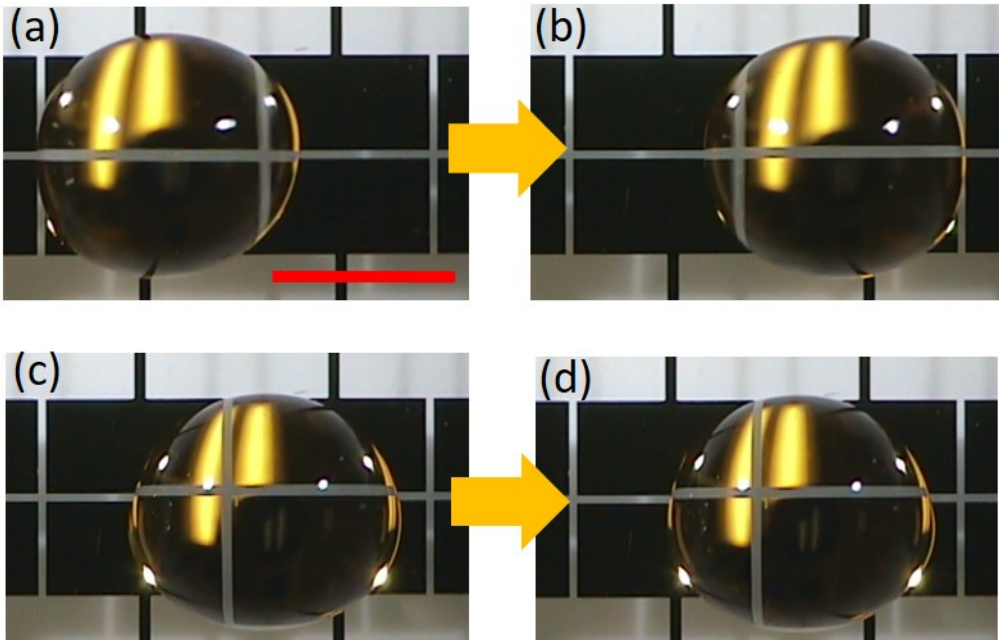

Figure 57. Transporting of 20 µg/mL protein droplet on Teflon surface. (a) and (b): At time t= 2s, the droplet can be transported with 125 V. (c) and (d): at t=80s, it pins on the surface. Scale bar: 1.5 mm.

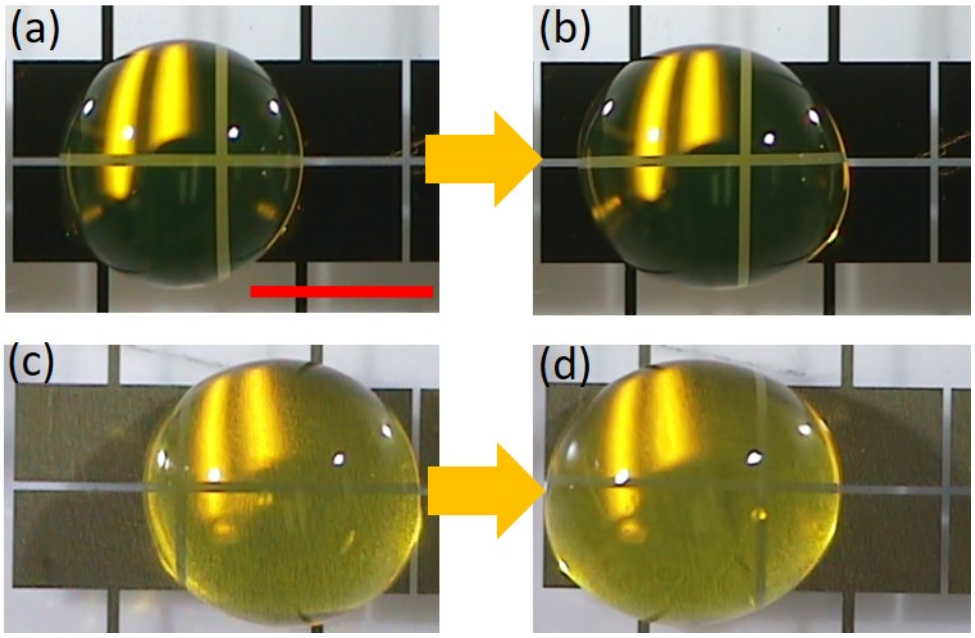

Figure 58. Transporting of 1 mg/mL protein droplet on Teflon surface and SLIPS. (a) and (b): At time t=2s, on Teflon surface, the droplet can not be transported with 125V. (c) and (d): At t=2s, the droplet can be transported on the SLIPS with 250 V. Scale bar:1.5 mm.

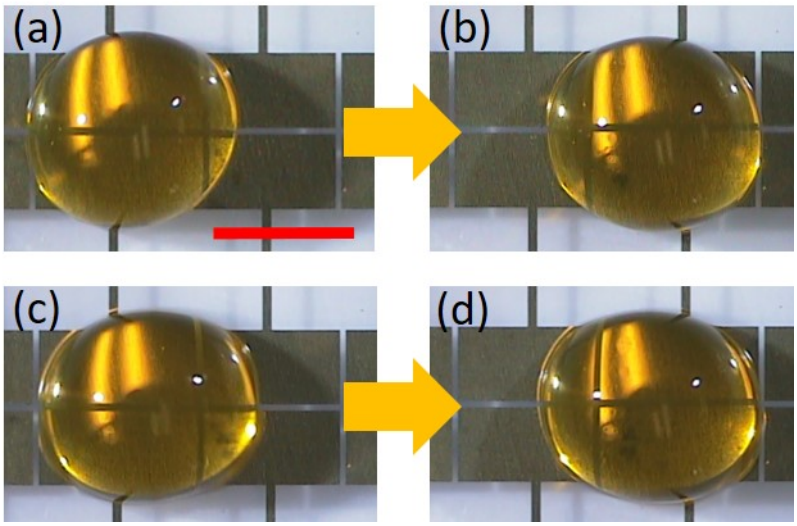

Figure 59. Transporting of 50 mg/mL protein droplet on SLIPS. (a) and (b): At time t= 0 min, the droplet can be transported with 250 V. (c) and (d): at t=10 min, it still can be transported. Scale bar: 1.5 mm.

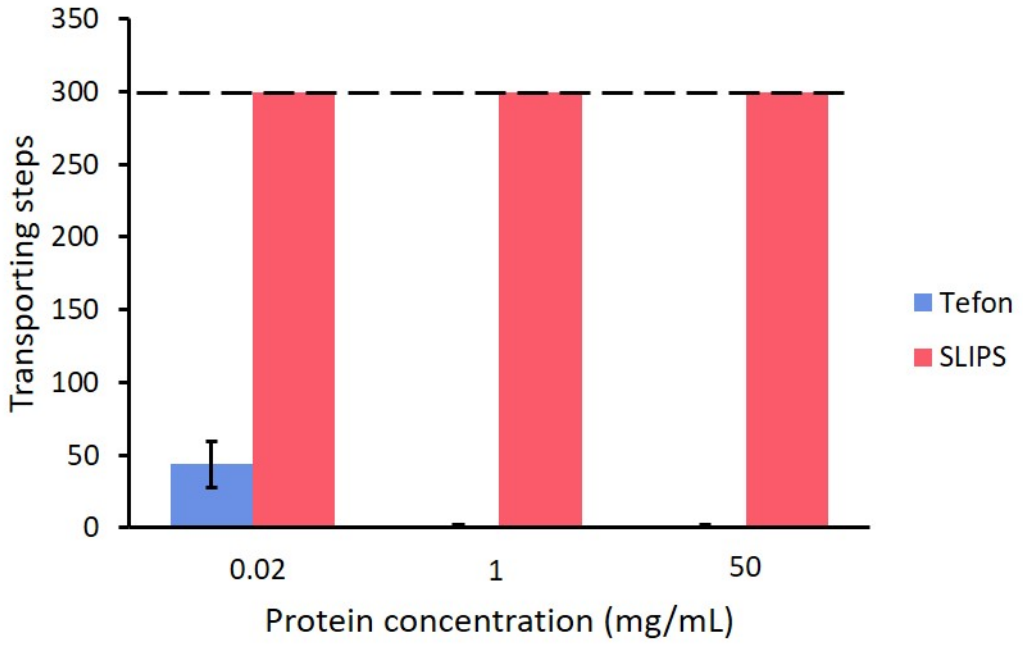

Figure 60. Transporting steps of protein droplets on Teflon and SLIPS. At the lowest concentration (0.02 mg/mL), the droplet can be transported less than 50 steps on Teflon surface. At higher concentrations (1 and 50 mg/mL), the droplets cannot be transported even 1 step. However, on the SLIPS, all the droplets can move more than 300 steps.

transported on Teflon because of the serious biofouling problem. However, such protein solution can move freely on SLIPS. To demonstrate the good anti-biofouling performance on SLIPS, the long term experiment is carried out for 50 mg/mL protein. After actuating for 10 min, the high concentrated protein can still be transported. Figure 60 is the summary for different concentrations on the two surfaces. At low concentration (20 μg/mL), the protein can be transported about 45 steps. However, if the concentration exceeds 1 mg/mL, it cannot be moved even one step. On the other side, they can be transported on SLIPS more than 300 steps. Therefore, the digital microfluidic device integrated with SLIPS is very robust for real applications.

3.3 CONCLUSION

An anti-biofouling digital microfluidic device is designed to transport bio-solutions, like protein solution, blood and DNA solution. In addition, dielectric droplets, such as IPA, propylene carbonate and light crude oil, are also be actuated. An electrode array is used to determine the transporting pathway of droplets. Upon the substrate, there are SU-8 and SLIPS layers. The former is aimed at enhancing the electrowetting effect, while the latter one is to prevent biofouling problem. Different conductive droplets are transported successfully, such as DI water, protein solution, saline, ionic liquid, blood, milk, DNA solution and honey. Some of them are bio-solutions or sticky fluids, which are challenging to transport. In addition, light crude oil, propylene carbonate and IPA are the representatives of dielectric fluids. All the fluids are immiscible to the lubricating oil, which is infused into porous film to form SLIPS. With electrowetting configuration, both dielectric and conductive droplets are tested. It turns out the contact angle of light crude oil does not change, nothing like what happens to DI water. Therefore, the driving force during the

transporting is from electrowetting, but dielectrophoresis. Meanwhile, the contact angle of ionic liquid is also changed to large extent by electrowetting on SLIPS. The different shapes of light crude oil and ionic liquid are demonstrated during transporting. For the former, the droplet is stretched along the electrode gap, while for the latter, it spread on the electrode region. It can be explained that the dielectrophoretic force is generating by the fringing field in the gap region, and the electrowetting force is exerted through electrode area. To show the anti-biofouling performance of SLIPS, conventional hydrophobic surfaces are selected as reference, like porous PTFE and flat Teflon. The results demonstrate that the solid hydrophobic surfaces are easily contaminated by the protein, and SLIPS surface owns the capability of anti-biofouling. More specifically, the contact angle of droplet on SLIPS during the evaporation process remains same, while the others decrease with time. Therefore, the protein is adsorbed to the solid surface, and not pinned on the SLIPS. Even for protein solution with high concentration, the results are same. On Teflon, the final pattern is a circular film, while on the SLIPS, the protein concentrates to a small island, meaning SLIPS is resistant to high concentration protein. The advancing and receding contact angles are important parameters for transporting of droplets. Two methods are used to measure the values. By infusing and pumping out the protein solution, the contact angles on Teflon surface are totally different, which means large contact angle hysteresis. On the other hand, the contact angles vary a little on SLIPS. The second way is to transport the droplet by hand, and measure the contact angle on the two sides. On SLIPS, the contact angle hysteresis is very small, while on Teflon, the value is so large that it is difficult to overcome. Electrowetting may also deteriorate the biofouling, which is proved the comparison of electrowetting on SLIPS and Teflon. When the protein droplet under many cycles of electrowetting, the contact angle change becomes very small, which means biofouling occurs. On SLIPS, the contact angle change remains same

even after several tens of actuations, revealing the good anti-biofouling performance. When the protein is dried on Teflon surface, it cannot be transported by water droplet, while on SLIPS, the device still works. Even after removing the protein, the surface is still contaminated on Teflon, where a new water droplet cannot be transported. It is a permanent damage to the Teflon surface after the protein drying, which is a challenging problem for conventional digital microfluidics. As for SLIPS, electrowetting works well even for high concentrated protein solution. If Teflon surface is utilized under same condition, the contact angle of protein cannot recover to the initial state after powering off. Similarly, different concentrations of protein droplets are tested on conventional digital microfluidic device and the anti-biofouling device. The result shows that on SLIPS, different concentrations are successfully transported for more than 300 steps, while on Teflon, the surface is contaminated easily and the droplets cannot be transported. Therefore, integration of digital microfluidics and SLIPS shows an impressive anti-biofouling performance.

4.0 A WIDE-SPECTRUM DIGITAL MICROFLUIDIC PLATFORM

Digital microfluidic device has a wide range of applications, including bio-solution assay, chemical reacting and genomics. Such device is based on droplets, which can be controlled by array of electrodes on a small chip. It owns many advantages compared to conventional laboratory level testing methods. The samples needed in digital microfluidics are tiny, highly reducing reagent consumption and increasing the chemical reaction rate. The most promising advantage is that the positions of droplets on the digital microfluidic device can be changed by computer program. This feature represents the high flexibility compared to laboratory level containers or microchannel based microfluidics. Conventional microfluidics require specific designed microchannel, as well as many mechanical components, such as pump to provide driving force, tube and connector to link the microchannel. Once fabricated, the microchannel based microfluidic devices are not able to change for other applications. On digital microfluidic platform, however, the transporting pathways of the droplets can be easily recomposed to meet different demands. The driving force of digital microfluidics originates from electric signal, which is controlled automatically. More specifically, the droplets are manipulated by electrowetting and dielectrophoresis, depending on the properties of the droplets. For conductive droplet, electrowetting is dominant, where the free charge in the droplet can be swiftly relocated, driving the droplet to move. For dielectric droplet, the effect of dielectrophoresis overwhelms, where strong non-uniform electric field attracts the dipoles of dielectric molecules. Both of the mechanisms can be integrated into a two-plate digital

microfluidics. However, if a dielectric droplet, especially with low dielectric constant, is placed on a single plate, the actuation is not simple as that of conductive droplet by electroweting. In addition, there are many conductive and non-conductive liquids have tends to adhere the solid surface, impeding or stopping the transporting by electric potential. Therefore, the digital microfluidics still face many problems to broaden the range of applications, and a wide-spectrum digital microfluidic device is highly demanded.

To overcome the current issues in digital microfluidics, a novel design is reported in this chapter. The device integrates two components of electrodes to actuate conductive and dielectric droplets respectively. The electrical force is considerable to drive different droplets, including the droplets with low dielectric constants. The surface of the device is also elaborately designed to lower the adhesion between droplets and surface. The slippery liquid infused porous surface (SLIPS) is utilized as the surface, which dramatically decreases the contact angle hysteresis of droplets, especially for many challenging fluids, like honey, bio-solution and oils. This chapter will demonstrate the capability to transport different types of droplets, elucidate the difference between conductive and dielectric droplet transporting, and end with conclusion.

4.1 DIGITAL MICROFLUIDIC DEVICE DESIGN AND FABRICATION

Figure 61 shows the schematic of wide-spectrum digital microfluidic device. An array of electrode couples are fabricated on the glass substrate, which is the power source to actuate conductive and dielectric droplets. They are controlled by computer program to power on and off. The SU-8 layer is to separate the SLIPS and substrate, and also serve as the dielectric layer to increase the electrowetting effect. The SLIPS is attached on the top of the device, which is designed to prevent

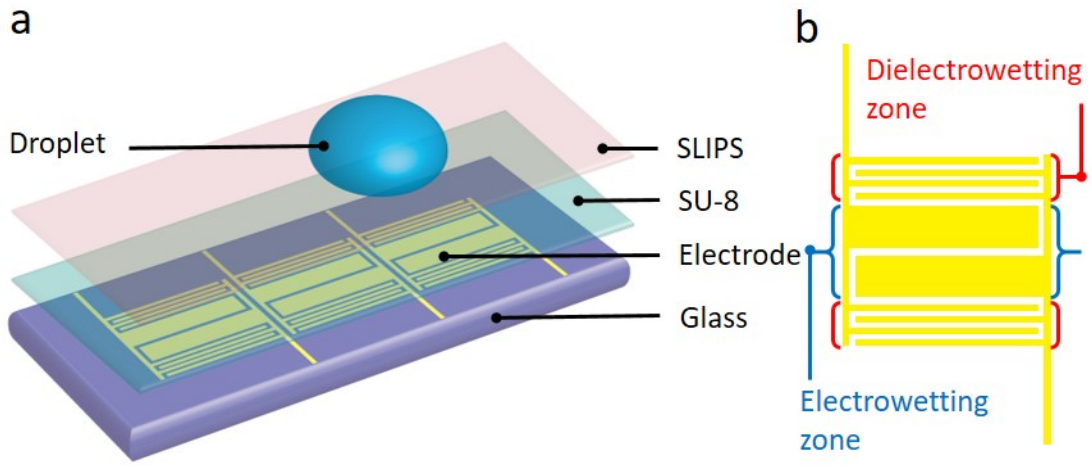

Figure 61. Schematic of wide-spectrum digital microfluidic device. (a) An array of electrode couples are fabricated on the glass substrate, which can be powered on or off by control to move the droplet on the top. One SLIPS layer and one SU-8 layer separate the droplet and electrode. The former is to decrease the surface adhesion of droplet and the latter is applied as high dielectric layer. (b) The structure of one electrode couple. Electrowetting zone is in the middle to actuate conductive liquids, with large area of solid electrodes. The dielectrowetting zone on the two sides to actuate dielectric liquids, utilizing interdigitated electrodes to generate large dielectrophoresis force.

droplet contacting with solid surface. For many sticky fluids, the adhesion to the solid surface is very strong, rendering the difficulty to remove the fluids from the surface. In this case, the electric field cannot drive the droplets to move because of the high contact angle hysteresis. The SLIPS is a lubricating liquid surface on the top, while the solid porous structure is to hold the liquid from escaping, making the liquid film stable. Therefore, the SLIPS combines the advantages of liquid and solid. It owns the nature of liquid with negligible shear stress, and the definite shape like a solid. In Figure 61(b), a close view shows the pattern of an electrode couple. In the middle, it is electrowetting zone with wide electrodes to actuate conductive fluids. On the two sides, the dielectrowetting zone is utilized to actuate dielectric liquids. The interdigital electrodes can generate strong fringing fields, which dramatically enhance the dielectrophoresis force to drive the

droplet with low dielectric constant. On such interdigital electrodes, the contact angle of dielectric droplet can be changed upon applying voltage. Such behavior seems like electrowetting, but really not. That is why it is named as dielectrowetting. In the subsequent experiments, it turns out the two zones are necessary in the device. Only one type of electrodes is not reliable to the other kind of liquids. For example, with purely interdigital electrodes, the dielectric liquids can be transported easily, while the conductive droplets cannot. Both dieletrowetting and electrowetting zones are indispensable.

As for fabrication process, the detailed information can refer to the previous chapters. The electrode pattern is formed with positive photoresist by conventional photolithography. Metal layers are deposited by electron-beam evaporation to form 10 nm Cr and 100 Ag, followed by lift off process. The SU-8 layer is spin coated, with thickness of 2 μm, which is exposed to ultraviolet light to strengthen the structure. Finally, the SLIPS film is attached uniformly to the top surface. The exact steps are described in the chapter of anti-biofouling digital microfluidic device.

4.2 RESULTS AND DISCUSSION

4.2.1 Surface characterizations

To emphasize the importance of SLIPS for the digital microfluidic device, such surface is compared with conventional Teflon surface, which owns the lowest coefficient of friction in solid materials. The testing fluid is honey, which is very sticky and prone to adhere to solid surface. If SLIPS is anti-sticky to honey, it is expectable to say it can resist most sticky fluids. In Figure 62, two honey droplets are place on SLIPS with a small distance. After linking the two equal sized

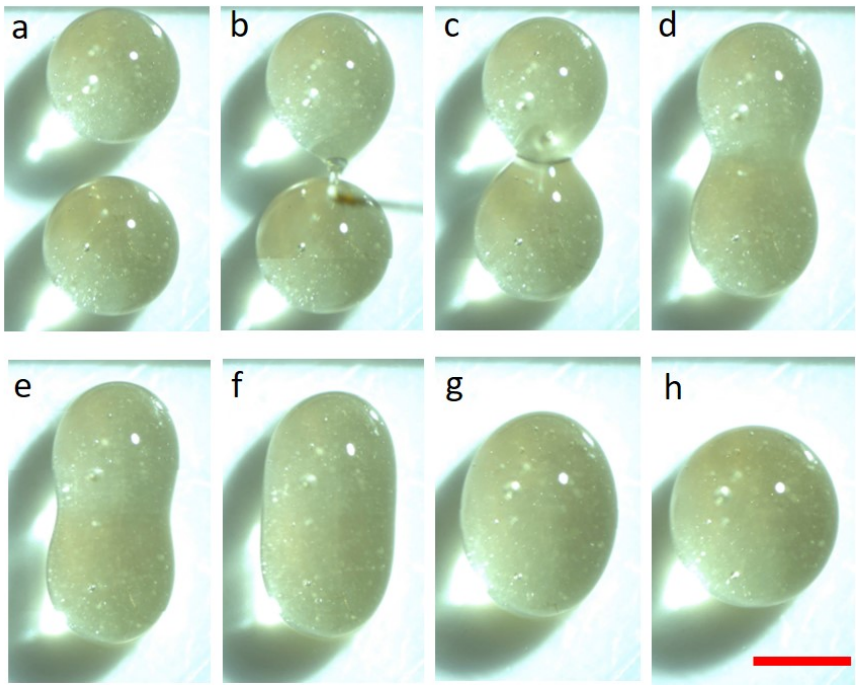

Figure 62. Coalescing two honey droplets on SLIPS. (a) Two 2-µL droplets. (b) 0s. (c) 0.6s. (d) 0.93s. (e) 1.16s. (f) 1.56s. (g) 2.76s. (h) 4.96s. Scale bar: 1.5 mm.

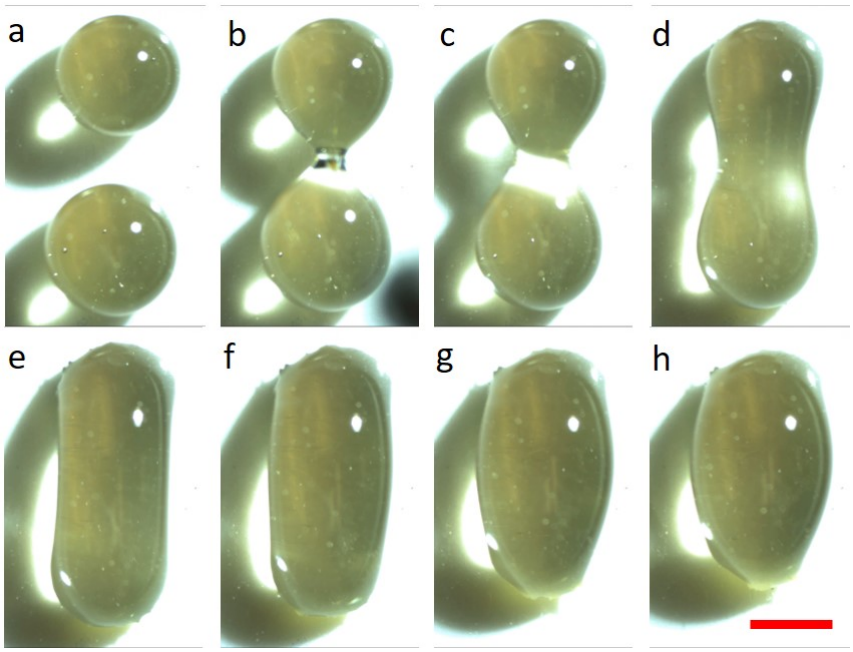

Figure 63. Coalescing two honey droplets on Teflon surface. (a) Two 2-µL droplets. (b) 0s. (c) 0.7s. (d) 2.3s. (e) 6.5s. (f) 17.9s. (g) 40s. (h) 62s. Scale bar: 1.5 mm.

droplets by a light pin, they tend to coalesce gradually. The necking area becomes larger and disappears after 1.56s. The final shape is one larger spherical droplet after 5s, which shows the coalescence completed. The above process is mainly under surface tension with very low surface friction. Therefore, the SLIPS is suitable to decrease the surface adhesion, which is necessary to wide-spectrum digital microfluidics. As the reference, when two honey droplets are placed on the Teflon surface, it is very hard to coalesce to be a spherical droplet. In Figure 63, after poking the two droplets, the necking area also turns to widen, but the speed is very slow. After 6.5s, the necking area still exists, while after 17.9s, it disappears. At 62s, the shape of the honey droplet is not spherical, but an irregular shape with two light ends and heavy center. Even longer time is not helpful to deform the shape again. On Teflon surface, the adhesion force is strong enough to resist the complete coalescence. Although the droplet deforms a lot, the final equilibrium state is when the adhesion force balances surface tension. The influence of the adhesion is not negligible, severely hindering the movement of sticky droplet. It can be concluded that even on the low friction solid surface, the digital microfluidic device will fail for many sticky fluids, and the SLIPS is an indispensable component for wide-spectrum device.

4.2.2 Droplet transporting

Conductive and dielectric droplets are performed to transport on the wide-spectrum digital microfluidic device, including bio-solutions and complex fluids. Figure 64 shows the transporting of some conductive liquids, like DI water at 300 V, 1 mg/mL protein solution at 300 V, detergent at 250 V and saline at 300 V. By sequentially powering on the left two electrode couples, the droplets are moved from right to left. Similarly, in Figure 65, DNA solution (350 V), glycerol (300 V), honey (300 V) and ionic liquid (250 V) are transported successfully. Not only conductive

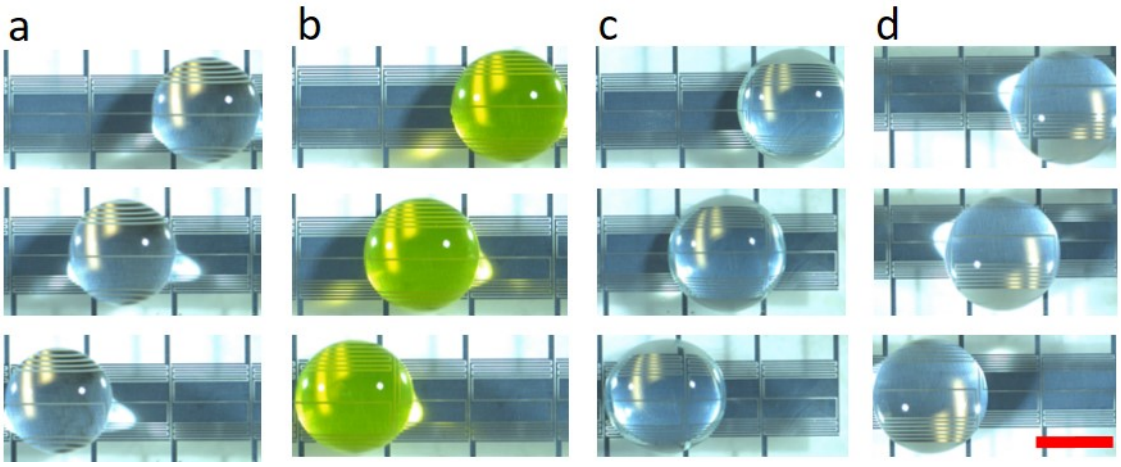

Figure 64. Transporting of conductive fluids. (a) DI water, 300 V. (b) 1 mg/mL protein, 300 V. (c) Detergent, 250 V. (d) Saline, 300 V. Scale bar: 1.5 mm.

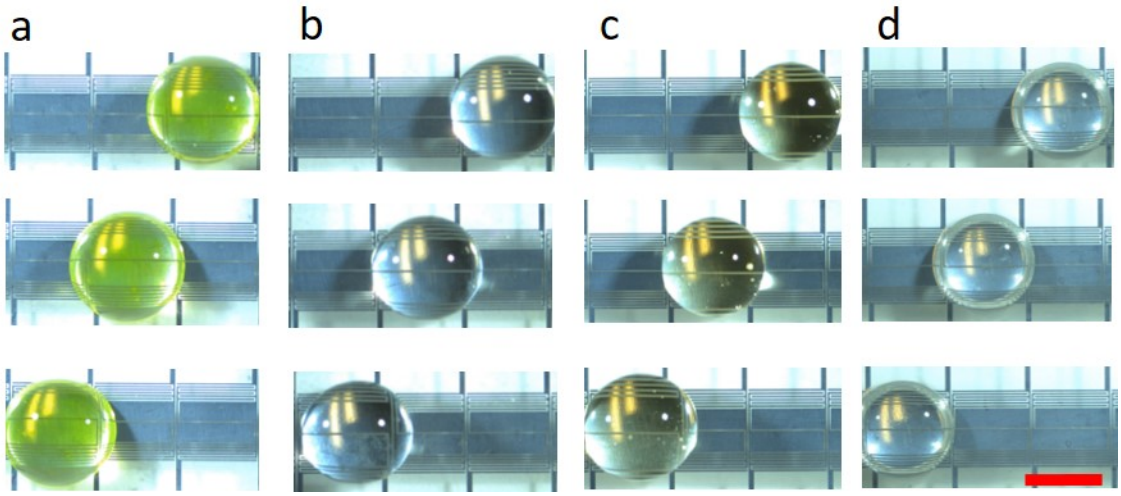

Figure 65. (Continued) transporting of conductive fluids. (a) DNA solution, 350 V. (b) Glycerol, 300 V. (c) Honey, 300 V. (d) Ionic liquid, 250 V. Scale bar: 1.5 mm.

fluids, dielectric liquids are also actuated to move on the digital microfluidic device. In Figure 66, IPA (250 V), propylene carbonate (300 V), fish oil (450 V) and vegetable oil (450 V) can be transported easily. Figure 67 shows the transporting of dodecane (450 V), low viscosity silicone oil (10 cSt, 450 V), medium viscosity silicone oil (100 cSt, 450 V) and high viscosity silicone oil

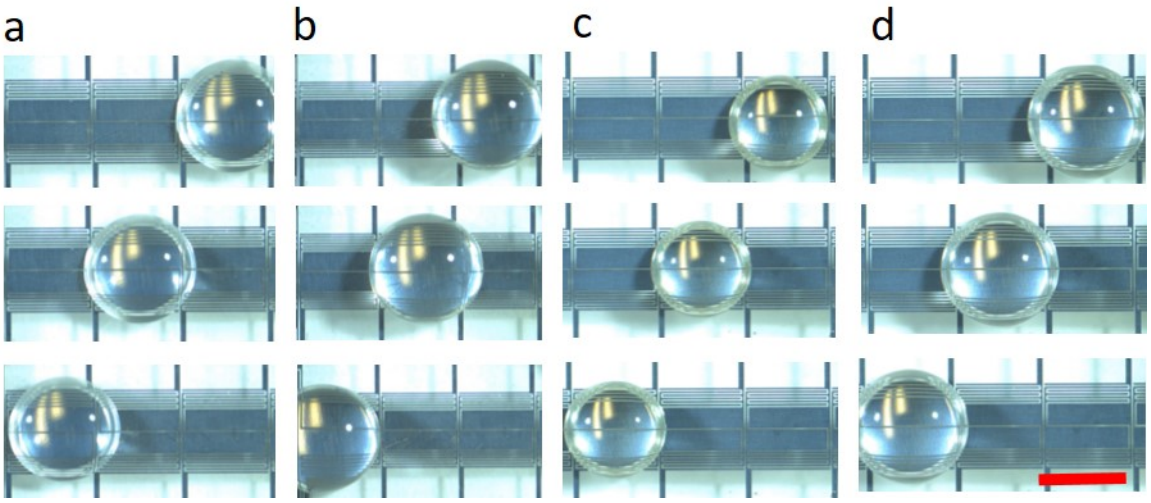

Figure 66. Transporting of dielectric fluids. (a) IPA, 250 V. (b) Propylene carbonate, 300 V. (c) Fish oil, 450 V. (d) Vegetable oil, 450 V. Scale bar: 1.5 mm.

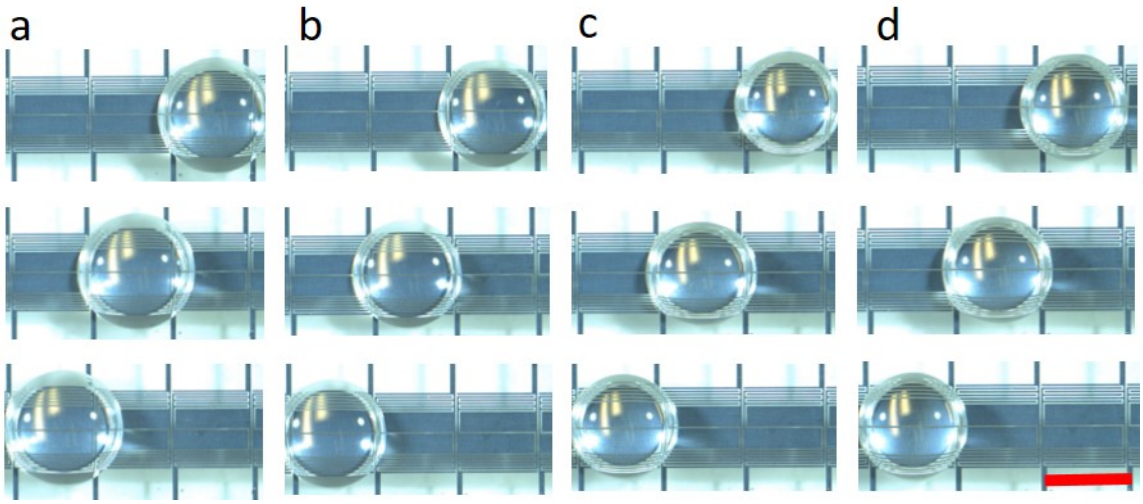

Figure 67. (Continued) Transporting of dielectric fluids. (a) Dodecane, 450 V. (b) Silicone oil (10 cSt), 450 V. (c) Silicone oil (100 cSt), 450 V. (d) Silicone oil (1000 cSt), 450 V. Scale bar: 1.5 mm.

(1000 cSt, 450 V). In addition, both light and heavy crude oil can be transported at 450 V, as shown in Figure 68. Therefore, the wide-spectrum digital microfluidic device works for different kinds of fluids, including conductive and non-conductive ones. For bio-solutions, the biofouling problem

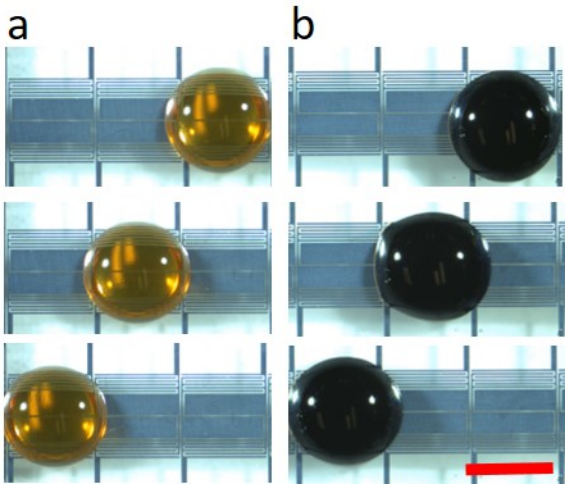

Figure 68. Transporting of crude oils. (a) Light crude oil, 450 V. (b) Heavy crude oil, 450 V. Scale bar: 1.5 mm.

is always serious for common conventional hydrophobic surfaces, which highly increases the contact angle hysteresis, impeding the transporting. SLIPS has been proved the capability of anti-biofouling, which is necessary for real applications of digital microfluidics. The sticky and high viscosity droplets can also move smoothly on the device with the integration of SLIPS.

4.2.3 Difference between electrowetting and dielectrowetting

To understand the inherent principles of droplet transporting, it is needed to distinguish electrowetting and dielectrowetting. Generally, electrowetting corresponds to conductive liquids, while dielectrowetting to dielectric liquids. Unlike electrowetting, dielectrowetting is a new term reported short time ago. The arrangement of the electrodes for dielectrowetting is totally different from electrowetting. Conventional electrowetting structure consist of top electrode inserted into droplet and bottom electrode, which is located underneath the dielectric layer. Upon applying voltage, the contact angle of the droplet will decrease remarkably. However, if such configuration

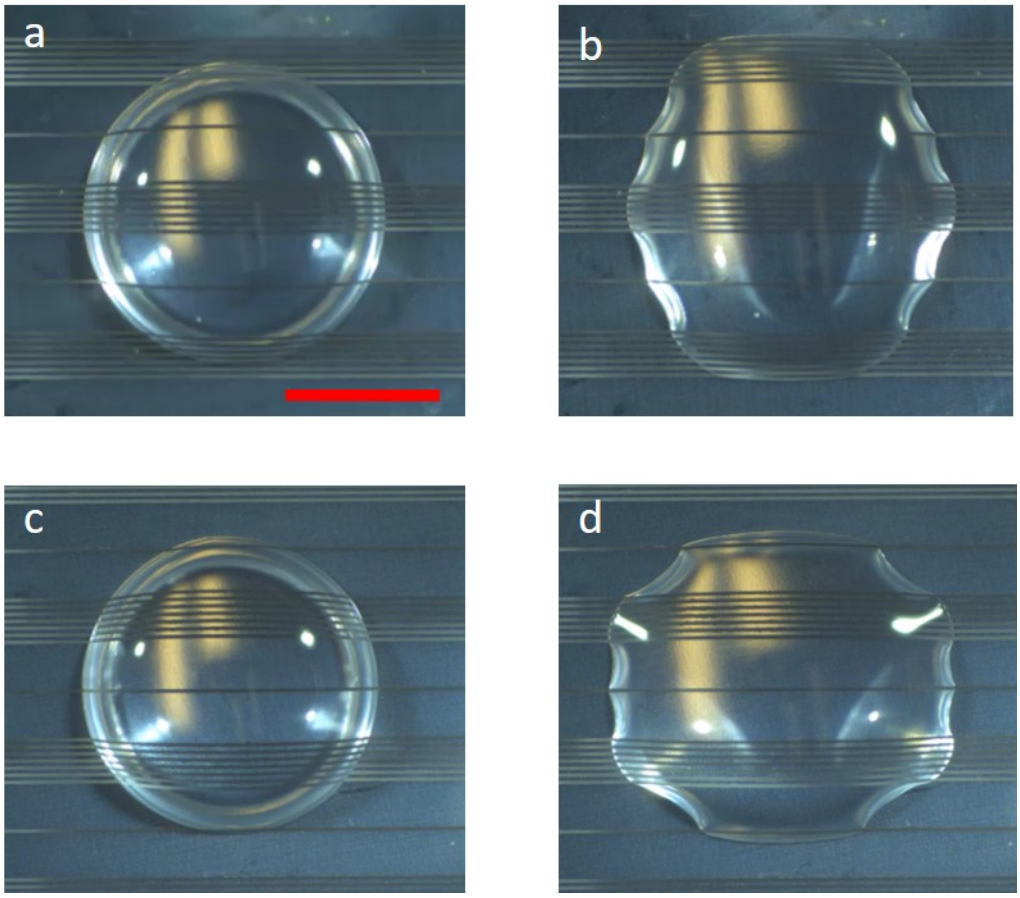

Figure 69. Spreading of 10 cSt silicone oil at different positions. (a) and (b) showing when the middle area of the droplet is at the dielectrowetting zone, the droplet is elongated vertically to the electrode direction. (c) and (d) showing when the middle area of the droplet is at the electrowetting zone, it is stretched along the electrode direction. Scale bar: 1.5 mm.

is applied to dielectric liquids, there is no contact angle change. On the other hand, dielectrowetting consists of interdigital electrodes, which can change the contact angle of non-conductive liquid. The mechanism is that the dense electrodes generate strong fringing field near the surface, and such non-uniform field induces a net dielectrophoretic force for dielectric liquid. With enough voltage applied, the force can drive the dielectric droplet to spread along the interdigital electrodes,

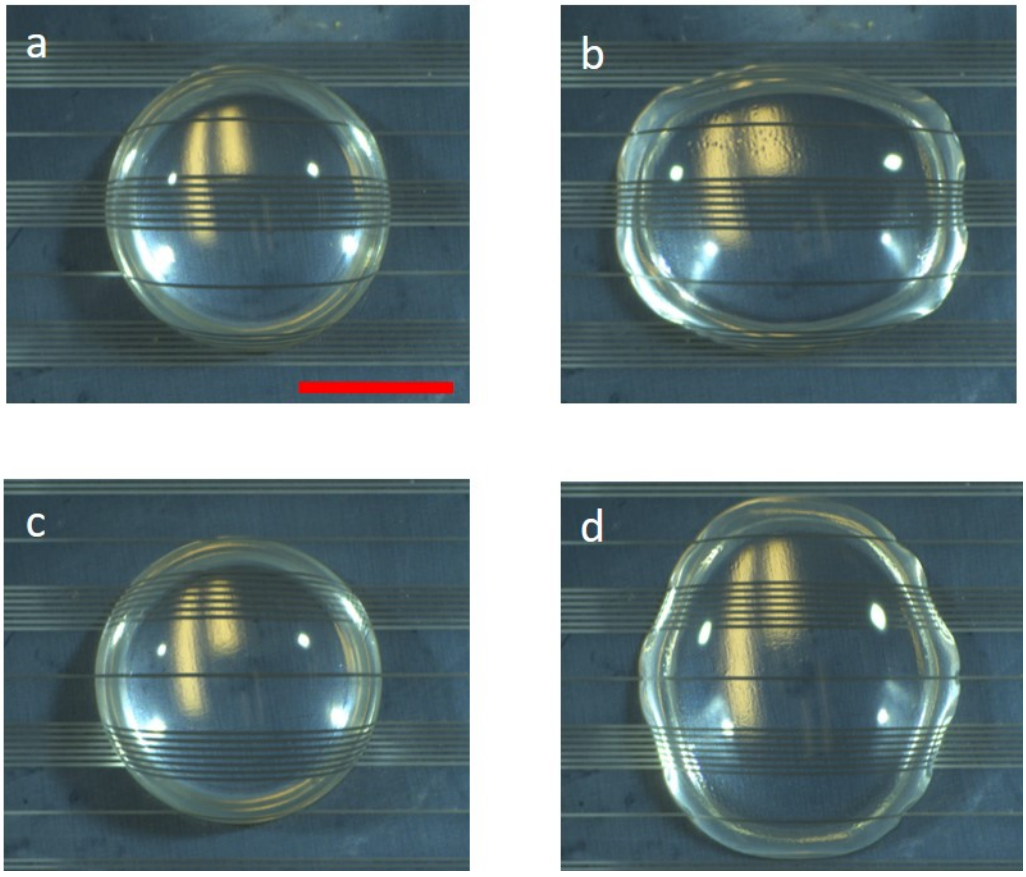

Figure 70. Spreading of ionic liquid at different positions. (a) and (b) showing when the middle area of the droplet is at the dielectrowetting zone, the droplet is elongated along the electrode direction. (c) and (d) showing when the middle area of the droplet is at the electrowetting zone, it is stretched vertically to the electrode direction. Scale bar: 1.5 mm.

resulting in the contact angle change in one direction. Therefore, the principle of dielectrowetting can be exploited to transport dielectric liquids.

Figure 69 shows the spreading of 10 cSt silicone oil at different positions. Since it is dielectric liquid, dielectrowetting dominates during the spreading. If the middle area of the droplet is at the dielectrowetting zone, the droplet is elongated vertically to the electrode direction, because the strong fringing field will attract the dielectric liquid, while the electrowetting zone has very small influence on it. If the middle area of the droplet is at the electrowetting zone, it is stretched

along the electrode direction, because the two dielectrowetting zones will induce more liquid in such regions and electrowetting zones at the two edges hold less liquid. It can be observed that at the gaps of electrowetting zones, the oil is stretched to some extent. This phenomenon also can be explained by the dielectrophoresis force, which is generated by the fringing field.

As for conductive liquid, the phenomena are opposite, as shown in Figure 70. Ionic liquid is highly conductive, which is actuated by electrowetting. When the middle area of the droplet is at the electrowetting zone, the droplet is elongated along the electrode direction, because the dielectrowetting zones at the two edges have very small influence on it. When the middle area of the droplet is at the electrowetting zone, it is stretched vertically to the electrode direction, because the two electrowetting zones at the two edges attract more liquid than the dielectrowetting zones. The dielectric and conductive liquids show the distinct difference between dielectrowetting and electrowetting.

4.2.4 Droplet transporting by interdigital electrodes

For dielectric droplet, the driving force is generated by the dielectrowetting zone, where interdigital electrodes are arranged. To visualize the transporting of different types of droplets actuated by such electrodes, the purely interdigital electrodes are exploited. If such structure works well for dielectric liquids, while inefficiently for conductive ones, it is proved that the dielectrowetting zone is essential to move dielectric droplets.

Figure 71(a) shows the structure of one electrode couple, with size and spacing same as previous ones. Different dielectric droplets are transported on such digital microfluidic device, such as dodecane, 1000 cSt silicone oil, heavy crude oil, vegetable oil and light crude oil, as shown in Figure 71(b)-(f). All the operations are at 450 V. Therefore, the interdigital electrodes can

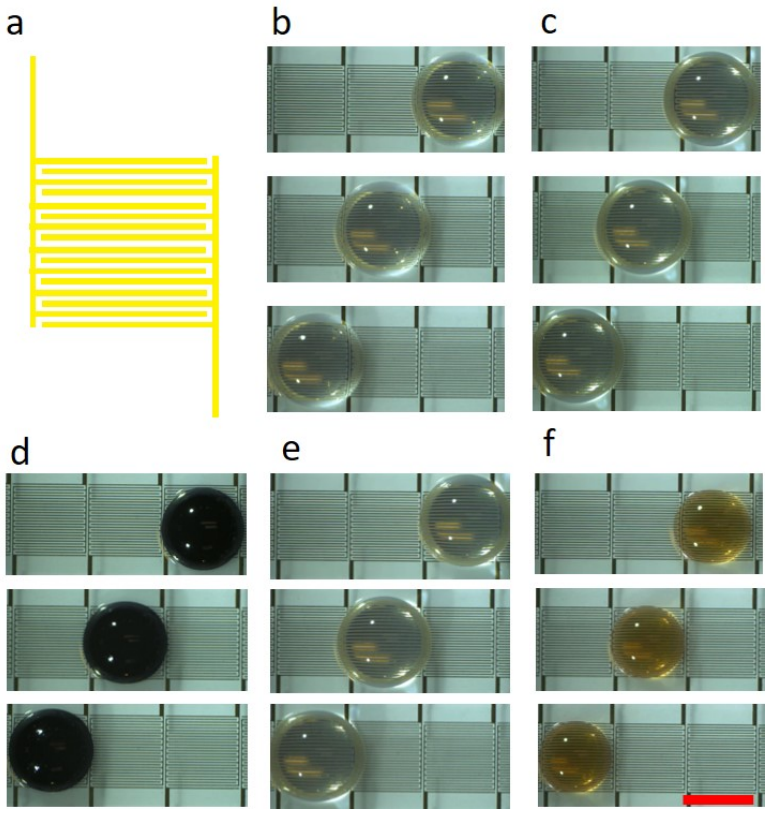

Figure 71. Transporting of dielectric droplets by interdigital electrodes. (a) Schematic of interdigital electrodes. (b) Dodecane, 450 V. (c) 1000cSt silicone oil, 450 V. (d) Thick crude oil, 450 V. (e) Vegetable oil, 450 V. (f) Thin crude oil. Scale bar: 1.5 mm.

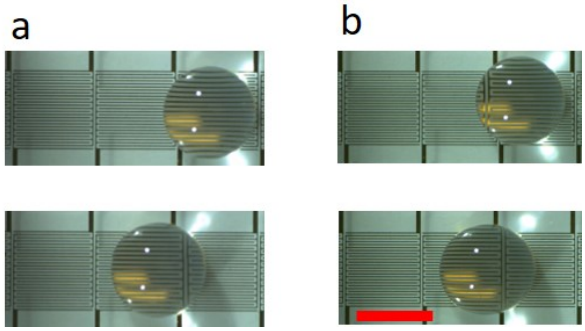

Figure 72. Transporting of conductive droplets by interdigital electrodes. (a) Saline, 300 V. Even after 3s, the droplet can not be transported to the second electrode couple. (b) DI water, 300 V. The transporting is not successful after 4s actuation. Scale bar: 1.5 mm.

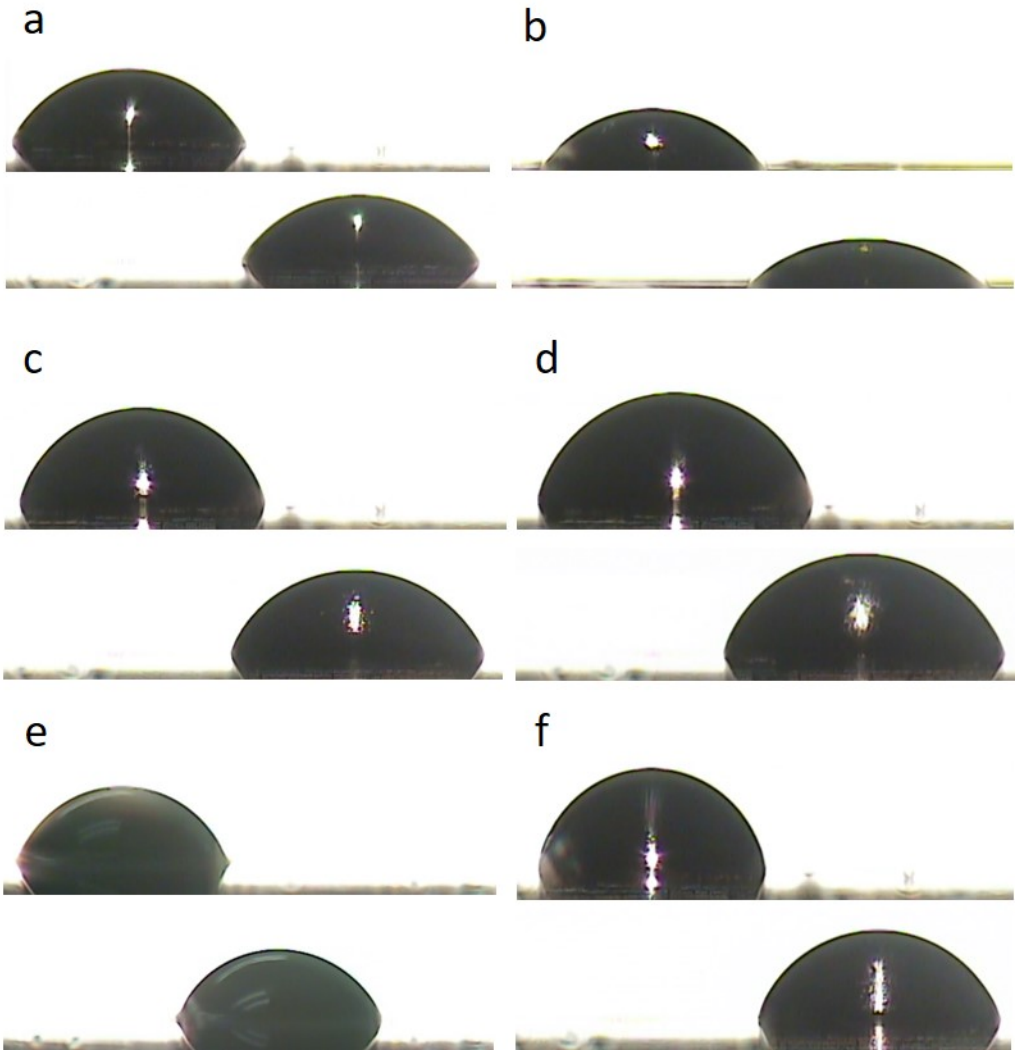

Figure 73. Side views of transporting of dielectric droplets. (a) Dodecane, 450 V, at 0s and 3.3s. (b) 10cSt silicone oil, 450 V, at 0s and 1.2s. (c) 100cSt silicone oil, 450 V, at 0s and 3.2s. (d) 1000cSt silicone oil, 450 V, at 0s and 7s. (e) Thick crude oil, 450 V, at 0s and 6s. (f) Vegetable oil, 450 V, at 0s and 3s.

actuate dielectric liquids easily, which is the indispensable part of the wide-spectrum digital microfluidic device. On the other hand, the purely interdigital electrodes are not efficient to conductive droplets. In Figure 72, saline and DI water are tested by powering on the middle electrode couple with 300 V. Even after 3s, the saline droplet cannot be transported to the right position of the middle region. As for DI water, the transporting is not successful, either, even after

4s actuation. This experiment demonstrates the limitation of interdigital electrodes, which are not suitable for conductive fluids.

Meanwhile, for dielectric liquid, the transporting is not only determined by the electrodes, but also by the properties of liquid, like dielectric constant, viscosity and density. In Figure 13, side views of different droplets at one transporting step are shown on the interdigital electrodes. Figure 73(a) shows the transporting of dodecane at 450 V, which can be achieve in 3.3s. Figure 73(b) to 73(d) show the different silicone oils in transporting. For 10cSt silicone oil, one step transporting is completed in 1.2s at 450 V, while for 100cSt and 1000cSt silicone oils, the times needed are 3.2s and 7s at the same condition. The transporting velocity should be determined by the viscosity, as well as influenced by the density and volume. In Figure 73(e), heavy crude oil is also transported in 6s at 450 V. In Figure 73(f), vegetable oil achieves the same process within 3s. Most of the dielectric droplets can be transported within 3.5s, while ones with high viscosities need longer time, but still less than 7s. Therefore, the dielectrowetting is efficient for dielectric droplet transporting, and not reliable for conductive droplet.

4.2.5 Droplet transporting by solid electrodes

It is well known the solid electrodes are utilized to actuate conductive droplets based on electrowetting mechanism. However, how it influences dielectric droplets is not studied yet. In Figure 74, different silicone oils are transported by the solid electrode couple, but the velocities are very low compared to the dielectrowetting method. For 10cSt silicone oil, 11.8s is required to transport the droplet from one electrode couple to the next. The time ranges are even longer for 100cSt and 1000cSt silicone oils, which are 50.3s and 62.9s, respectively. All the operations are at 450s, same as dielectrowetting. Within 10s, the two oils only deform a little, meaning that the

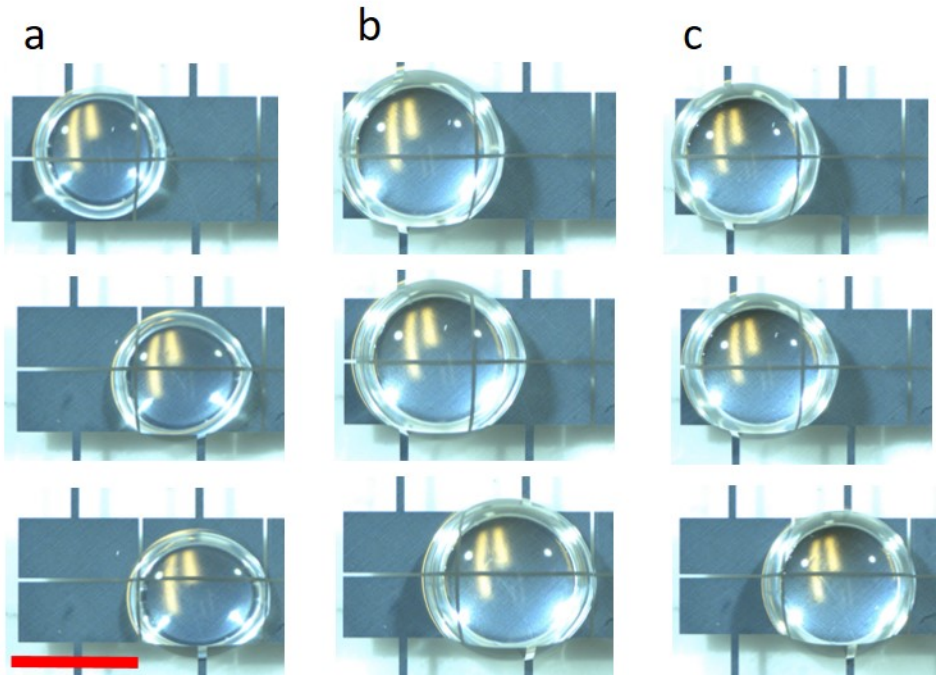

Figure 74. Transporting of dielectric droplets by solid electrodes. (a) 10cSt silicone oil, 450 V, at 0s, 6.8s and 11.8s. (b) 100cSt silicone oil, 450 V, at 0s, 8.3s and 50.3s. (a) 1000cSt silicone oil, 450 V, at 0s, 8.3s and 62.9s. Scale bar: 1.5 mm.

solid electrodes are not efficient for dielectric droplet transporting. If the droplets are conductive, the results are totally different, as shown in Figure 75. The saline droplet can be transported within 0.3s and the DI water droplet can achieve it in 1.5s at 300 V. However, when the dielectric liquids are applied to the same electrodes, the transporting is not successful, as shown in Figure 76. In fact, the dodecane and heavy crude oil only deform a little at 450 V, without any signs of transporting even after 40s actuations. It is suspected that the weak driving force for dielectric liquid is from the gap region of solid electrode couple, because the fringing field is generated in such region. Figure 77(a) shows that when voltage applied, the vegetable droplet stretches a little around the gap region. If the volume of the droplet is decreased, the transporting effect is more notable, as shown from Figure 77(b) to 77(d). When the droplet is small enough, the transporting

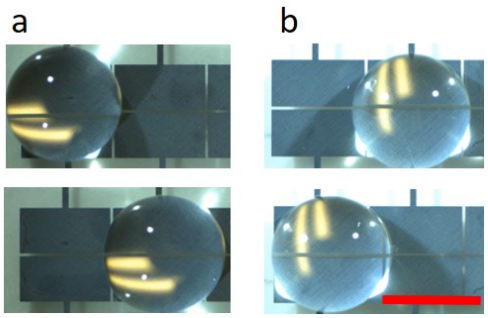

Figure 75. Transporting of conductive droplets by solid electrodes. (a) Saline, 300 V, at 0s and 0.3s. (b) DI water, 300 V, at 0s and 1.5s. Scale bar: 1.5 mm.

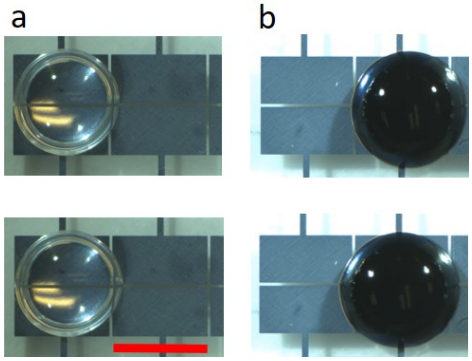

Figure 76. Transporting of dielectric droplets by solid electrodes. (a) Dodecane, 450 V, at 0s and 30s. (b) Thick crude oil, 450 V, at 0s and 30s. Scale bar: 1.5 mm.

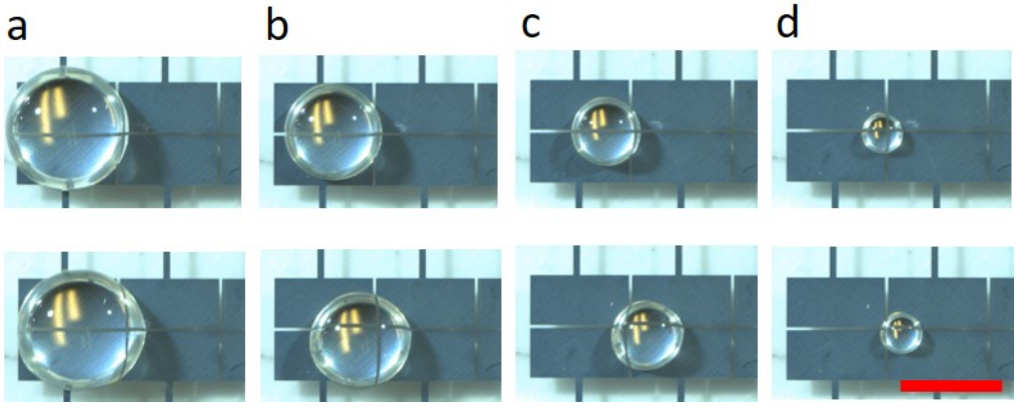

Figure 77. Size effect of droplet on the transporting of vegetable oil by solid electrodes. (a) 0s and 8.2s. (b) 0s and 8.8s. (c) 0s and 5.4s. (d) 0s and 4.5s. All at 450 V. Scale bar: 1.5 mm.

can be achieved around 5s. Therefore, the dielectrowetting can be seen as the amplification of the single gap region. With dense arrange of fringing fields, the dielectrophoretic force is large enough to actuate the droplet with low dielectric constant, which is not achievable for solid electrodes.

4.2.6 Applications of wide-spectrum digital microfluidics

Since the wide-spectrum digital microfluidics can transport both conductive and dielectric fluids, it is promising to integrate the conductive and dielectric droplet manipulations on a single chip. Figure 78(a) shows the coalescence of protein solution and silicone oil. The concentration of protein is 1 mg/mL and the viscosity of silicone oil is 100cSt. When activating the middle electrode couple with 300 V, the two droplet will contact each other and coalesce swiftly. Finally, the protein droplet is enclosed by the oil. Such core-shell structure will reduce the evaporation process of protein solution. To compare the difference between core-shell droplet and bare protein droplet, the experiment is carried out, as shown in Figure 78(b). After 18 min, the bare droplet is dried, while the protein droplet in the oil shrinks. As the time goes, the evaporation speed of core-shell protein decreases. The total drying time of the core-shell droplet is about 3.5h, after which a tiny protein dot is formed in the silicone oil. The protein dot can be transported by moving the oil droplet, as shown in Figure 79(a) and (b), where the voltage is 450 V. In addition, the protein can be dissolved again by coalescing another water droplet. As shown in Figure 79(c) and (d), activating the middle electrode couple at 450 V, the water and silicone oil forms another core-shell structure. When the protein dot contacts water, it becomes dissolved slowly, as shown from 79(e) to (i). About 1 min later, the protein is dissolved into water uniformly. Figure 79(j) shows the transporting of core-shell droplet by powering on the electrode couple on the left side at 450 V.

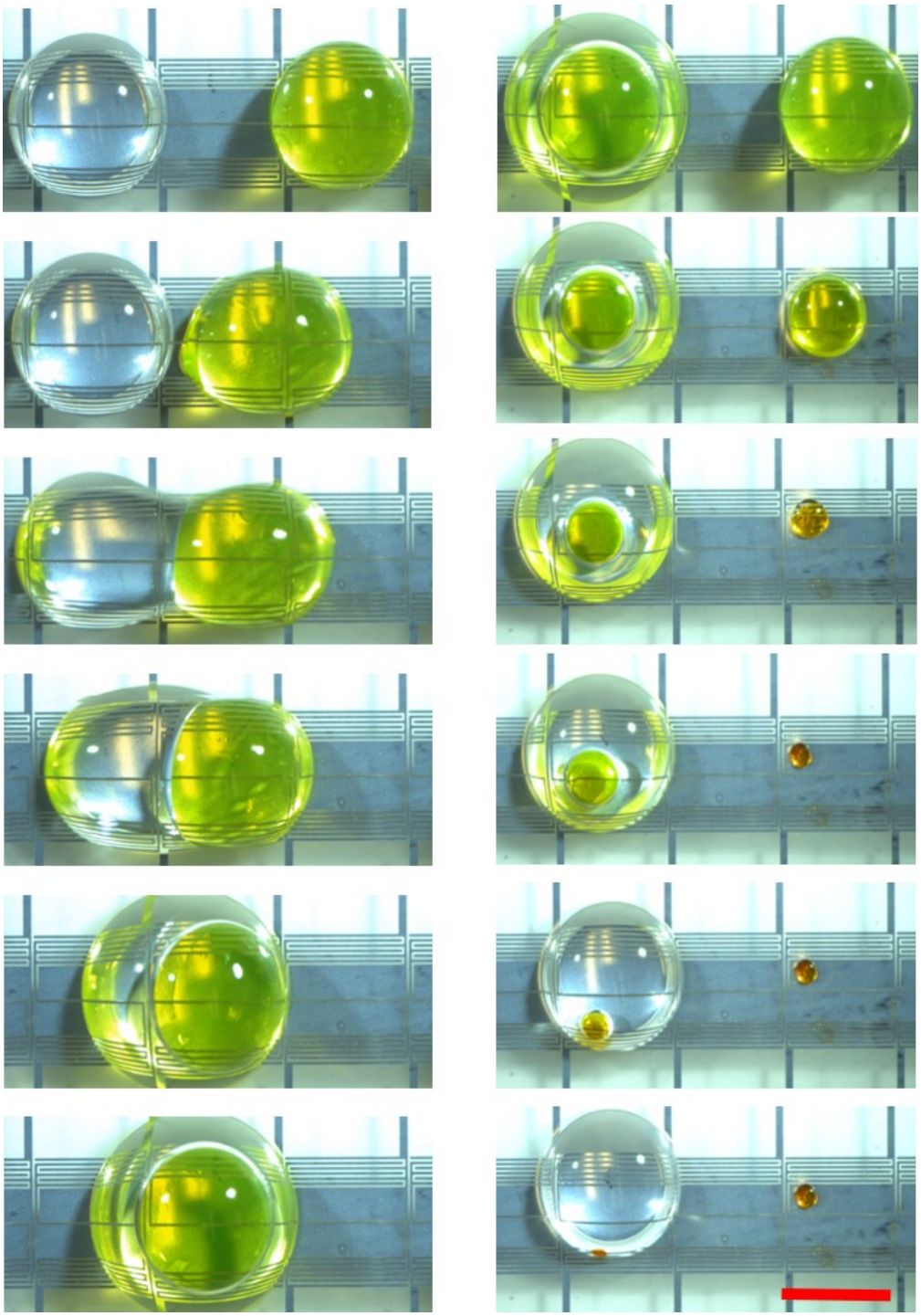

Figure 78. Water-silicone oil coalescence. (a) By powering on the middle electrode couple with 300 V, the protein solution is immersed by 100cSt silicone oil. 0s and 8.2s. (b) Drying of protein in oil and air environment at 0min, 12min, 16min, 18min, 2h and 3.5h. Scale bar: 1.5 mm.

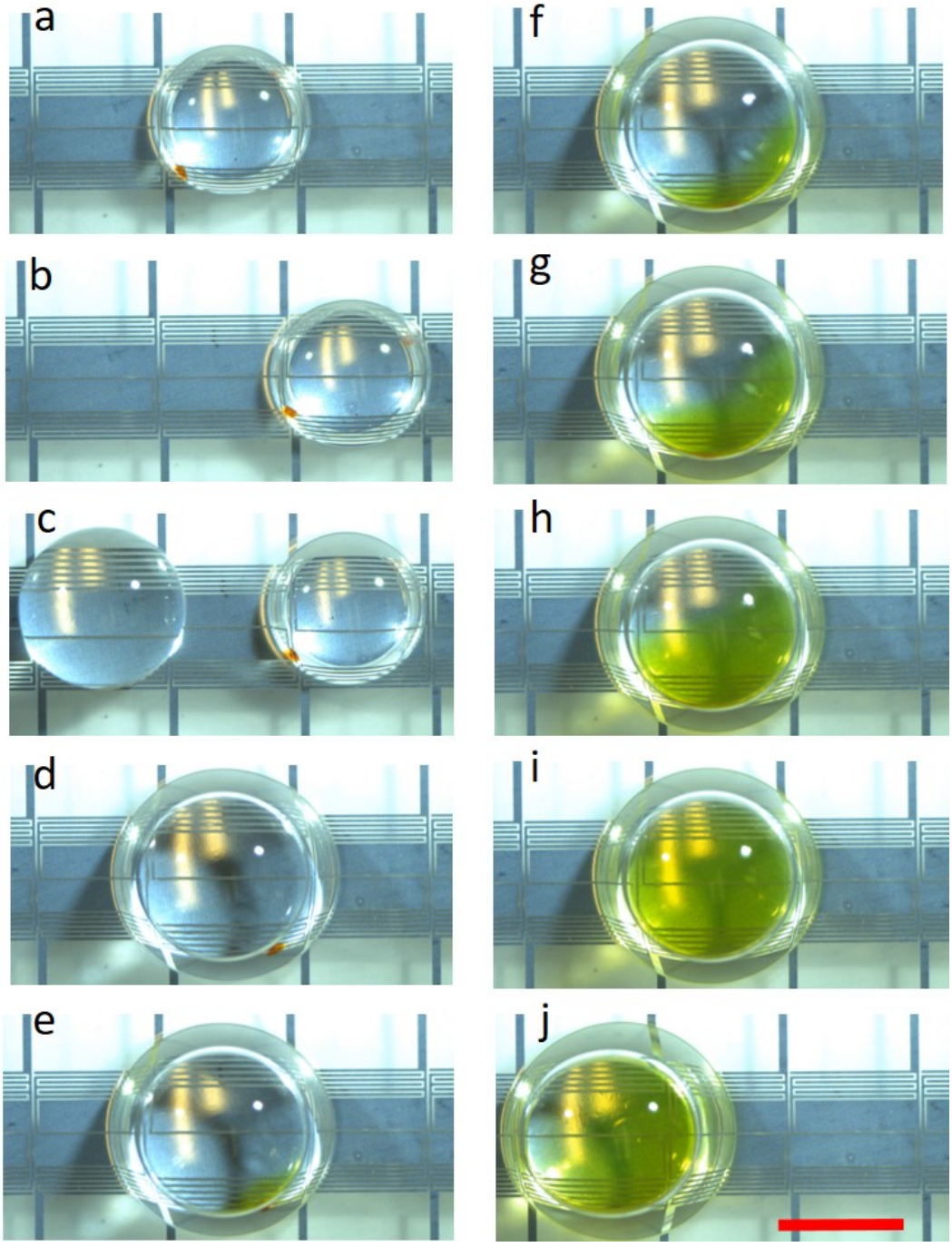

Figure 79. (Continued) Water-silicone oil coalescence. (a)-(b)Dried protein transported by silicone oil, 450 V. (c)-(d) DI water and silicone oil coalesce by powering on the middle electrode couple, 450 V. (e)-(i) Dried protein dissolving into water at 6s, 12s, 30s, 48s and 68s. (j) Water-oil coalescence transporting, 450 V. Scale bar: 1.5 mm.

Therefore, the wide-spectrum digital microfluidic device can be applied to transport water, oil or the combination, as well as solid solute.

4.2.7 Contact angle change by electrowetting and dielectrowetting

Dieletrowetting is that when voltage is applied to the dense interdigital electrodes, the contact angle of dielectric liquid on it will change. This phenomenon is similar to electrowetting, where contact angle of conductive droplet is decreased when applying voltage to the droplet and electrode beneath it. It is necessary to distinguish them from the view of physical principles, because the different behaviors will determine the transporting methods of conductive and dielectric droplets.

In Figure 80, light crude oil is utilized the testing liquid by electrowetting and dielectrowetting. When the droplet is on the interdigital electrodes, the contact angle will decrease with voltage applied. The contact angle change is 8^o at 250 V, and 19.2^o at 450 V, which increases with voltage. However, with electrowetting configuration, there is no contact angle change, even when high voltage applied. Figure 80 (b) and (c) show the difference between dielectrowetting and dielectrowetting. With dielectrowetting, the contact angle is 73.6^o at 0 V, and 44.6^o at 450 V, while with electrowetting, the contact angle remains same.

If the dielectric liquid is 10cSt silicone oil, the phenomenon is same. In Figure 81(a), as the voltage increases to 450 V, electrowetting has no effect on the oil, while the contact angle change is 16^o at 450 V with dielectrowetting. In Figure 81(b), the initial contact angle is 60^o, and it becomes 43.8^o at 450 V with dielectrowetting. On the other hand, the contact angles at 0 V and 450 V are same with electrowetting, as shown in Figure 81(c).

As for the dielectric liquid with low dielectric constant, it is more difficult to actuate it with electrical potential. In this case, dielectrowetting still works, as shown in Figure 82, where

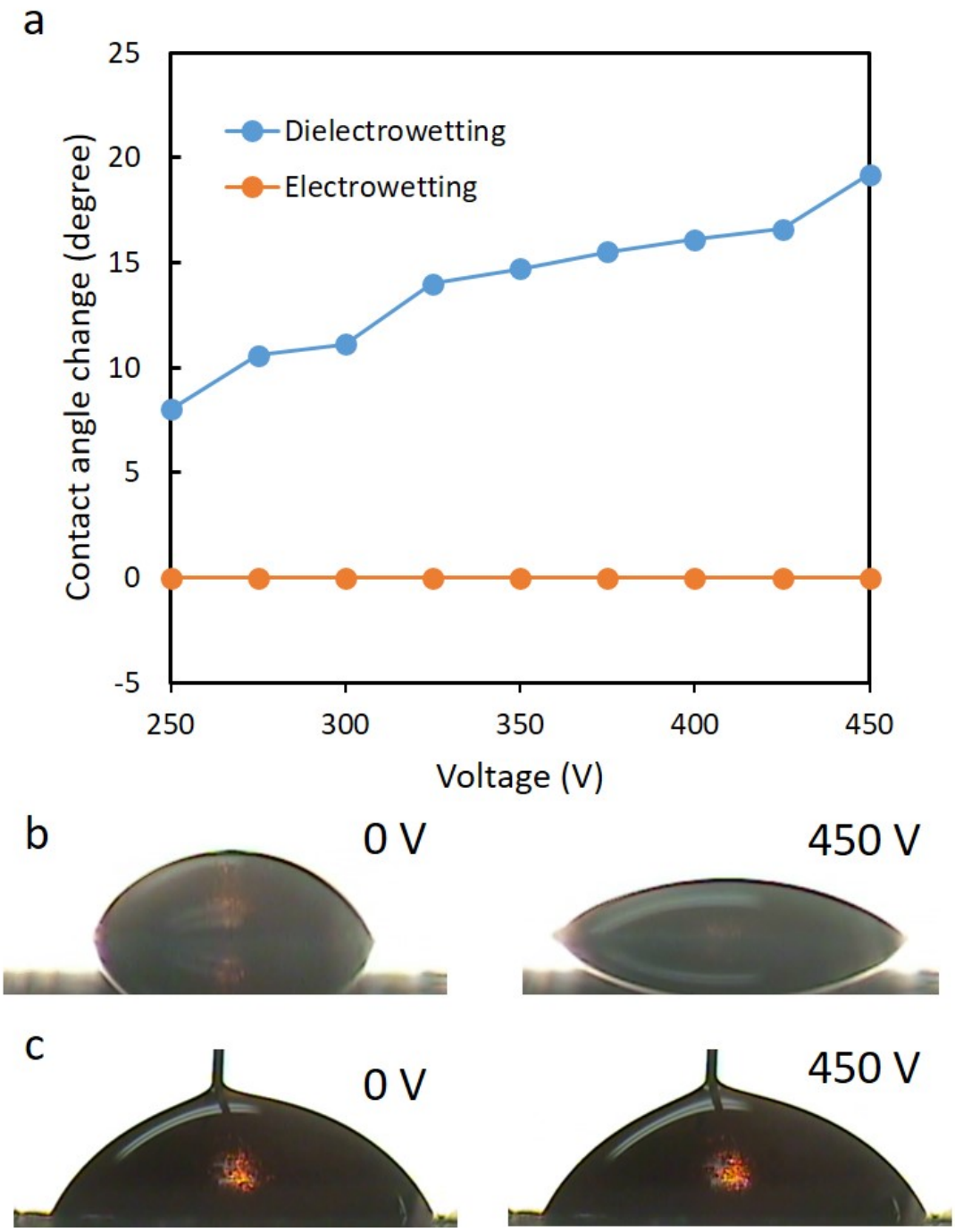

Figure 80. Dielectrowetting and electrowetting effects on light crude oil. (a) As the voltage increases to 450 V, electrowetting has no effect on the oil, while the contact angle change can be 20º with dielectrowetting. (b) With dielectrowetting, the contact angle is 73.6º at 0 V, and 44.6º at 450 V. (c) With electrowetting, the contact angle remains same.

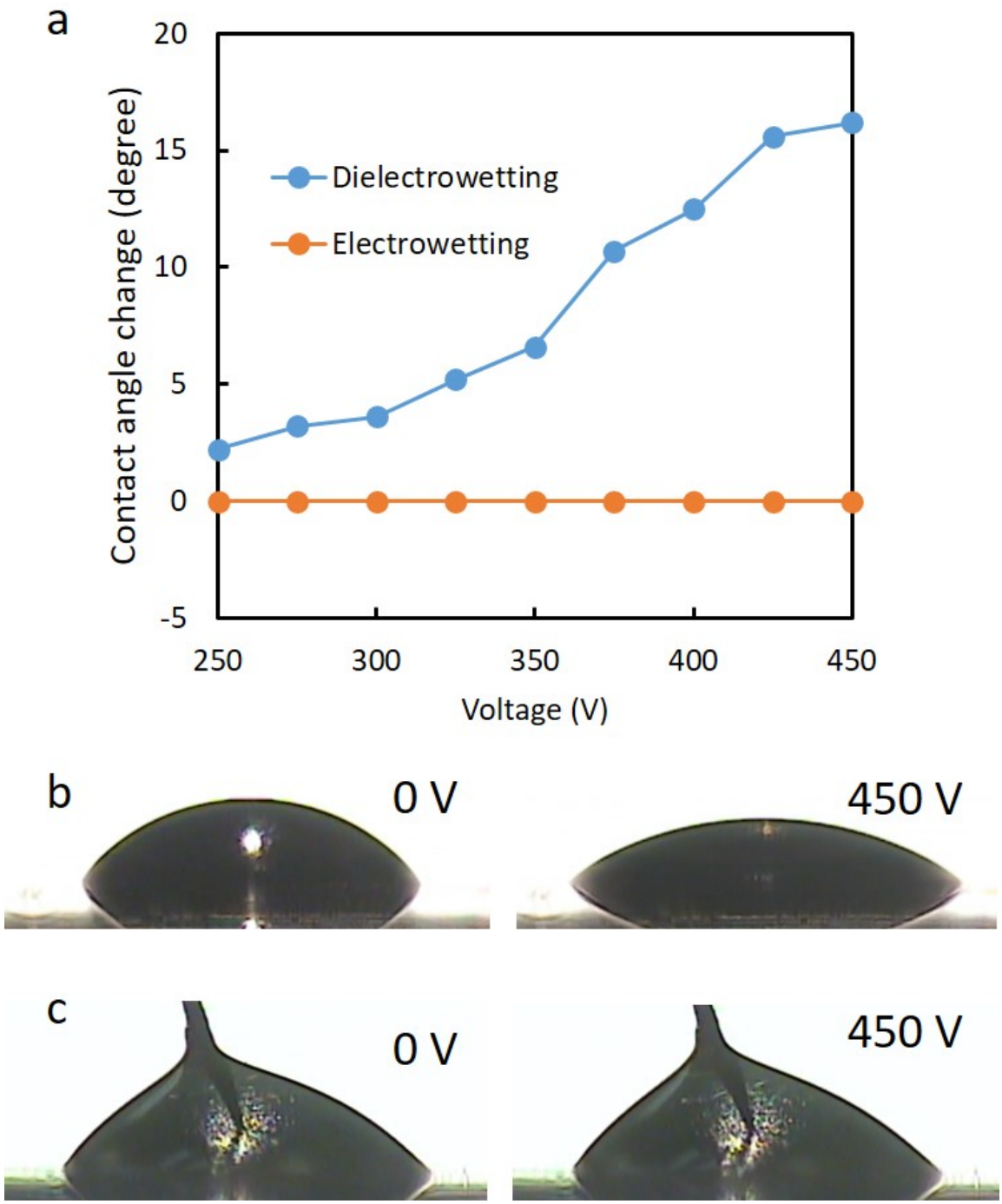

Figure 81. Dielectrowetting and electrowetting effects on 10 cSt silicone oil. (a) As the voltage increases to 450 V, electrowetting has no effect on the oil, while the contact angle change can be 16^{o} with dielectrowetting. (b) With dielectrowetting, the contact angle is 60^{o} at 0 V, and 43.8^{o} at 450 V. (c) With electrowetting, the contact angle remains same.

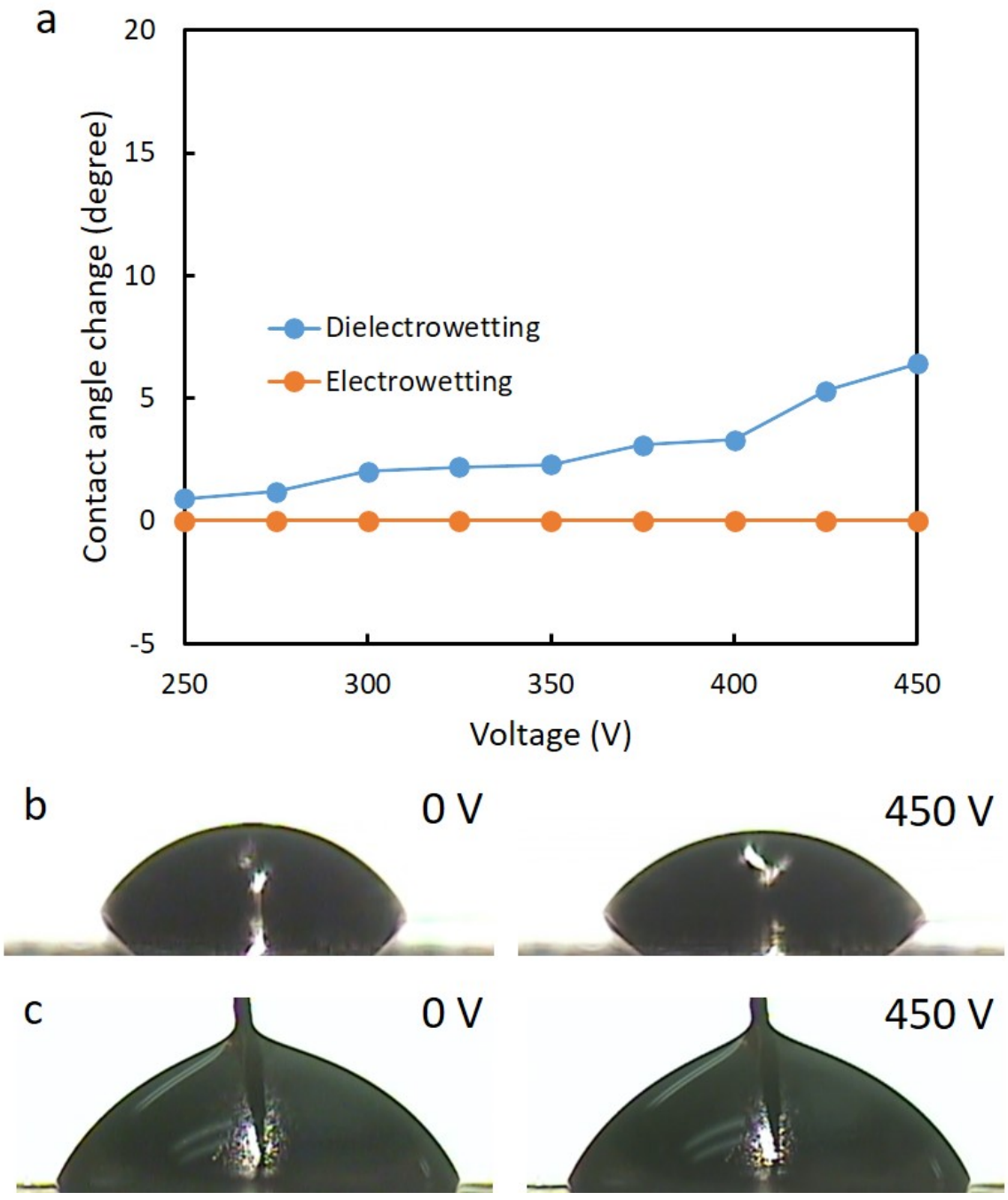

Figure 82. Dielectrowetting and electrowetting effects on dodecane. (a) As the voltage increases to 450 V, electrowetting has no effect on the oil, while the contact angle change is 6.4^{o} with dielectrowetting. (b) With dielectrowetting, the contact angle is 65.2^{o} at 0 V, and 58.8^{o} at 450 V. (c) With electrowetting, the contact angle remains same.

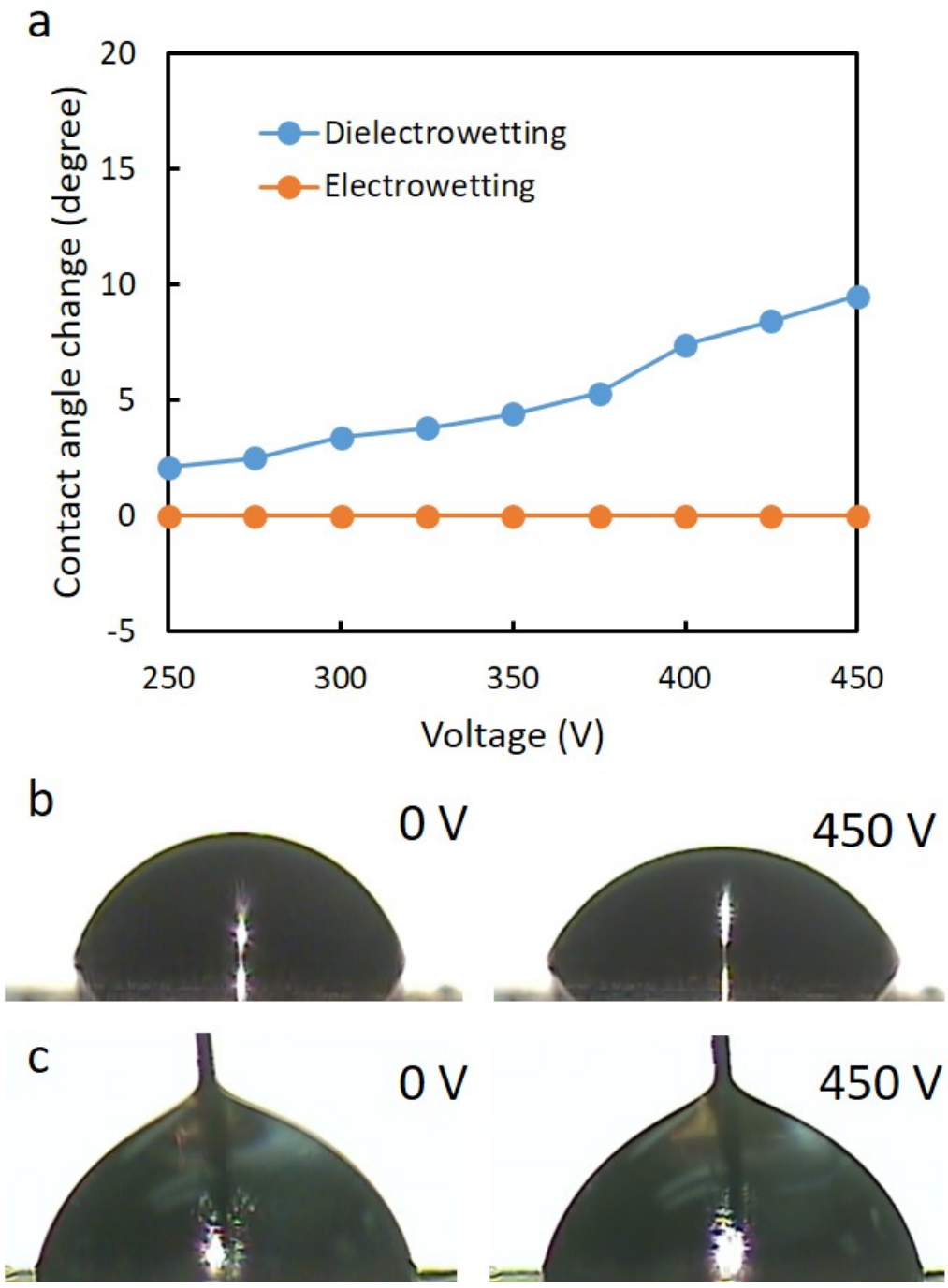

Figure 83. Dielectrowetting and electrowetting effects on 1000 cSt silicone oil. (a) As the voltage increases to 450 V, electrowetting has no effect on the oil, while the contact angle change is 9.5° with dielectrowetting. (b) With dielectrowetting, the contact angle is 77.5° at 0 V, and 68° at 450 V. (c) With electrowetting, the contact angle remains same.

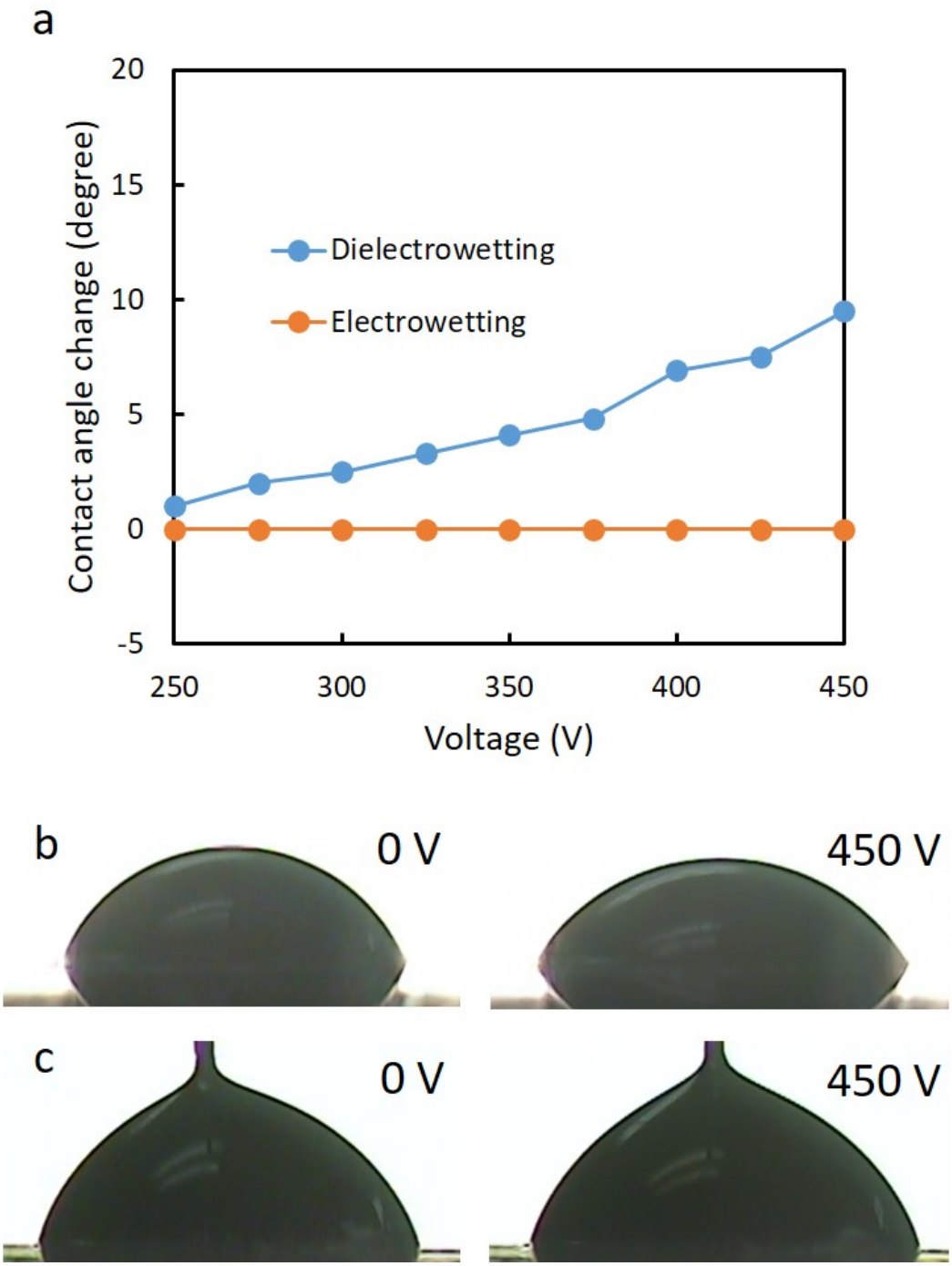

Figure 84. Dielectrowetting and electrowetting effects on heavy crude oil. (a) As the voltage increases to 450 V, electrowetting has no effect on the oil, while the contact angle change is 9.5^{o} with dielectrowetting. (b) With dielectrowetting, the contact angle is 71.9^{o} at 0 V, and 62.4^{o} at 450 V. (c) With electrowetting, the contact angle remains same.

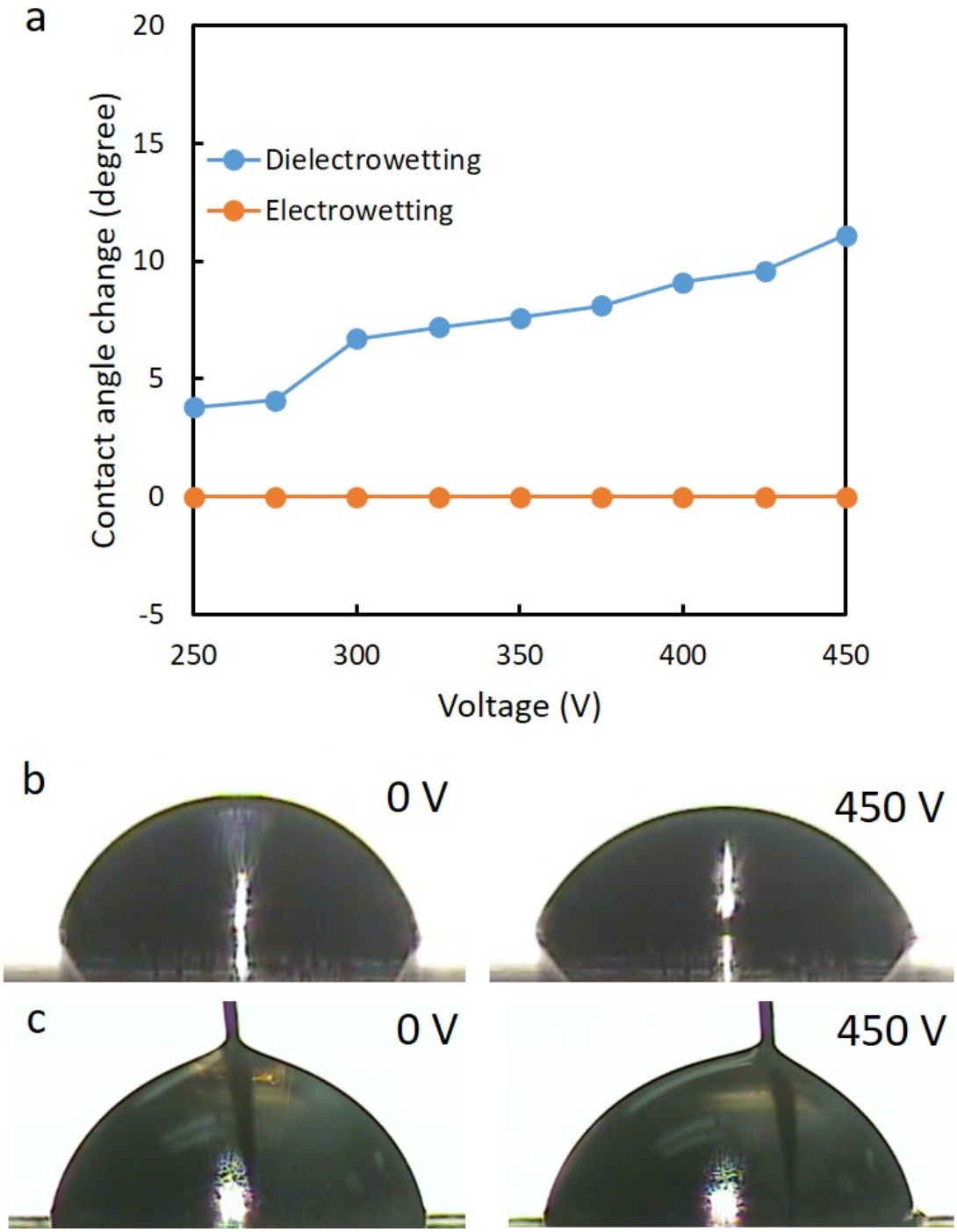

Figure 85. Dielectrowetting and electrowetting effects on vegetable oil. (a) As the voltage increases to 450 V, electrowetting has no effect on the oil, while the contact angle change can be 11.1^{o} with dielectrowetting. (b) With dielectrowetting, the contact angle is 80.2^{o} at 0 V, and 71.4^{o} at 450 V. (c) With electrowetting, the contact angle remains same.

dodecane is used as the dielectric liquid. The dielectric constant of dodecane is 2.0, which is one of lowest values for liquid. At 450 V, the contact angle change is about 6.4^{o} under dielectrowetting. The change is much lower than those of light crude oil and 10cSt silicone oil, but it is still enough to drive the droplet to move. Figure 82(b) shows the side views of contact angle with dielectrowetting, which is 65.2^{o} at 0 V and 58.8^{o} at 450 V. However, the contact angle remains same with electrowetting.

Figure 83 shows the contact angle change of silicone oil with high viscosity. As the voltage increases to 450 V, electrowetting has no effect on the 1000cSt silicone oil, but dielectrowetting can change the contact angle by 9.5^{o}. The contact angle change is much smaller than that of 10cSt silicone oil, representing that it is harder to be transported. Figure 83(b) shows the contact angle is 77.5^{o} at 0 V, and 68^{o} at 450 V with dielectrowetting. As the reference, the contact angle remains same with electrowetting.

Heavy crude oil is another droplet which is difficult to drive. The contact angle change is 9.5^{o} at 450 V with dielectrowetting, as shown in Figure 84(a). Also, it is not influenced by electrowetting effect. Figure 84(b) and (c) show the contact angles with dielectrowetting and electrowetting. For the former case, the contact angle is 71.9^{o} at 0 V and 62.4^{o} at 450 V.The last dielectric liquid tested is vegetable oil, as shown in Figure 85(a). The contact angle change is 11.1^{o} at 450 V with dielectrowetting. In Figure 85(b), the initial angle is 80.2^{o} and it changes to 71.4^{o} at 450 V. Figure 85(c) shows there is no contact angle change with electrowetting.

In addition to dielectric liquids, conductive droplets are also tested under both dielectrowetting and electrowetting conditions. In Figure 86(a), the contact angle change of DI water with dielectrowetting is 3.3^{o} at 275 V and 19.2^{o} at 450 V. However, with electrowetting, the contact angle can be 50.5^{o} at 275 V. Figure 86(b) shows that with dielectrowetting, the contact

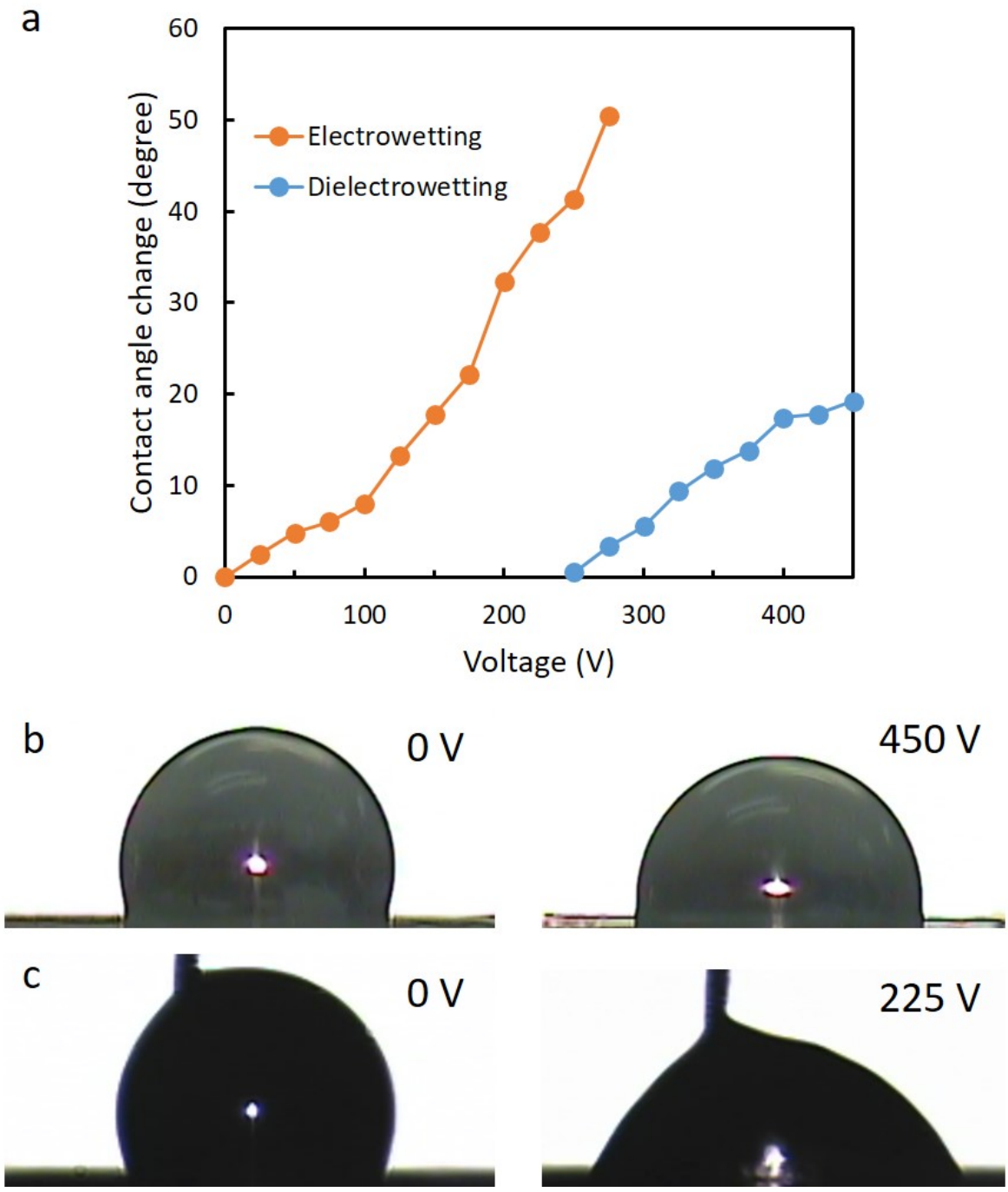

Figure 86. Dielectrowetting and electrowetting effects on DI water. (a) As the voltage increases to 275 V, electrowetting changes the contact angle by 50.5°, while the contact angle change is only 19.2° with dielectrowetting at 450 V. (b) With dielectrowetting, the contact angle is 113° at 0 V, and 93.8° at 450 V. (c) With electrowetting, the contact angle is 75.3° at 225 V.

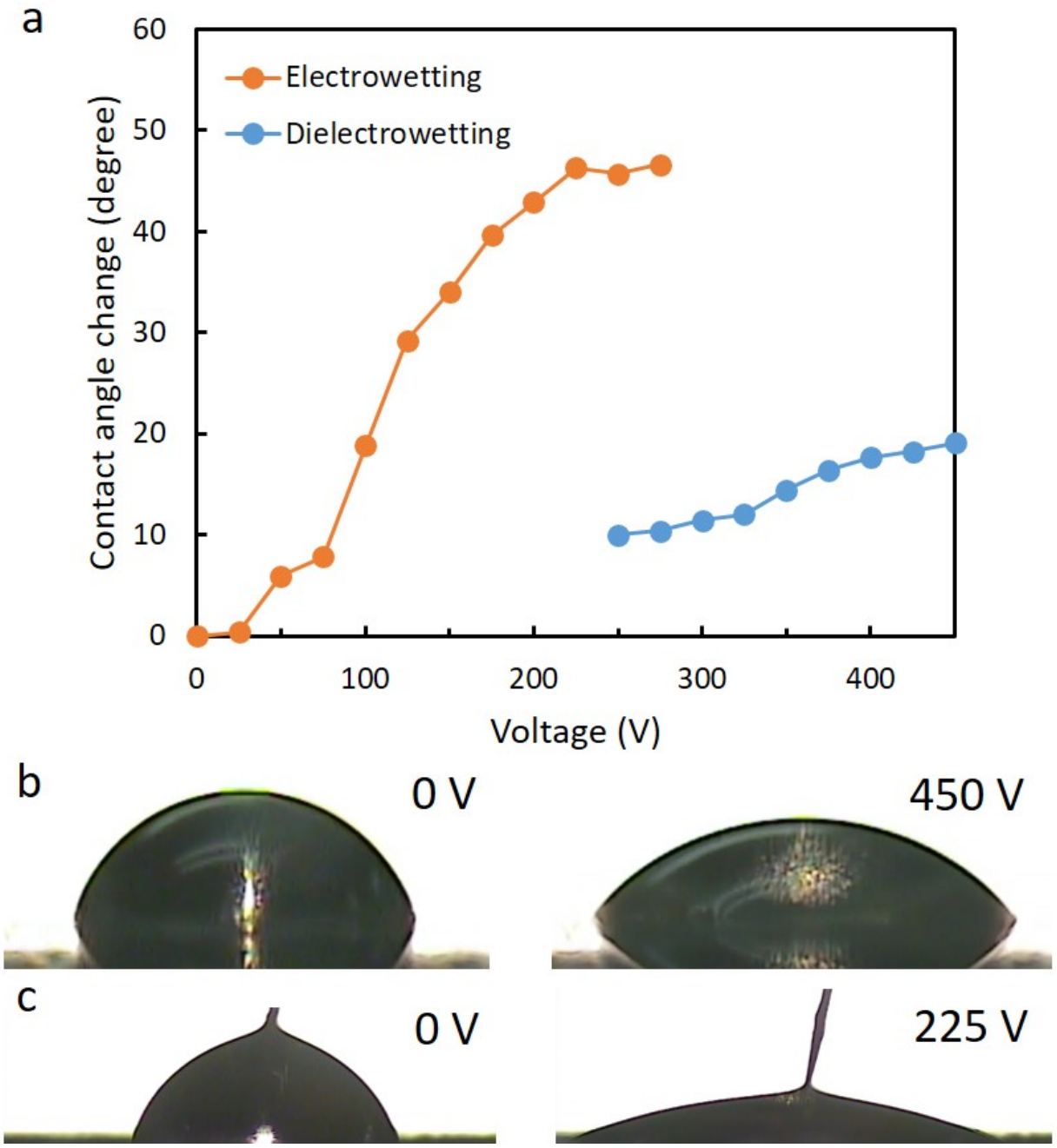

Figure 87. Dielectrowetting and electrowetting effects on ionic liquid. (a) As the voltage increases to 275 V, electrowetting changes the contact angle by 46.6°, while the contact angle change is only 19.1° with dielectrowetting at 450 V. (b) With dielectrowetting, the contact angle is 70.2° at 0 V, and 56.9° at 450 V. (c) With electrowetting, the contact angle decreases to 23.6° at 225 V.

angle is 113^{o} at 0 V, and 93.8^{o} at 450 V. Figure 86(c) shows that with electrowetting, the contact angle is as low as 75.3^{o} at 225 V. Therefore, dielectrowetting is not efficient for conductive droplet, although the contact angle can be changed to certain extent.

Ionic liquids are salt liquids with good electrical conductivity, which are powerful solvents and electrolytes. Figure 87(a) shows the contact angle changes of one ionic liquid. With electrowetting, the contact angle change is 46.6^{o} at 275 V. As for dielectrowetting, the change is 10^{o} at 275 V and 19^{o} at 450 V. Figure 87(b) shows the initial contact angle is 70.2^{o}, and it becomes 56.9^{o} at 450 V. Figure 87(c) shows the contact angle can be as low as 23.6^{o} at 225 V. For ionic liquid, dielectrowetting is also not applicable as electrowetting.

4.3 CONCLUSION

A wide-spectrum digital microfluidic device is design to transport both conductive and dielectric droplets. A unit electrode couple consists of electrowetting and dielectrowetting zone. The former is responsible for transporting conductive droplets, while the latter is for dielectric droplets. Two layers are added to the substrate. One is SU-8 layer, acting as the dielectric layer for enhancing electrowetting. The other one is SLIPS film as the top surface to reduce the adhesion between droplet and surface. In the electrowetting zone, free charges are relocated upon applying voltage, resulting in the movement of conductive droplets. In the dielectrowetting zone, strong fringing field is generated by the interdigital electrodes, which will exert considerable dielectrophoretic force to actuate dielectric droplets. Honey droplets on Teflon and SLIPS are tested to demonstrate the different surface properties. On Teflon, the adhesion is strong enough to resist the coalescence and the final shape is irregular. However, on SLIPS, the adhesion is so weak that the two droplets

coalescent into a spherical one within several seconds. Different kinds of conductive droplets are transported successfully on the device, including DI water, protein solution, detergent, saline, DNA solution, glycerol, honey and ionic liquid. These liquids are highly representative for conductive droplets. Some of them are sticky fluids, and some are bio-solutions, which are difficult to transport on conventional digital microfluidic device. In addition, different types of dielectric liquids are actuated by the wide-spectrum digital microfluidic device, including IPA, propylene carbonate, fish oil, vegetable oil, dodecane, silicone oils with different viscosities, light and heavy crude oils. All the operations for one step can be achieved within several seconds. The different mechanisms of dielectrowetting and electrowetting are elucidated by the specific designed electrodes. Depending on the properties of the droplets, the spreading shapes upon applying voltages are opposite. It can be utilized to characterize the distinction of dielectrowetting and electrowetting. To better show the function of dielectrowetting zone, the purely interdigital electrodes are designed to transport droplets. Dodecane, 1000cSt silicone oil, heavy crude oil, vegetable oil and light crude oil can be moved smoothly on such device. However, saline and DI water cannot work well, which means dielectrowetting is not efficient to actuate conductive droplets. The transporting speeds of dielectric droplets are measured, showing the viscosity, density or other parameters influence the results. The solid electrodes are conventional configuration for electrowetting. Although it can actuate silicone oils slowly, the manipulations are not acceptable for real applications. For dodecane and heavy crude oil, the electrodes can only change the shapes of droplets slightly. The droplet size effect is also demonstrated by the vegetable oil. Smaller droplets can be transported faster, perhaps because the driving force is from the gap region, where fringing field is generated. Since the conductive and dielectric droplets can be transported at the same time, many applications can be achieved, including coalescence of oil and

protein solution, slowing evaporation, transporting solute and combination of water and oil. Contact angle changes by electrowetting and dielectrowetting are totally different scenarios. With dielectrowetting, dielectric droplets can decrease their contact angles. However, their contact angles do not change with electrowetting configuration. Light and heavy crude oils, silicone oils, vegetable oil and dodecane are performed to prove the validity. On the other hand, if the droplets are conductive liquids, such as DI water and ionic liquid, and actuated by dielectrowetting, the contact angle changes are much smaller than electrowetting configuration. Therefore, the dielectrowetting zone is only suitable for dielectric fluids, while the electrowetting zone is indispensable for conductive ones.

5.0 FINAL CONCLUSION

This dissertation present several progresses in digital microfluidics. Not only electrowetting, dielectrowettting can also be applied to manipulate droplets, including conductive and dielectric ones. This is the first time to apply this principle to digital microfluidics. Dielectrowetting is a counterpart concept for electrowtting, in the terms of changing contact angles of droplets. However, for dielectric fluids, dielectrowetting is the only effective method to actuate, while for conductive fluids, electrowetting is commonly used. Dense interdigital electrodes are arranged on the substrate to form dielectrowetting configuration. Upon voltage applied, strong fringing fields are generated by such electrodes, which are only confined near the surface. If dielectric droplet is placed on such region, a net dielectrophoretic force is induced by the non-uniform fields. As a result, the droplet spreads along the electrode direction, changing the apparent contact angle. For propylene carbonate, such effect is strong enough to spread the droplet to be a light liquid film, namely, complete wetting. Therefore, the manipulations can be achieved on a single plate.

Another problem is highly demanded to solve for digital microfluidic device, in order to apply it into biological assay and diagnostics. When hydrophobic surface comes into contact with bio-solutions, it is vulnerable to be stained due to hydrophobic interaction. As a result, the droplet is firmly pinned onto the surface, which means large contact angle hysteresis. At this condition, it is very hard or impossible to actuate droplet on digital microfluidic device. The biofouling issue impedes the real application of digital microfluidics. Here, a reasonable thought to overcome such

challenge is to modify the surface. In this dissertation, a slippery liquid infused porous surface (SLIPS) is introduced to achieve the anti-biofouling goal by decreasing the contact angle hysteresis. Since the surface is covered by a light liquid film, it separates droplet and solid substrate to avoid potential contaminations. Many kinds of droplets can be moved smoothly on such surface, as long as the fluids is immiscible to the infused lubricating liquid. Different concentrations of protein droplets are tested under electrowetting on SLIPS and conventional Teflon surface. It turns out the protein is not able to stain the SLIPS, even under hundreds of actuations. However, electrowetting loses efficacy easily for protein droplets on Teflon surface because of biofouling. Both sessile and moving droplets are tested on the two surfaces, further evidencing the capability of anti-biofouling performance for SLIPS.

With the integration of SLIPS and digital microfluidics, it is desirable to transport different types of droplets, including some sticky and viscous ones. The pathway adopted is to combine electrowetting and dielectrowetting, realizing the goal of transporting conductive and dielectric droplets. For one electrode couple, the center area is electrowetting zone, which is responsible for actuating conductive droplets. On the two sides, dielectrowetting zones can elevate dielectrophoretic force to move dielectric droplets. On the top, SLIPS remarkably reduces the adhesion between droplets and substrate, making it possible to transport complex fluids, such as heavy crude oil and honey. Such wide-spectrum digital microfluidic device is applicable to actuate both conductive and dielectric droplets on a single platform, which can broaden the working range of digital microfluidics, such as biological assay, chemical synthesis, genomics and food industry.

BIBLIOGRAPHY

[1] P. S. Dittrich and A. Manz, "Lab-on-a-chip: Microfluidics in drug discovery", *Nature Reviews Drug Discovery,* vol. 5, pp. 210-218, 2006.

[2] P. Abgrall and A. Gue, "Lab-on-chip technologies: Making a microfluidic network and coupling it into a complete microsystem—A review", *J. Micromech. Microeng.*, vol. 17, pp. 15-49, 2007.

[3] D. P. Parekh, C. Ladd, L. Panich, K. Moussa, and M. D. Dickey, "3D printing of liquid metals as fugitive inks for fabrication of 3D microfluidic channels", *Lab Chip,* vol. 16, pp. 1812-1820, 2016.

[4] C. Hu, S. Lin, W. B. Li, H. Sun, Y. F. Chen, C. W. Chan, *et al.*, "A one-step strategy for ultra-fast and low-cost mass production of plastic membrane microfluidic chips", *Lab Chip,* vol. 16, pp. 3909-3918, 2016.

[5] https://www.illumina.com/science/technology/digital-microfluidics.html

[6] A. G. Hati, D. C. Bassett, J. M. Ribe, P. Sikorski, D. A. Weitz, and B. T. Stokke, "Versatile, cell and chip friendly method to gel alginate in microfluidic devices", *Lab Chip,* vol. 16, pp. 3718-3727, 2016.

[7] B. G. Chung, K. H. Lee, A. Khademhosseini, and S. H. Lee, "Microfluidic fabrication of microengineered hydrogels and their application in tissue engineering", *Lab Chip,* vol. 12, pp. 45-59, 2012.

[8] O. Cybulski, S. Jakiela, and P. Garstecki, "Whole Teflon valves for handling droplets", *Lab Chip,* vol. 16, pp. 2198-2210, 2016.

[9] H. Gong, A. T. Woolley, and G. P. Nordin, "High density 3D printed microfluidic valves, pumps, and multiplexers", *Lab Chip,* vol. 16, pp. 2450-2458, 2016.

[10] J. Hansson, M. Hillmering, T. Haraldsson, and W. van der Wijngaart, "Leak-tight vertical membrane microvalves", *Lab Chip,* vol. 16, pp. 1439-1446, 2016.

[11] E. Dolgin, "Devices: Artificial inspiration", *Nature,* vol. 489, pp. 12-14, 2012.

[12] E. Samiei, M. Tabrizian, and M. Hoorfar, "A review of digital microfluidics as portable platforms for lab-on a-chip applications", *Lab Chip,* vol. 16, pp. 2376-2396, 2016.

[13] H. H. Shen, S. K. Fan, C. J. Kim, and D. J. Yao, "EWOD microfluidic systems for biomedical applications", *Microfluid. Nanofluid.,* vol. 16, pp. 965-987, 2014.

[14] V. Srinivasan, V. K. Pamula, and R. B. Fair, "An integrated digital microfluidic lab-on-a-chip for clinical diagnostics on human physiological fluids", *Lab Chip,* vol. 4, pp. 310-315, 2004.

[15] N. Vergauwe, D. Witters, F. Ceyssens, S. Vermeir, B. Verbruggen, R. Puers, *et al.*, "A versatile electrowetting-based digital microfluidic platform for quantitative homogeneous and heterogeneous bio-assays", *J. Micromech. Microeng.,* vol. 21, 2011.

[16] A. R. Wheeler, "Putting electrowetting to work", *Science,* vol. 322, pp. 539-540, 2008.

[17] D. Witters, N. Vergauwe, S. Vermeir, F. Ceyssens, S. Liekens, R. Puers, *et al.*, "Biofunctionalization of electrowetting-on-dielectric digital microfluidic chips for miniaturized cell-based applications", *Lab Chip,* vol. 11, pp. 2790-2794, 2011.

[18] H. Yang, V. N. Luk, M. Abeigawad, I. Barbulovic-Nad, and A. R. Wheeler, "A World-to-Chip Interface for Digital Microfluidics", *Analytical Chemistry,* vol. 81, pp. 1061-1067, 2009.

[19] K. Choi, A. H. Ng, R. Fobel, and A. R. Wheeler, "Digital microfluidics", *Annual review of analytical chemistry,* vol. 5, pp. 413-440, 2012.

[20] L.-Y. Chung, H.-H. Shen, Y.-H. Chung, C.-C. Chen, C.-H. Hsu, H.-Y. Huang, *et al.*, "In vitro dynamic fertilization by using EWOD device", in *Micro Electro Mechanical Systems (MEMS), 2015 28th IEEE International Conference on*, 2015, pp. 519-522.

[21] R. Fobel, A. E. Kirby, A. H. C. Ng, R. R. Farnood, and A. R. Wheeler, "Paper Microfluidics Goes Digital", *Adv. Mater.,* vol. 26, pp. 2838-2843, 2014.

[22] S. L. Freire and A. R. Wheeler, "Proteome-on-a-chip: Mirage, or on the horizon?", *Lab Chip,* vol. 6, pp. 1415-1423, 2006.

[23] P. C. Gach, K. Iwai, P. W. Kim, N. J. Hillson, and A. K. Singh, "Droplet microfluidics for synthetic biology", *Lab Chip,* vol. 17, pp. 3388-3400, 2017.

[24] J. L. Garcia-Cordero and Z. H. Fan, "Sessile droplets for chemical and biological assays", *Lab Chip,* vol. 17, pp. 2150-2166, 2017.

[25] A. Huebner, S. Sharma, M. Srisa-Art, F. Hollfelder, and J. B. Edel, "Microdroplets: a sea of applications?", *Lab Chip,* vol. 8, pp. 1244-1254, 2008.

[26] E. M. Miller and A. R. Wheeler, "A digital microfluidic approach to homogeneous enzyme assays", *Analytical Chemistry,* vol. 80, pp. 1614-1619, 2008.

[27] F. Mugele, J. C. Baret, and D. Steinhauser, "Microfluidic mixing through electrowetting-induced droplet oscillations", *Appl. Phys. Lett.*, vol. 88, 2006.

[28] A. H. Ng, M. D. Chamberlain, H. Situ, V. Lee, and A. R. Wheeler, "Digital microfluidic immunocytochemistry in single cells", *Nature Commun.*, vol. 6, p. 7513, 2015.

[29] A. H. Ng, B. B. Li, M. D. Chamberlain, and A. R. Wheeler, "Digital microfluidic cell culture", *Annual review of biomedical engineering*, vol. 17, pp. 91-112, 2015.

[30] J. Noordmans, H. Wormeester, and H. J. Busscher, "Simultaneous monitoring of protein adsorption at the solid–liquid interface from sessile solution droplets by ellipsometry and axisymmetric drop shape analysis by profile", *Colloids and surfaces B: Biointerfaces*, vol. 15, pp. 227-233, 1999.

[31] P. Paik, V. K. Pamula, M. G. Pollack, and R. B. Fair, "Electrowetting-based droplet mixers for microfluidic systems", *Lab Chip*, vol. 3, pp. 28-33, 2003.

[32] J. Z. Chen, S. M. Troian, A. A. Darhuber, and S. Wagner, "Effect of contact angle hysteresis on thermocapillary droplet actuation", *J. Appl. Phys.*, vol. 97, pp. 014906-014914, 2005.

[33] F. Mugele and J. C. Baret, "Electrowetting: From basics to applications", *J. Phys.: Condens. Matter*, vol. 17, pp. 705-774, 2005.

[34] W. C. Nelson and C. J. Kim, "Droplet actuation by electrowetting-on-dielectric (EWOD): A review", *J. Adhesion Sci. Technol.*, vol. 26, pp. 1747-1771, 2012.

[35] F. Lapierre, M. Jonsson-Niedziolka, Y. Coffinier, R. Boukherroub, and V. Thomy, "Droplet transport by electrowetting: lets get rough!", *Microfluid. Nanofluid.*, vol. 15, pp. 327-336, 2013.

[36] S. Millefiorini, A. H. Tkaczyk, R. Sedev, J. Efthimiadis, and J. Ralston, "Electrowetting of ionic liquids", *J Am Chem Soc*, vol. 128, pp. 3098-3101, 2006.

[37] Y.-P. Zhao and Y. Wang, "Fundamentals and applications of electrowetting", *Reviews of Adhesion and Adhesives*, vol. 1, pp. 114-174, 2013.

[38] M. J. Jebrail and A. R. Wheeler, "Digital Microfluidic Method for Protein Extraction by Precipitation", *Analytical Chemistry*, vol. 81, pp. 330-335, 2009.

[39] A. E. Kirby and A. R. Wheeler, "Digital Microfluidics: An Emerging Sample Preparation Platform for Mass Spectrometry", *Analytical Chemistry*, vol. 85, pp. 6178-6184, 2013.

[40] V. N. Luk and A. R. Wheeler, "A Digital Microfluidic Approach to Proteomic Sample Processing", *Analytical Chemistry*, vol. 81, pp. 4524-4530, 2009.

[41] L. Malic, D. Brassard, T. Veres, and M. Tabrizian, "Integration and detection of biochemical assays in digital microfluidic LOC devices", *Lab Chip,* vol. 10, pp. 418-431, 2010.

[42] B. Berge and J. Peseux, "Variable focal lens controlled by an external voltage: An application of electrowetting", *Eur. Phys. J. E,* vol. 3, pp. 159-163, 2000.

[43] S. K. Chung, K. Ryu, and S. K. Cho, "Electrowetting propulsion of water-floating objects", *Appl. Phys. Lett.,* vol. 95, pp. 014107-014109, 2009.

[44] S. K. Chung, Y. Zhao, and S. K. Cho, "On-chip creation and elimination of microbubbles for a micro-object manipulator", *J. Micromech. Microeng.,* vol. 18, pp. 095009-095021, 2008.

[45] Y. Zhao, S. K. Chung, U. C. Yi, and S. K. Cho, "Droplet manipulation and microparticle sampling on perforated microfilter membranes", *J. Micromech. Microeng.,* vol. 18, pp. 025030-025040, 2008.

[46] A. G. Banpurkar, K. P. Nichols, and F. Mugele, "Electrowetting-based microdrop tensiometer", *Langmuir,* vol. 24, pp. 10549-10551, 2008.

[47] J. Yuan and S. K. Cho, "Mechanism and flow measurement of AC electrowetting propulsion on free surface", *Expt. Fluids,* vol. 56, pp. 56-67, 2015.

[48] J. Q. Yuan, J. Feng, and S. K. Cho, "Cheerios effect controlled by electrowetting", *Langmuir,* vol. 31, pp. 8502-8511, 2015.

[49] T. Krupenkin and J. A. Taylor, "Reverse electrowetting as a new approach to high-power energy harvesting", *Nature Commun.,* vol. 2, 2011.

[50] B. Sun, K. Zhou, Y. Lao, J. Heikenfeld, and W. Cheng, "Scalable fabrication of electrowetting displays with self-assembled oil dosing", *Appl. Phys. Lett.,* vol. 91, 2007.

[51] I. A. Eydelnant, B. B. Li, and A. R. Wheeler, "Microgels on-demand", *Nature Commun.,* vol. 5, 2014.

[52] L. K. Fiddes, V. N. Luk, S. H. Au, A. H. C. Ng, V. Luk, E. Kumacheva, *et al.*, "Hydrogel discs for digital microfluidics", *Biomicrofluidics,* vol. 6, 2012.

[53] V. N. Luk, L. K. Fiddes, V. M. Luk, E. Kumacheva, and A. R. Wheeler, "Digital microfluidic hydrogel microreactors for proteomics", *Proteomics,* vol. 12, pp. 1310-1318, 2012.

[54] M. G. Pollack, R. B. Fair, and A. D. Shenderov, "Electrowetting-based actuation of liquid droplets for microfluidic applications", *Appl. Phys. Lett.,* vol. 77, pp. 1725-1726, 2000.

[55] M. G. Pollack, A. D. Shenderov, and R. B. Fair, "Electrowetting-based actuation of droplets for integrated microfluidics", *Lab Chip,* vol. 2, pp. 96-101, 2002.

[56] M. Abdelgawad and A. R. Wheeler, "The digital revolution: a new paradigm for microfluidics", *Adv. Mater.*, vol. 21, pp. 920-925, 2009.

[57] M. J. Jebrail, M. S. Bartsch, and K. D. Patel, "Digital microfluidics: a versatile tool for applications in chemistry, biology and medicine", *Lab Chip,* vol. 12, pp. 2452-2463, 2012.

[58] M. J. Jebrail, A. H. C. Ng, V. Rai, R. Hili, A. K. Yudin, and A. R. Wheeler, "Synchronized Synthesis of Peptide-Based Macrocycles by Digital Microfluidics", *Angew Chem Int Edit,* vol. 49, pp. 8625-8629, 2010.

[59] M. J. Jebrail, A. Sinha, S. Vellucci, R. F. Renzi, C. Ambriz, C. Gondhalekar, *et al.*, "World-to-Digital-Microfluidic Interface Enabling Extraction and Purification of RNA from Human Whole Blood", *Analytical Chemistry,* vol. 86, pp. 3856-3862, 2014.

[60] S. K. Cho, H. Moon, and C.-J. Kim, "Creating, transporting, cutting, and merging liquid droplets by electrowetting-based actuation for digital microfluidic circuits", *J. Microelectromech. Syst.*, vol. 12, pp. 70-80, 2003.

[61] S. K. Fan, W. J. Chen, T. H. Lin, T. T. Wang, and Y. C. Lin, "Reconfigurable liquid pumping in electric-field-defined virtual microchannels by dielectrophoresis", *Lab Chip,* vol. 9, pp. 1590-1595, 2009.

[62] S. K. Fan, P. W. Huang, T. T. Wang, and Y. H. Peng, "Cross-scale electric manipulations of cells and droplets by frequency-modulated dielectrophoresis and electrowetting", *Lab Chip,* vol. 8, pp. 1325-1331, 2008.

[63] S. K. Fan, H. P. Lee, C. C. Chien, Y. W. Lu, Y. Chiu, and F. Y. Lin, "Reconfigurable liquid-core/liquid-cladding optical waveguides with dielectrophoresis-driven virtual microchannels on an electromicrofluidic platform", *Lab Chip,* vol. 16, pp. 847-854, 2016.

[64] D. Chatterjee, B. Hetayothin, A. R. Wheeler, D. J. King, and R. L. Garrell, "Droplet-based microfluidics with nonaqueous solvents and solutions", *Lab Chip,* vol. 6, pp. 199-206, 2006.

[65] T. B. Jones, J. D. Fowler, Y. S. Chang, and C. J. Kim, "Frequency-based relationship of electrowetting and dielectrophoretic liquid microactuation", *Langmuir,* vol. 19, pp. 7646-7651, 2003.

[66] S.-K. Fan, Y.-W. Hsu, and C.-H. Chen, "Encapsulated droplets with metered and removable oil shells by electrowetting and dielectrophoresis", *Lab Chip,* vol. 11, pp. 2500-2508, 2011.

[67] S.-K. Fan and F.-M. Wang, "Multiphase optofluidics on an electro-microfluidic platform powered by electrowetting and dielectrophoresis", *Lab Chip,* vol. 14, pp. 2728-2738, 2014.

[68] J. Cao, P. Cheng, and F. J. Hong, "A numerical analysis of forces imposed on particles in conventional dielectrophoresis in microchannels with interdigitated electrodes", *J. Electrostatics,* vol. 66, pp. 620-626, 2008.

[69] N. Crews, J. Darabi, P. Voglewede, F. Guo, and A. Bayoumi, "An analysis of interdigitated electrode geometry for dielectrophoretic particle transport in micro-fluidics", *Sensor Actuat B-Chem,* vol. 125, pp. 672-679, 2007.

[70] G. McHale, C. V. Brown, M. I. Newton, G. G. Wells, and N. Sampara, "Dielectrowetting driven spreading of droplets", *Phys. Rev. Lett.,* vol. 107, pp. 186101-186104, 2011.

[71] G. McHale, C. V. Brown, M. I. Newton, G. G. Wells, and N. Sampara, "Developing interface localized liquid dielectrophoresis for optical applications", *Proc. SPIE,* vol. 8557, p. 855703, 2012.

[72] C. V. Brown, G. McHale, and C. L. Trabi, "Dielectrophoresis-Driven Spreading of Immersed Liquid Droplets", *Langmuir,* vol. 31, pp. 1011-1016, 2015.

[73] G. McHale, C. V. Brown, and N. Sampara, "Voltage-induced spreading and superspreading of liquids", *Nature Commun.,* vol. 4, pp. 2619-2625, 2013.

[74] C. V. Brown, W. Al-Shabib, G. G. Wells, G. McHale, and M. I. Newton, "Amplitude scaling of a static wrinkle at an oil-air interface created by dielectrophoresis forces", *Appl. Phys. Lett.,* vol. 97, pp. 242904-242907, 2010.

[75] C. V. Brown, G. McHale, and N. J. Mottram, "Analysis of a static undulation on the surface of a thin dielectric liquid layer formed by dielectrophoresis forces", *J. Appl. Phys.,* vol. 110, pp. 024107-024112, 2011.

[76] C. V. Brown, G. G. Wells, M. I. Newton, and G. McHale, "Voltage-programmable liquid optical interface", *Nature Photonics,* vol. 3, pp. 403-405, 2009.

[77] Z. Brabcova, G. McHale, and G. G. Wells, "Near axisymmetric partial wetting using interface-localized liquid dielectrophoresis", *Langmuir,* vol. 32, pp. 10844-10850, 2016.

[78] A. Russell, E. Kreit, and J. Heikenfeld, "Scaling dielectrowetting optical shutters to higher resolution: Microfluidic and optical implications", *Langmuir,* vol. 30, pp. 5357-5362, 2014.

[79] A. C. Russell, W. L. Hsieh, K. C. Chen, and J. Heikenfeld, "Experimental and numerical insights into isotropic spreading and deterministic dewetting of dielectrowetted films", *Langmuir,* vol. 31, pp. 637-642, 2015.

[80] S. Xu, H. W. Ren, and S. T. Wu, "Dielectrophoretically tunable optofluidic devices", *J. Phys. D: Appl. Phys.,* vol. 46, pp. 483001-483014, 2013.

[81] R. Zhao, B. Cumby, A. Russell, and J. Heikenfeld, "Large area and low power dielectrowetting optical shutter with local deterministic fluid film breakup", *Appl. Phys. Lett.,* vol. 103, pp. 223510-223514, 2013.

[82] D. R. Absolom and A. W. Neumann, "Modification of substrate surface properties through protein adsorption", *Colloids and surfaces,* vol. 30, pp. 25-45, 1987.

[83] N. Barnthip, P. Parhi, A. Golas, and E. A. Vogler, "Volumetric interpretation of protein adsorption: kinetics of protein-adsorption competition from binary solution", *Biomaterials,* vol. 30, pp. 6495-6513, 2009.

[84] M. M. Ouberai, K. Xu, and M. E. Welland, "Effect of the interplay between protein and surface on the properties of adsorbed protein layers", *Biomaterials,* vol. 35, pp. 6157-6163, 2014.

[85] M. Rabe, D. Verdes, and S. Seeger, "Understanding protein adsorption phenomena at solid surfaces", *Advances in colloid and interface science,* vol. 162, pp. 87-106, 2011.

[86] G. Raffaini and F. Ganazzoli, "Protein Adsorption on a Hydrophobic Surface: A Molecular Dynamics Study of Lysozyme on Graphite", *Langmuir,* vol. 26, pp. 5679-5689, 2010.

[87] W. van der Vegt, W. Norde, H. C. van der Mei, and H. J. Busscher, "Kinetics of interfacial tension changes during protein adsorption from sessile droplets on FEP–Teflon", *J. Colloid. Interf. Sci.,* vol. 179, pp. 57-65, 1996.

[88] E. A. Vogler, "Protein adsorption in three dimensions", *Biomaterials,* vol. 33, pp. 1201-1237, 2012.

[89] G. Zardeneta, H. Mukai, V. Marker, and S. B. Milam, "Protein interactions with particulate Teflon: implications for the foreign body response", *Journal of oral and maxillofacial surgery,* vol. 54, pp. 873-878, 1996.

[90] S. O. Lumsdon, J. Green, and B. Stieglitz, "Adsorption of hydrophobin proteins at hydrophobic and hydrophilic interfaces", *Colloids and Surfaces B: Biointerfaces,* vol. 44, pp. 172-178, 2005.

[91] C. Beverung, C. Radke, and H. Blanch, "Protein adsorption at the oil/water interface: characterization of adsorption kinetics by dynamic interfacial tension measurements", *Biophysical chemistry,* vol. 81, pp. 59-80, 1999.

[92] D. Brassard, L. Malic, F. Normandin, M. Tabrizian, and T. Veres, "Water-oil core-shell droplets for electrowetting-based digital microfluidic devices", *Lab Chip,* vol. 8, pp. 1342-1349, 2008.

[93] S. H. Au, P. Kumar, and A. R. Wheeler, "A new angle on pluronic additives: advancing droplets and understanding in digital microfluidics", *Langmuir,* vol. 27, pp. 8586-8594, 2011.

[94] V. N. Luk, G. C. Mo, and A. R. Wheeler, "Pluronic additives: a solution to sticky problems in digital microfluidics", *Langmuir,* vol. 24, pp. 6382-6389, 2008.

[95] G. Perry, V. Thomy, M. R. Das, Y. Coffinier, and R. Boukherroub, "Inhibiting protein biofouling using graphene oxide in droplet-based microfluidic microsystems", *Lab Chip,* vol. 12, pp. 1601-1604, 2012.

[96] J.-Y. Yoon and R. L. Garrell, "Preventing biomolecular adsorption in electrowetting-based biofluidic chips", *Analytical Chemistry,* vol. 75, pp. 5097-5102, 2003.

[97] M. Karlsson, J. Ekeroth, H. Elwing, and U. Carlsson, "Reduction of irreversible protein adsorption on solid surfaces by protein engineering for increased stability", *J Biol Chem,* vol. 280, pp. 25558-25564, 2005.

[98] M. K. Sarvothaman, K. S. Kim, B. Seale, P. M. Brodersen, G. C. Walker, and A. R. Wheeler, "Dynamic Fluoroalkyl Polyethylene Glycol Co-Polymers: A New Strategy for Reducing Protein Adhesion in Lab-on-a-Chip Devices", *Adv Funct Mater,* vol. 25, pp. 506-515, 2015.

[99] T. N. Krupenkin, J. A. Taylor, T. M. Schneider, and S. Yang, "From rolling ball to complete wetting: The dynamic tuning of liquids on nanostructured surfaces", *Langmuir,* vol. 20, pp. 3824-3827, 2004.

[100] U. Manna, A. H. Broderick, and D. M. Lynn, "Chemical Patterning and Physical Refinement of Reactive Superhydrophobic Surfaces", *Adv. Mater.,* vol. 24, pp. 4291-+, 2012.

[101] P. Papadopoulos, L. Mammen, X. Deng, D. Vollmer, and H. J. Butt, "How superhydrophobicity breaks down", *P Natl Acad Sci USA,* vol. 110, pp. 3254-3258, 2013.

[102] A. Tuteja, W. Choi, M. L. Ma, J. M. Mabry, S. A. Mazzella, G. C. Rutledge, *et al.*, "Designing superoleophobic surfaces", *Science,* vol. 318, pp. 1618-1622, 2007.

[103] H. F. Bohn and W. Federle, "Insect aquaplaning: Nepenthes pitcher plants capture prey with the peristome, a fully wettable water-lubricated anisotropic surface", *P Natl Acad Sci USA,* vol. 101, pp. 14138-14143, 2004.

[104] J. B. Boreyko, G. Polizos, P. G. Datskos, S. A. Sarles, and C. P. Collier, "Air-stable droplet interface bilayers on oil-infused surfaces", *P Natl Acad Sci USA,* vol. 111, pp. 7588-7593, 2014.

[105] D. Daniel, J. V. I. Timonen, R. P. Li, S. J. Velling, and J. Aizenberg, "Oleoplaning droplets on lubricated surfaces", *Nat Phys,* vol. 13, pp. 1020-+, 2017.

[106] X. Hou, Y. H. Hu, A. Grinthal, M. Khan, and J. Aizenberg, "Liquid-based gating mechanism with tunable multiphase selectivity and antifouling behaviour", *Nature,* vol. 519, pp. 70-73, 2015.

[107] K. C. Park, P. Kim, A. Grinthal, N. He, D. Fox, J. C. Weaver, *et al.*, "Condensation on slippery asymmetric bumps", *Nature,* vol. 531, pp. 78-82, 2016.

[108] T. S. Wong, S. H. Kang, S. K. Y. Tang, E. J. Smythe, B. D. Hatton, A. Grinthal, *et al.*, "Bioinspired self-repairing slippery surfaces with pressure-stable omniphobicity", *Nature,* vol. 477, pp. 443-447, 2011.

[109] X. Yao, Y. H. Hu, A. Grinthal, T. S. Wong, L. Mahadevan, and J. Aizenberg, "Adaptive fluid-infused porous films with tunable transparency and wettability", *Nat Mater,* vol. 12, pp. 529-534, 2013.

[110] J. Barman, R. Pant, A. K. Nagarajan, and K. Khare, "Electrowetting on dielectrics on lubricating fluid-infused smooth/rough surfaces with negligible hysteresis", *J. Adhesion Sci. Technol.,* vol. 31, pp. 159-170, 2017.

[111] E. Bormashenko, R. Pogreb, Y. Bormashenko, H. Aharoni, E. Shulzinger, R. Grinev, *et al.*, "Progress in low voltage reversible electrowetting with lubricated polymer honeycomb substrates", *Rsc. Adv.,* vol. 5, pp. 32491-32496, 2015.

[112] Z. Brabcova, G. McHale, G. G. Wells, C. V. Brown, and M. I. Newton, "Electric field induced reversible spreading of droplets into films on lubricant impregnated surfaces", *Appl. Phys. Lett.,* vol. 110, p. 121603, 2017.

[113] E. Jenner and B. D'Urso, "Wetting states on structured immiscible liquid coated surfaces", *Appl. Phys. Lett.,* vol. 103, 2013.

[114] K. S. Khalil, S. R. Mahmoudi, N. Abu-dheir, and K. K. Varanasi, "Active surfaces: Ferrofluid-impregnated surfaces for active manipulation of droplets", *Appl. Phys. Lett.,* vol. 105, 2014.

[115] G. Mistura and M. Pierno, "Drop mobility on chemically heterogeneous and lubricant-impregnated surfaces", *Adv Phys-X,* vol. 2, pp. 591-607, 2017.

[116] C. Semprebon, G. McHale, and H. Kusumaatmaja, "Apparent contact angle and contact angle hysteresis on liquid infused surfaces", *Soft Matter,* vol. 13, pp. 101-110, 2017.

[117] J. D. Smith, R. Dhiman, S. Anand, E. Reza-Garduno, R. E. Cohen, G. H. McKinley, *et al.*, "Droplet mobility on lubricant-impregnated surfaces", *Soft Matter,* vol. 9, pp. 1772-1780, 2013.

[118] X. D. He, W. B. Qiang, C. Du, Q. F. Shao, X. P. Zhang, and Y. Q. Deng, "Modification of lubricant infused porous surface for low-voltage reversible electrowetting", *J Mater Chem A,* vol. 5, pp. 19159-19167, 2017.

[119] G. Chaniel, M. Frenkel, V. Multanen, and E. Bormashenko, "Paradoxical coffee-stain effect driven by the Marangoni flow observed on oil-infused surfaces", *Colloid. Surface. A,* vol. 522, pp. 355-360, 2017.

[120] T. Darmanin and F. Guittard, "Recent advances in the potential applications of bioinspired superhydrophobic materials", *J Mater Chem A,* vol. 2, pp. 16319-16359, 2014.

[121] X. Q. Dou, D. Zhang, C. L. Feng, and L. Jiang, "Bioinspired Hierarchical Surface Structures with Tunable Wettability for Regulating Bacteria Adhesion", *Acs Nano,* vol. 9, pp. 10664-10672, 2015.

[122] A. K. Epstein, T. S. Wong, R. A. Belisle, E. M. Boggs, and J. Aizenberg, "Liquid-infused structured surfaces with exceptional anti-biofouling performance", *P Natl Acad Sci USA*, vol. 109, pp. 13182-13187, 2012.

[123] A. Grinthal and J. Aizenberg, "Mobile interfaces: Liquids as a perfect structural material for multifunctional, antifouling surfaces", *Chem Mater*, vol. 26, pp. 698-708, 2013.

[124] H. L. Liu, P. C. Zhang, M. J. Liu, S. T. Wang, and L. Jiang, "Organogel-based Thin Films for Self-Cleaning on Various Surfaces", *Adv. Mater.*, vol. 25, pp. 4477-4481, 2013.

[125] N. MacCallum, C. Howell, P. Kim, D. Sun, R. Friedlander, J. Ranisau, *et al.*, "Liquid-Infused Silicone As a Biofouling-Free Medical Material", *Acs Biomater Sci Eng*, vol. 1, pp. 43-51, 2015.

[126] P. Wang, D. Zhang, and Z. Lu, "Slippery liquid-infused porous surface bio-inspired by pitcher plant for marine anti-biofouling application", *Colloids and Surfaces B: Biointerfaces*, vol. 136, pp. 240-247, 2015.

[127] P. Wang, D. Zhang, Z. Lu, and S. M. Sun, "Fabrication of Slippery Lubricant-Infused Porous Surface for Inhibition of Microbially Influenced Corrosion", *ACS Appl. Mater. Interfaces*, vol. 8, pp. 1120-1127, 2016.

[128] P. Wang, D. Zhang, S. M. Sun, T. P. Li, and Y. Sun, "Fabrication of Slippery Lubricant-Infused Porous Surface with High Underwater Transparency for the Control of Marine Biofouling", *ACS Appl. Mater. Interfaces*, vol. 9, pp. 972-982, 2017.

[129] C. Q. Wei, G. F. Zhang, Q. H. Zhang, X. L. Zhan, and F. Q. Chen, "Silicone Oil-Infused Slippery Surfaces Based on Sol-Gel Process-Induced Nanocomposite Coatings: A Facile Approach to Highly Stable Bioinspired Surface for Biofouling Resistance", *ACS Appl. Mater. Interfaces*, vol. 8, pp. 34810-34819, 2016.

[130] Q. Wei, C. Schlaich, S. Prevost, A. Schulz, C. Bottcher, M. Gradzielski, *et al.*, "Supramolecular Polymers as Surface Coatings: Rapid Fabrication of Healable Superhydrophobic and Slippery Surfaces", *Adv. Mater.*, vol. 26, pp. 7358-7364, 2014.

[131] X. Yao, Y. L. Song, and L. Jiang, "Applications of Bio-Inspired Special Wettable Surfaces", *Adv. Mater.*, vol. 23, pp. 719-734, 2011.

[132] P. F. Zhang, H. W. Chen, L. W. Zhang, T. Ran, and D. Y. Zhang, "Transparent self-cleaning lubricant-infused surfaces made with large-area breath figure patterns", *Appl Surf Sci*, vol. 355, pp. 1083-1090, 2015.

[133] D. C. Leslie, A. Waterhouse, J. B. Berthet, T. M. Valentin, A. L. Watters, A. Jain, *et al.*, "A bioinspired omniphobic surface coating on medical devices prevents thrombosis and biofouling", *Nat Biotechnol*, vol. 32, pp. 1134-1140, 2014.

[134] C. Howell, T. L. Vu, C. P. Johnson, X. Hou, O. Ahanotu, J. Alvarenga, *et al.*, "Stability of Surface-Immobilized Lubricant Interfaces under Flow", *Chem Mater,* vol. 27, pp. 1792-1800, 2015.

[135] P. Kim, M. J. Kreder, J. Alvarenga, and J. Aizenberg, "Hierarchical or Not? Effect of the Length Scale and Hierarchy of the Surface Roughness on Omniphobicity of Lubricant-Infused Substrates", *Nano Lett,* vol. 13, pp. 1793-1799, 2013.

[136] J. Barman, A. K. Nagarajan, and K. Khare, "Controlled electro-coalescence/non-coalescence on lubricating fluid infused slippery surfaces", *Rsc. Adv.,* vol. 5, pp. 105524-105530, 2015.

[137] X. M. Dai, B. B. Stogin, S. K. Yang, and T. S. Wong, "Slippery Wenzel State", *Acs Nano,* vol. 9, pp. 9260-9267, 2015.

[138] X. M. Dai, N. Sun, S. O. Nielsen, B. B. Stogin, J. Wang, S. K. Yang, *et al.*, "Hydrophilic directional slippery rough surfaces for water harvesting", *Sci Adv,* vol. 4, 2018.

[139] C. L. Hao, J. Li, Y. Liu, X. F. Zhou, Y. H. Liu, R. Liu, *et al.*, "Superhydrophobic-like tunable droplet bouncing on slippery liquid interfaces", *Nature Commun.,* vol. 6, 2015.

[140] C. L. Hao, Y. H. Liu, X. M. Chen, J. Li, M. Zhang, Y. H. Zhao, *et al.*, "Bioinspired Interfacial Materials with Enhanced Drop Mobility: From Fundamentals to Multifunctional Applications", *Small,* vol. 12, pp. 1825-1839, 2016.

[141] Y. Huang, B. B. Stogin, N. Sun, J. Wang, S. K. Yang, and T. S. Wong, "A Switchable Cross-Species Liquid Repellent Surface", *Adv. Mater.,* vol. 29, 2017.

[142] J. T. Luo, N. R. Geraldi, J. H. Guan, G. McHale, G. G. Wells, and Y. Q. Fu, "Slippery Liquid-Infused Porous Surfaces and Droplet Transportation by Surface Acoustic Waves", *Phys Rev Appl,* vol. 7, 2017.

[143] S. K. Yang, X. M. Dai, B. B. Stogin, and T. S. Wong, "Ultrasensitive surface-enhanced Raman scattering detection in common fluids", *P Natl Acad Sci USA,* vol. 113, pp. 268-273, 2016.

[144] S. Y. Wu and W. Hsu, "Wireless EWOD/DEP chips powered and controlled through LC circuits and frequency modulation", *Lab Chip,* vol. 14, pp. 3101-3109, 2014.

[145] M. G. Yoon, S. H. Byun, and S. K. Cho, "Inherent amplitude demodulation of an AC-EWOD (electrowetting on dielectric) droplet", *Lab Chip,* vol. 13, pp. 662-668, 2013.

[146] B. Berge, "Electrocapillarité et mouillage de films isolants par l'eau", *Comptes Rendus l'Académie Sciences. Série 2,* vol. 317, pp. 157-163, 1993.

[147] U.-C. Yi and C.-J. Kim, "Characterization of electrowetting actuation on addressable single-side coplanar electrodes", *J. Micromech. Microeng.,* vol. 16, pp. 2053-2059, 2006.

[148] T. B. Jones, "On the relationship of dielectrophoresis and electrowetting", *Langmuir,* vol. 18, pp. 4437-4443, 2002.

[149] T. B. Jones, "Liquid dielectrophoresis on the microscale", *J. Electrostatics,* vol. 51, pp. 290-299, 2001.

[150] S. K. Fan, T. H. Hsieh, and D. Y. Lin, "General digital microfluidic platform manipulating dielectric and conductive droplets by dielectrophoresis and electrowetting", *Lab Chip,* vol. 9, pp. 1236-1242, 2009.

[151] W. Wang and T. Jones, "Microfluidic actuation of insulating liquid droplets in a parallel-plate device", *J. Phys.: Conf. Series,* vol. 301, pp. 012057-012060, 2011.

[152] T. B. Jones, K. L. Wang, and D. J. Yao, "Frequency-dependent electromechanics of aqueous liquids: Electrowetting and dielectrophoresis", *Langmuir,* vol. 20, pp. 2813-2818, 2004.

[153] J. Cui, D. Daniel, A. Grinthal, K. Lin, and J. Aizenberg, "Dynamic polymer systems with self-regulated secretion for the control of surface properties and material healing", *Nat Mater,* vol. 14, p. 790, 2015.

[154] X. M. Li, J. Y. Shao, H. M. Tian, Y. C. Ding, and X. M. Li, "Fabrication of high-aspect-ratio microstructures using dielectrophoresis-electrocapillary force-driven UV-imprinting", *J. Micromech. Microeng.,* vol. 21, p. 065010, 2011.

[155] F. Mugele, A. Klingner, J. Buehrle, D. Steinhauser, and S. Herminghaus, "Electrowetting: a convenient way to switchable wettability patterns", *J. Phys.: Condens. Matter,* vol. 17, pp. 559-576, 2005.

[156] R. A. Hayes and B. J. Feenstra, "Video-speed electronic paper based on electrowetting", *Nature,* vol. 425, pp. 383-385, 2003.

[157] J. Heikenfeld and A. J. Steckl, "High-transmission electrowetting light valves", *Appl. Phys. Lett.,* vol. 86, p. 151121, 2005.

[158] S. Kuiper and B. H. W. Hendriks, "Variable-focus liquid lens for miniature cameras", *Appl. Phys. Lett.,* vol. 85, pp. 1128-1130, 2004.